

JYU DISSERTATIONS 336

---

**Antti Neuvonen**

**Toward an Understanding of Hydrogen-Bonding Bifunctional Organocatalyst Conformations and Their Activity in Asymmetric Mannich Reactions**

---



UNIVERSITY OF JYVÄSKYLÄ  
FACULTY OF MATHEMATICS  
AND SCIENCE

JYU DISSERTATIONS 336

---

**Antti Neuvonen**

**Toward an Understanding of Hydrogen-  
Bonding Bifunctional Organocatalyst  
Conformations and Their Activity in  
Asymmetric Mannich Reactions**

Esitetään Jyväskylän yliopiston matemaattis-luonnontieteellisen tiedekunnan suostumuksella  
julkisesti tarkastettavaksi joulukuun 11. päivänä 2020 kello 12.

Academic dissertation to be publicly discussed, by permission of  
the Faculty of Mathematics and Science of the University of Jyväskylä,  
on December 11, 2020 at 12 o'clock noon.



JYVÄSKYLÄN YLIOPISTO  
UNIVERSITY OF JYVÄSKYLÄ

JYVÄSKYLÄ 2020

Editors

Petri Pihko

Department of Chemistry, University of Jyväskylä

Ville Korkiakangas

Open Science Centre, University of Jyväskylä

Copyright © 2020, by University of Jyväskylä

Permanent link to this publication: <http://urn.fi/URN:ISBN:978-951-39-8464-9>

ISBN 978-951-39-8464-9 (PDF)

URN:ISBN:978-951-39-8464-9

ISSN 2489-9003

## ABSTRACT

Neuvonen, Antti

Toward an Understanding of Hydrogen-Bonding Bifunctional Organocatalyst Conformations and Their Activity in Asymmetric Mannich Reactions

Jyväskylä: University of Jyväskylä, 2020, 77 p.

(JYU Dissertations

ISSN 2489-9003; 336)

ISBN 978-951-39-8464-9 (PDF)

Small molecule catalysts capable of simultaneously activating and coordinating reactive substrates through weak interactions, in a highly selective fashion, typically suffer from a lack of generality. Moreover, the interplay of several weak interactions in catalyst-substrate complexes is often not well understood. The aim of this thesis is to explain the factors governing the complexation and the activation of hydrogen bonding substrates with conformationally flexible bifunctional thiourea-tertiary amine organocatalysts during the catalytic cycle. Enantioselective Mannich reactions were used as model reactions. The catalyst family discovered in a prior study was further screened and developed to improve selectivity, reactivity and to expand the catalyst utility in related reactions. Computational and kinetic studies were conducted to establish a model explaining the observed selectivity and reactivity patterns. Additionally, conformational preference of the catalyst upon anion binding was studied with an array of anions in the solid state and in the solution to correlate the anion size and shape with observed catalyst folding. The thesis is based on three peer-reviewed publications.

Keywords: bifunctional organocatalysis, organic synthesis, anion binding, hydrogen bonding, kinetic experiments

## TIIVISTELMÄ (ABSTRACT IN FINNISH)

Neuvonen, Antti

Kohti vetysitoutuvien bifunktionaalisten organokatalyyttien konformaatioiden ja niiden aktiivisuuden ymmärtämistä asymmetrisissä Mannich-reaktioissa

Jyväskylä: University of Jyväskylä, 2020, 77 p.

(JYU Dissertations

ISSN 2489-9003; 336)

ISBN 978-951-39-8464-9 (PDF)

Katalyyttisten pienmolekyylien, jotka kykenevät samanaikaisesti aktivoimaan ja koordinoimaan heikoin vuorovaikutuksin lähtöaineita, toimintatapa ei usein ole yleistettävissä. Lisäksi useiden heikkojen vuorovaikutusten yhteisvaikutuksia katalyyttien ja substraattien sitoutumisessa ei usein ymmärretä. Tämän väitöskirjan tarkoituksena on selvittää vetysitoutuvien lähtöaineiden sitoutumiseen ja aktivointiin vaikuttavat tekijät katalyyttisen kierron eri vaiheissa käytettäessä konformaatioiltaan mukautuvaa, tioureaan ja tertiääriseen amiiniin perustuvaa bifunktionaalista organokatalyyttiä. Tutkimuksessa mallireaktioina käytettiin enantioselektiivisiä Mannich-reaktioita. Aikaisemmassa tutkimuksessa kehitetty katalyyttiperheen toimintaa selvitettiin ja kehitettiin edelleen selektiivisyyden, reaktiivisuuden ja käytettävyyden parantamiseksi uusilla lähtöaineilla. Havaitun selektiivisyyden ja reaktiivisuuden selittävän mallin luomiseksi suoritettiin laskennallisia ja reaktiokineettisiä kokeita. Konformaatioiden määräytymistä katalyytin sitoutuessa anioneihin tutkittiin sekä kiinteässä tilassa että liuoksissa. Anionin muodon ja koon vaikutusta katalyytin konformaatioon tutkittiin käyttäen valittua joukkoa anioneita. Tämä väitöskirja perustuu kolmeen vertaisarvioituun julkaisuun.

Avainsanat: bifunktionaalinen organokatalyyysi, orgaaninen synteesi, anionisitoutuminen, vetysitoutuminen, kineettiset kokeet

**Author** Antti Neuvonen  
Department of Chemistry  
University of Jyväskylä  
antti.j.neuvonen@gmail.com

**Supervisor** Petri Pihko  
Department of Chemistry  
University of Jyväskylä

**Reviewers** Lukasz Pilarski  
Department of Chemistry – BMC  
Uppsala University

Andrei Malkov  
Department of Chemistry  
Loughborough University

**Opponent** Tõnis Kanger  
Department of Chemistry and Biotechnology  
Tallinn University of Technology

## ACKNOWLEDGEMENTS

The experimental work presented in this thesis was mostly carried out at the Department of Chemistry, University of Jyväskylä during years 2011–2015 while the writing was completed in 2019–2020. The research was financed by the Department of Chemistry of the University of Jyväskylä and additional financial support was kindly provided by the Emil Aaltonen foundation.

I wish to express my gratitude to Professor Petri Pihko who gave me the opportunity and provided the means to conduct high-level research in inspiring surroundings. The research would not have reached this level without the collaboration between three interdisciplinary research groups. I am thankful for the fruitful collaboration with the co-authors of the papers included in my thesis. So, thank you Imre, Tamás, Ádám, Kari, Filip, and Dimitris!

My stay in Jyväskylä would not have been as joyful without all the Pihko group members that welcomed me into the group, helped me to get established in a new town and in a new lab, and continue to be a wonderful group of peers and friends. And not to forget members of the Rissanen group who took me along the frequent pastime activities...

Kiitos Vantaan kavereiden sain nautittua ajoittaisista, hyvin ansaituista reissuista kotipuoleen ja pitää taukoa akateemisesta elämästä. Te autoitte pitämään mielen kirkkaana.

Haluan syvästi kiittää entistä esimiestäni Reijo Partasta CABB Oy:ssä sekä nykyisiä ja entisiä kollegojani tutustuttamisestani teollisen mittakaavan operaatioihin orgaanisessa hienokemiassa, mikä auttoi väitöskirjan tutkimuksen asettamisesta oikean perspektiiviin. Olen kiitollinen kaikesta tuesta, rohkaisusta ja joustavuudesta, joita sain teiltä väitöskirjani kirjoitusvaiheen loppuunsaattamiseksi.

Kaiken tässä väitöskirjassa saavutetun taustalla on ollut vakaa pohja elämälle, josta en voi kiittää perhettäni kylliksi. Jokaisessa tämän venyneen 4-vuotisen rupeaman ylä- ja alamäessä olen voinut luottaa isäni ja äitini tukeen, josta sydämellinen kiitos teille! Kiitos Lauri motivoivista keskusteluista saunan lauteilla, vertaistuesta ja veljellisestä kirjavuudesta väitöskirjan loppumetreille.

Kokkola 15.11.2020

Antti Neuvonen

## FIGURE

FIGURE 1.	Structures of <i>R</i> and <i>S</i> enantiomers of SDHI fungicide Penflufen. .	16
FIGURE 2.	Simplified depiction of an energy diagram of a non-catalyzed reaction and a catalytic reaction, TS denoting a transition state. ....	17
FIGURE 3.	Simplified energy diagram of a catalytic enantioselective reaction. ....	19
FIGURE 4.	Factors affecting the strength of ion-dipole interaction .....	27
FIGURE 5.	Factors affecting the interaction energy between two stationary dipoles.....	27
FIGURE 6.	Directions of dipoles and distance of H-bond donors in reported H-bond catalytic moieties. <sup>54</sup> .....	29
FIGURE 8.	Activity of Takemoto catalyst is results in simultaneous function of thiourea H-bond donor moiety and a tertiary amine Brønsted base.....	31
FIGURE 9.	Energy diagram of a normal primary kinetic isotope effect.....	39
FIGURE 10.	Energy diagram of an inverse secondary kinetic isotope effect.....	41
FIGURE 11.	Catalysts studied in enantioselective Mannich reactions with $\beta$ -ketoesters. ....	46
FIGURE 12.	Hypothesis for failed application of pyrrolidine derived $\beta$ -ketoamide <b>56</b> versus sterically challenging $\beta$ -ketoester <b>55e</b> . ....	49
FIGURE 13.	Relative reaction rate as a function of Hammett constant ( $\sigma$ ). Reprinted with permission from ACS Catalysis, 2017, 7, 3284-3294. Copyright 2017 American Chemical Society. ....	52
FIGURE 14.	Hydrogen bond network of bifunctional catalyst <b>54</b> and urea.....	55
FIGURE 15.	Computational comparison of plausible dispersion interactions with urea-thiourea catalyst <b>54</b> ( <b>1a</b> in figure) and Takemoto catalyst <b>39</b> ( <b>2a</b> in figure). Phenyl and cyclohexyl imines = red, dimethylmalonate = blue. Dispersion interactions = green, catalyst = light grey. Reprinted with permission from ACS Catalysis, 2017, 7, 3284-3294. Copyright 2017 American Chemical Society.....	57
FIGURE 16.	Observed catalyst <b>53</b> and catalyst <b>53</b> salt conformers in solid state. Reprinted with permission from Journal of Organic Chemistry, 2019, 84, 15009-15019. Copyright 2019 American Chemical Society. ....	58
FIGURE 17.	Solid state structures of catalyst <b>52</b> and <b>53</b> halide salts. Adapted with permission from Journal of Organic Chemistry, 2019, 84, 15009-15019. Copyright 2019 American Chemical Society. ....	61
FIGURE 18.	Solid-state structure of catalyst 52 TFA salt.....	62
FIGURE 19.	Solid-state structure of C <sub>2</sub> -symmetric 2:1:1 catalyst-urea-acetonitrile complex. <sup>11</sup> One catalyst molecule is presented as space-fill model and urea, acetonitrile, and second catalyst molecule as wireframe model. H-Bonding moieties in second catalyst molecule are colored according to atom colors and the rest colored green for clarity.....	63



## TABLE

TABLE 1.	Distance dependencies of idealized non-covalent interactions.....	26
TABLE 2.	Strength and type of interaction in hydrogen bonds.....	28
TABLE 3.	Selected results from expanding nucleophile scope in asymmetric Mannich reaction.....	48

## SCHEME

SCHEME 1.	Epimerization of Thalidomide enantiomers.....	16
SCHEME 2.	Proposed catalytic cycle of a Suzuki reaction.....	18
SCHEME 3.	First Mannich reaction reported in 1917.....	21
SCHEME 4.	Selected examples of enantioselective catalytic Mannich-type reactions of Silyl enol ethers.....	22
SCHEME 5.	Selected examples of Mannich-type reactions catalyzed by chiral secondary amines.....	23
SCHEME 6.	Selected examples of enantioselective Mannich reactions with $\beta$ -dicarbonyl substrates.....	24
SCHEME 7.	Conformational freedom of few common moieties in H-bond organocatalysts.....	32
SCHEME 8.	Rate acceleration by enolate and transition state stabilization in a Michael reaction.....	34
SCHEME 9.	Organocatalytic enantioselective chlorolactonization reaction studied with RPKA.....	38
SCHEME 10.	Selected example of primary kinetic isotope effect in catalytic reaction.....	40
SCHEME 11.	General scheme of enantioselective Mannich reaction studied in reference 123.....	44
SCHEME 12.	Properties of $\beta$ -dicarbonyl compounds. a) see ref. 133, b) see ref. 132, c) see ref. 130 d) see ref. 131, e) see ref. 129.....	45
SCHEME 13.	Diastereoselective organocatalytic generation of the key quaternary stereocenter in (-)-Nakadomarin A total synthesis. <sup>143</sup> .....	49
SCHEME 14.	Initial hypothesis for catalytic cycles of enantioselective Mannich reaction leading to both enantiomers.....	50
SCHEME 15.	Model reaction used in determination of Hammett relationship. X denotes the <i>para</i> -substituent.....	51
SCHEME 16.	Model reaction used in determination of 2° KIE. X denotes the <i>para</i> -substituent.....	53
SCHEME 17.	H-bond acceptor (red) and donor (blue) sites in Mannich reaction substrates and product.....	54
SCHEME 18.	An example of extreme product inhibition in a Lewis acid catalyzed Schmidt reaction.....	56

## LIST OF PUBLICATIONS

This thesis consists of an introduction based on the related literature, an overview of the author's work and of the following publications. The publications are referred to in the text by their Roman numerals.

- I            Neuvonen, A. J.; Pihko, P. M. Enantioselective Mannich Reaction of  $\beta$ -Keto Esters with Aromatic and Aliphatic Imines Using a Cooperatively Assisted Bifunctional Catalyst. *Org. Lett.* **2014**, *16*, 5152-5155.
- II            Neuvonen, A. J.; Földes, T.; Madarász, Á.; Pápai, I. Pihko, P. M. Organocatalysts Fold To Generate an Active Site Pocket for the Mannich Reaction. *ACS Catalysis*, **2017**, *7*, 3284-3294.
- III           Neuvonen, A. J.; Noustas, D.; Topić, F.; Rissanen, K.; Földes, T.; Pápai, I.; Pihko, P. M. Dynamic Refolding of Ion-Pair Catalysts in Response to Different Anions. *J. Org. Chem.* **2019**, *84*, 15009-15019.

## **AUTHOR'S CONTRIBUTION**

In publication I, the author designed and carried out the experiments and analyses. The publication was written with the co-author.

In publication II, the author designed and carried out the experiments and analyses. Computational analysis was performed in the research group of Imre Pápai. The publication was written with the co-authors.

In publication III, the author designed and carried out the experiments and analyses together with Dimitris Noutsias and Filip Topić, focusing on the solid-state structures. The computational analyses were performed in the research group of Imre Pápai. The publication was written with the co-authors.

## ABBREVIATIONS

1° KIE	primary kinetic isotope effect
2° KIE	secondary kinetic isotope effect
$\alpha$	the closest position to a functional group
$\beta$	the second-closest position to a functional group
$\gamma$	the third-closest position to a functional group
$\epsilon$	dielectric constant
$\epsilon_0$	permeability of vacuum
$\mu$	dipole moment
$\rho$	Hammett reaction constant
$\sigma$	Hammett substituent constant or a bonding orbital
$\sigma^*$	antibonding orbital
$\theta$	angle
Boc	<i>tert</i> -butyloxycarbonyl
D	deuterium atom, $^2\text{H}$
DBU	1,8-Diazabicyclo[5.4.0]undec-7-ene
DMF	<i>N,N</i> -dimethyl formamide
DMSO	dimethyl sulfoxide
dr	diastereomeric ratio
<i>E</i>	energy
<i>ee</i>	enantiomeric excess (%)
EIE	equilibrium isotope effect
equiv.	equivalent
er	enantiomeric ratio
Et	ethyl
g	gram
<i>G</i>	Gibbs energy
GC	gas chromatography
GC-MS	gas chromatography with mass spectrometric detection
H	hydrogen (protium) atom
ha	hectare
H-bond	hydrogen bond
hfacac	hexafluoroacetylacetone
HFIP	hexafluoro isopropanol
HPLC	high-performance liquid chromatography
HRMS	high-resolution mass spectrometry
I	intermediate
<i>in situ</i>	Latin for "in position"
<i>iPr</i>	<i>iso</i> -propyl
<i>k</i>	rate constant
$K_{\text{eq}}$	equilibrium constant
$k_{\text{obs}}$	observed rate constant
$k_{\text{rel}}$	relative rate
LUMO	lowest unoccupied molecular orbital

M	mol/L
Me	methyl
mol	mole, $6.022 \times 10^{23}$ particles
NMR	nuclear magnetic resonance
Ph	phenyl
$pK_a$	acid dissociation constant
PMP	<i>para</i> -methoxy phenyl
$q$	electric charge (eV)
$r$	distance (Å)
$R$	ideal gas constant
$R_e$	enantiotopic face leading to <i>R</i> enantiomer
RPKA	reaction progress kinetic analysis
rt	room temperature
SDHI	succinate dehydrogenase inhibitor
$S_i$	enantiotopic face leading to <i>S</i> enantiomer
$T$	temperature
<i>t</i> Bu	<i>tert</i> -butyl
TDI	turnover frequency determining intermediate
TDTS	turnover frequency determining transition state
THF	tetrahydrofuran
TON	turnover number
TOF	turnover frequency
TS	transition state
Ts	<i>para</i> -toluenesulfonyl
XRD	X-ray diffraction
$ZpE$	zero-point energy

# CONTENTS

ABSTRACT

TIIVISTELMÄ (ABSTRACT IN FINNISH)

ACKNOWLEDGEMENTS

FIGURES, TABLES AND SCHEMES

LIST OF PUBLICATIONS

AUTHOR'S CONTRIBUTION

ABBREVIATIONS

CONTENTS

1	INTRODUCTION TO CATALYSIS AND ITS ROLE IN SOCIETY .....	15
1.1	Catalysis is All Around Us, but It is Difficult Understand.....	15
1.2	Catalysis in the Scope of this Dissertation .....	17
1.2.1	General Principles of Catalysis.....	17
1.2.2	Introduction to Asymmetric Catalysis.....	18
1.2.3	Enantioselective Mannich-Type Reactions.....	20
2	UNDERSTANDING CATALYTIC REACTIONS IN BIFUNCTIONAL ORGANOCATALYSIS .....	25
2.1	Non-covalent Interactions .....	25
2.2	Brønsted Acids and Hydrogen Bond Donors in Noncovalent Activation of Electrophiles .....	28
2.3	Basic Design Concepts of Catalysts for Enantioselective Reactions .....	30
2.3.1	Conceptualization of Catalyst Design.....	30
2.3.2	Primary Interactions Between Catalyst and Substrates.....	30
2.3.3	Chiral Backbone in Enantioselective Catalysts .....	31
2.3.4	Secondary Interactions Between Catalyst and Substrates.....	32
2.4	Experimental Kinetic Methods Help to Reveal Reaction Mechanisms .....	35
2.4.1	General Considerations in Experimental Kinetic Measurements of Organocatalytic Reactions.....	35
2.4.2	Factors for Selecting Experimental Methods .....	35
2.4.3	Reaction Order.....	37
2.4.4	Kinetic Isotope Effects .....	38
2.4.5	Linear Free Energy Relationships.....	41
2.4.6	Computational Methods Compliment Experimental Results.....	42
3	RESULTS AND DISCUSSION .....	43
3.1	Aim of the Work .....	43
3.2	Expanding the Scope of Enantioselective Organocatalytic Mannich Reactions <sup>1</sup> .....	44

3.3	Understanding the Mechanism of Mannich Reactions Catalyzed by Bifunctional Organocatalysts <sup>II</sup> .....	49
3.3.1	The Approach .....	49
3.3.2	Key Findings of Kinetic Studies .....	50
3.3.3	Inhibition Experiments as a Proxy for Complex Formation Studies.....	53
3.4	Weak Interactions and Enhanced Activity in H-bond Catalysis .....	56
3.5	Solving the Active Catalyst and Catalyst Salt Conformations <sup>III</sup> .....	58
3.5.1	The Native Conformation of Free Catalyst .....	58
3.5.2	Structure Elucidation of Catalyst Salts in Solid State and in Solution.....	59
4	SUMMARY AND CONCLUSIONS .....	64
	REFERENCES.....	65
	ORIGINAL PAPERS	

# 1 INTRODUCTION TO CATALYSIS AND ITS ROLE IN SOCIETY

## 1.1 Catalysis is All Around Us, but It is Difficult Understand

Biological catalytic processes are a significant factor in the vital functions of all known forms of life, and thus they have been an essential part of life on Earth for billions of years. On the other hand, catalysis has proven to be the main driver of new innovations in chemical research and industrial processes which enable the modern healthcare and food supply.<sup>1</sup> Despite the many successful implementations and the general understanding of catalytical processes there is still a long journey ahead to fully understand the phenomena behind asymmetric catalysis.<sup>2</sup>

Catalytic applications form the backbone of sustainable energy, fertilizer, and materials industries, comprising of e.g. fuel and power production,<sup>3</sup> ammonia production<sup>4</sup>, monomer production for polymeric materials and polymerization,<sup>1</sup> and fine chemical production.<sup>5</sup> Shortly put, in things that have changed societies in the modern era throughout the globe. In these cases, metal catalysis is mostly used. Catalysis by organic small molecules is still a niche area in chemical industries. However, as pharmaceutical and agrochemical<sup>6</sup> active ingredients are required to be more effective and selective, approaches to introduce chirality<sup>7</sup> and enantiomeric purity have been taken. To reach these goals, new activation modes and the use of *asymmetric organocatalysis* is bound to find more and more industrial applications.<sup>8</sup>

Penflufen (**1**), an SDHI fungicide, is used as a racemic mixture despite the *S*-enantiomer being almost 5 times as effective against apple scab (*Venturia inaequalis*) as the *R*-enantiomer at 25 g/ha application rate (FIGURE 1).<sup>9</sup> This means that the same efficacy could be reached with 40% less material if only pure *S*-enantiomer was used. In this case the benefits of using a pure enantiomer are clear but the availability of feasible enantioselective large-scale manufacturing processes limits the availability of the pure *S*-enantiomer.



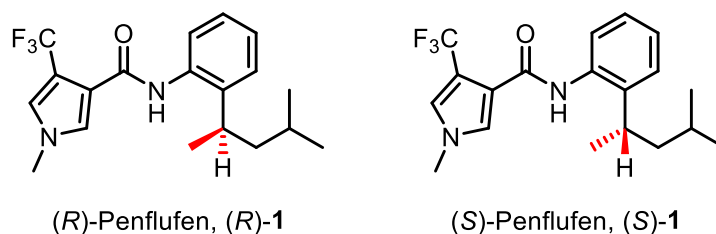
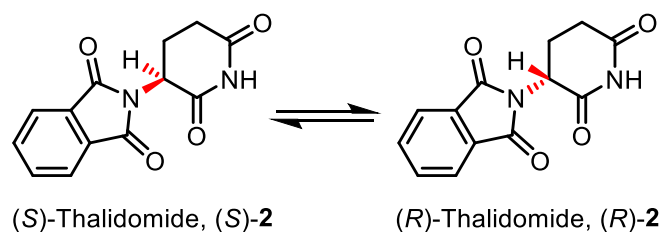


FIGURE 1. Structures of *R* and *S* enantiomers of SDHI fungicide Penflufen.

In pharmaceuticals such racemic active ingredient mixtures caused “the biggest man-made medical disaster”.<sup>10</sup> Whereas the *S*-enantiomer of Thalidomide (**2**) is an effective sedative and anti-emetic in treatment of morning sickness in pregnant women, the *R*-enantiomer is teratogenic to the unborn child and caused permanent physical defects to over 10 000 children. In this case even the enantioselective synthesis of the active ingredient does not solve the problem as the stereocenter epimerizes in physiological conditions to result a racemic mixture (SCHEME 1).



SCHEME 1. Epimerization of Thalidomide enantiomers.

Although the examples above are just individual cases, they remind us of the fact that these differences of activity in biocatalytic processes are often not obvious from the molecular structure even to the experts in the area, revealing the limits of human understanding, especially in understanding structure-activity relationships.

Still today the development of catalysts for enantioselective transformations is mostly relying on trial and error, and chemical intuition.<sup>11</sup> Despite the outlook from nearly 20 years ago<sup>12</sup> and the exponential increase in computation power, computational design of enantioselective catalysts has not yet become mainstream and many alternative approaches are still in early development.<sup>13,14,15</sup> Due to the high development effort, tailor-made catalysts that are required to reach high yields and selectivity are much more expensive than more widely used general catalysts. A better understanding of the structure-activity relationship would reduce the labor cost of catalyst development but not necessarily the material cost of catalyst itself. To reduce the cost of catalysis and to increase the feasibility of catalytic processes, high turnover frequency (TOF) and turnover number (TON) are essential. These targets should be among the main drivers for any catalysis development efforts.

Both governmental bodies, such as “Europe 2020 Strategy” by European Union <sup>16</sup>, and non-governmental organizations <sup>17</sup> are advocating resource efficiency as the solution to lower human impact on the nature. Additionally, sustainability goals are becoming increasingly important to customers and stakeholders across industries. Catalysis is widely considered to be a significant part of the solution.<sup>18,19</sup>

## 1.2 Catalysis in the Scope of this Dissertation

### 1.2.1 General Principles of Catalysis

Molecules and polymeric materials exhibiting catalytic activity have been grouped and labeled, based on structure and activity, into numerous catalysis subcategories. However, few fundamental principles apply to all forms of catalysis.<sup>20,21</sup> In a catalytic reaction a catalyst interacts with the starting material(s), intermediate(s), or other species in the reaction. Hence the reaction mechanism is changed leading to the formation of reaction products *via* a lower-energy pathway (FIGURE 2).

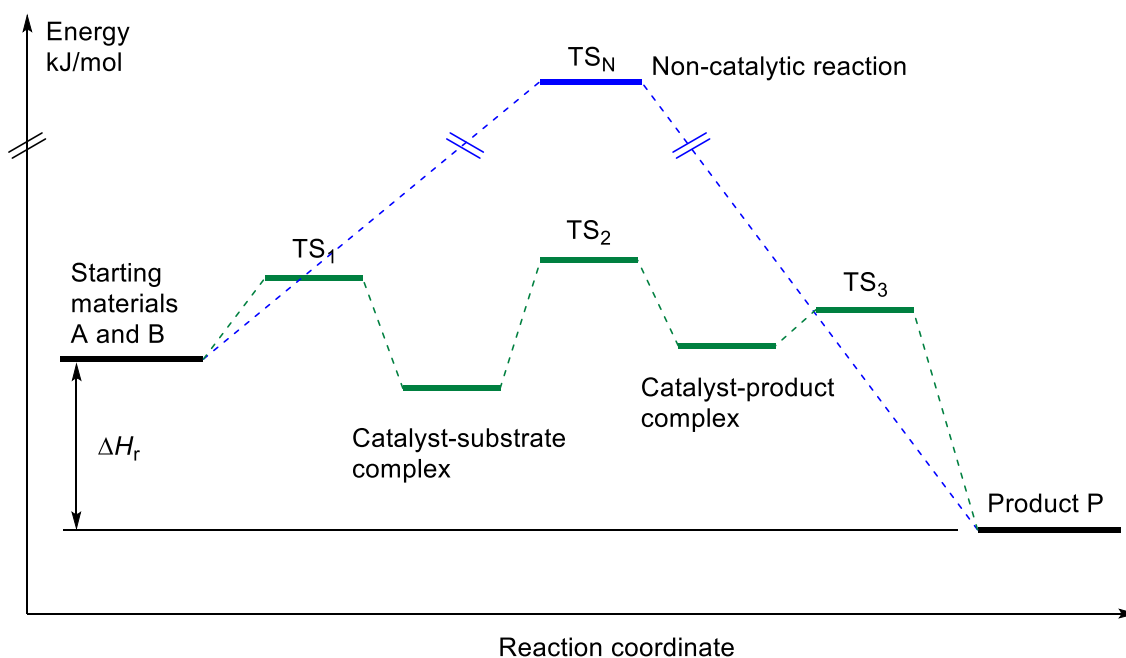
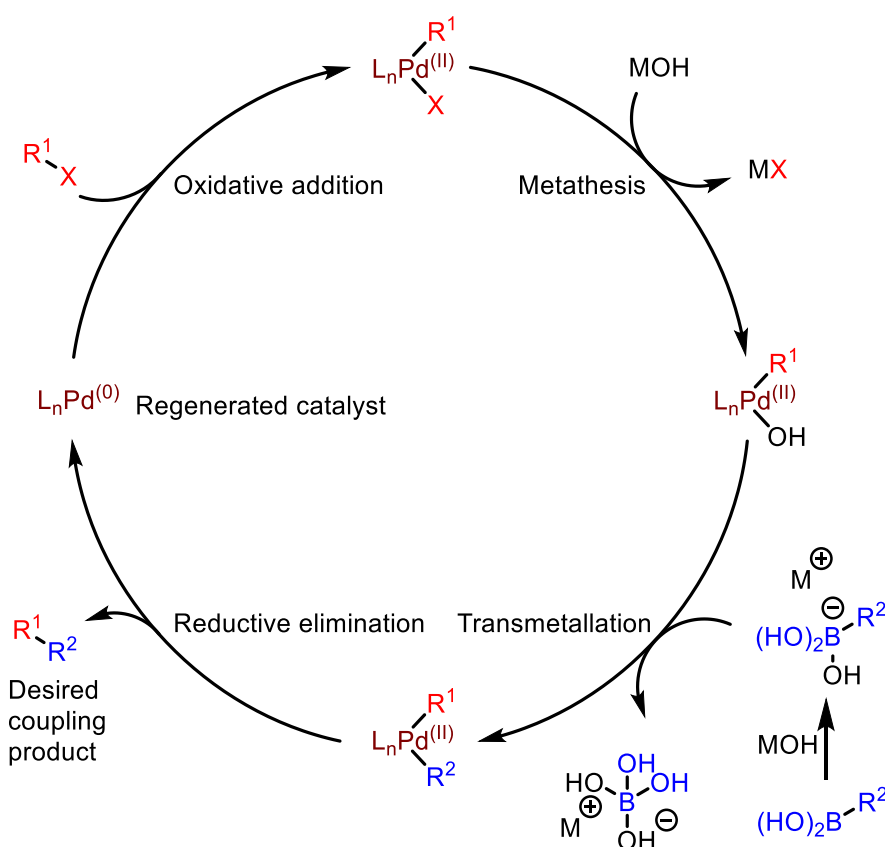


FIGURE 2. Simplified depiction of an energy diagram of a non-catalyzed reaction and a catalytic reaction, TS denoting a transition state.

A lower energy in the TOF determining transition state leads to an increased rate of product formation. Since the starting materials and products in a catalytic reaction and non-catalytic reaction are the same, the reaction enthalpy ( $\Delta H$ ) is not altered and thus the equilibrium of the reaction does not change. In

2011 Kozuch and Shaik<sup>21</sup> published an article introducing an “Energetic Span Model” which refined the terminology describing the factors governing TOF, namely the TOF-determining transition state (TDTS) and TOF-determining intermediate (TDI).

Another general principle in catalysis is that the catalyst is regenerated after participating in the catalytic reaction. The regeneration of catalyst allows the presentation of the consecutive reactions as a catalytic cycle where reaction starting materials enter the cycle and product together with potential side products leave the cycle (SCHEME 2). This presentation helps us to understand the concepts of TOF and TON, TOF being the number of cycles per time unit and TON being the number of times a single catalyst molecule, on average, completes a cycle. This presentation however does not explain the deactivation of catalyst through irreversible complexation or through side reactions which result in the observed TON.



SCHEME 2. Proposed catalytic cycle of a Suzuki reaction.<sup>22</sup>

## 1.2.2 Introduction to Asymmetric Catalysis

Main purpose of asymmetric catalysis is to have access to a compound which can exist as stereoisomers<sup>23</sup> known as enantiomers<sup>24</sup> and to obtain it as a pure enantiomer. Without any external factor promoting the formation of one enantiomer over the other in a reaction, the enantiomers would be obtained as a

racemic mixture, with 1:1 ratio of enantiomers. The enantiomeric selectivity of a reaction is typically governed by a difference in the rate of formation.<sup>2</sup> However, in the case of reversible reactions or epimerizable stereocenters, thermodynamic or kinetic equilibrium in chiral environment can also favor formation of one enantiomer over the other. Examples of such enrichment of enantiomers are crystallization-induced asymmetric transformations<sup>25,26</sup> and dynamic kinetic resolutions (DKR)<sup>27</sup>.

In the development of asymmetric catalysis, the aim is to increase the reaction rate against the non-catalyzed reaction as well as to promote the formation of the desired enantiomer over the undesired enantiomer. The rates of enantiomer formation are controlled by the energies in the stereoselectivity determining transition state.<sup>2</sup> Thus, to achieve high selectivity, it is mandatory for a catalyst to differentiate the enantioselectivity determining transition states.

In enantioselective catalysis the reaction energy diagram (FIGURE 2) transforms to account for two pathways leading to *R* and *S* enantiomers (FIGURE 3). In this example of kinetic control, enantioselectivity arises from the energy difference  $\Delta G$  of diastereomeric transition states  $TS_2(R)$  and  $TS_2(S)$ .<sup>2</sup> In FIGURE 3 a scenario is depicted where prior to the bond forming reaction two slightly different diastereotopic substrate-catalyst complexes  $I_1(R)$  and  $I_1(S)$  are formed that would lead to different product enantiomers. This complexation can be reversible, and in that case the enantiomeric ratio is determined in the bond forming reaction between two substrates.

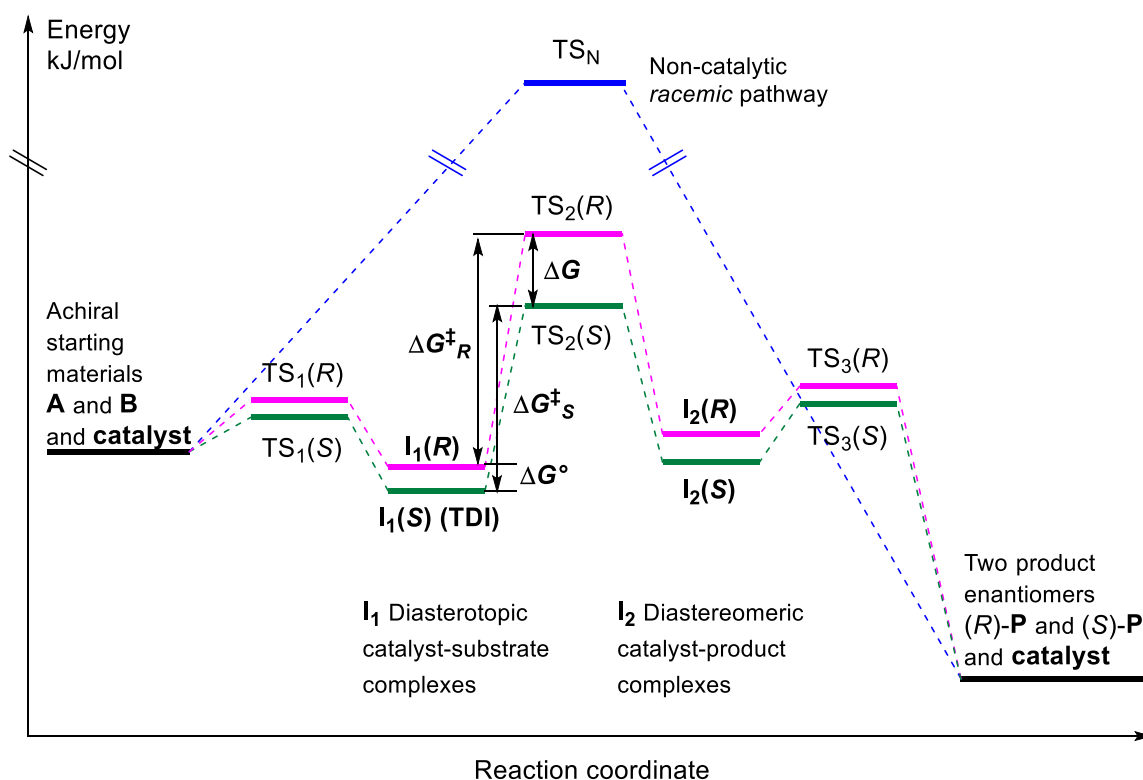


FIGURE 3. Simplified energy diagram of a catalytic enantioselective reaction.

The enantiomeric ratio, a key performance indicator in enantioselective catalysis, arises from the energy difference ( $\Delta G$ ) of enantioselectivity determining transition states<sup>2</sup> or difference in energetic span ( $\delta E$ )<sup>21</sup>. The ratio of enantiomers can be derived from rate law:

$$rate = k[A][B][catalyst] \quad (1)$$

$$\frac{rate(S)}{rate(R)} = \frac{k_S[A][B][catalyst]}{k_R[A][B][catalyst]} = \frac{k_S}{k_R} \quad (2)$$

$$k_S = e^{\frac{-\Delta G^\ddagger_S}{RT}} \quad (3)$$

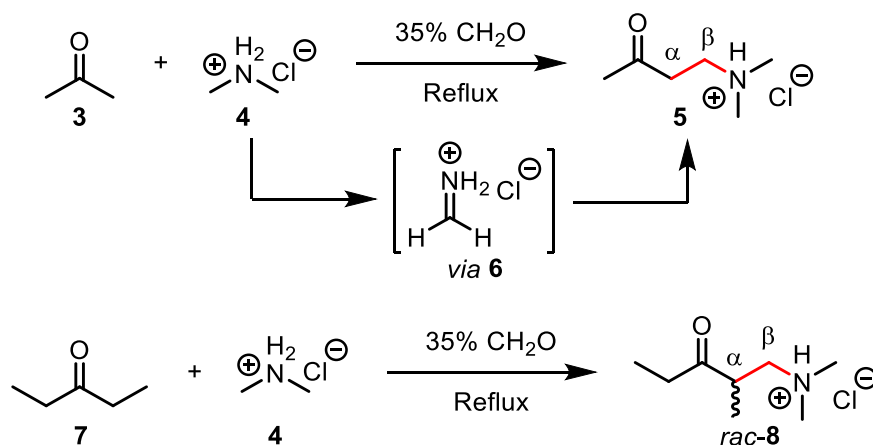
Considering a common TDI ( $I_1(S)$ ) for both pathways the enantiomeric ratio can be written as:

$$\Delta G = \Delta G^\ddagger_R + \Delta G^0 - \Delta G^\ddagger_S \quad (4)$$

$$er = e^{\frac{-\Delta G}{RT}} = e^{\frac{-(\Delta G^\ddagger_R + \Delta G^0 - \Delta G^\ddagger_S)}{RT}} \quad (5)$$

### 1.2.3 Enantioselective Mannich-Type Reactions

The first Mannich reactions were described already a century ago in 1917 by Mannich in a publication titled "Synthesis of  $\beta$ -Ketonic Bases".<sup>28</sup> The three-component reaction between acetone (**3**), dimethylammonium hydrochloride (**4**) and formaldehyde yields a linear  $\beta$ -unsubstituted amine **5** with two new covalent bonds (SCHEME 3). One of the new bonds is formed in a reaction between dimethylammonium hydrochloride and formaldehyde and the second bond in a C-C bond forming reaction between in situ formed iminium species **6** and acetone. However, the reaction using diethyl ketone (**7**) instead of acetone yields a branched compound **8** with a stereocenter in the  $\alpha$  position. As no molecules capable of chiral induction are present, the reaction most likely yields a racemic mixture of enantiomers.



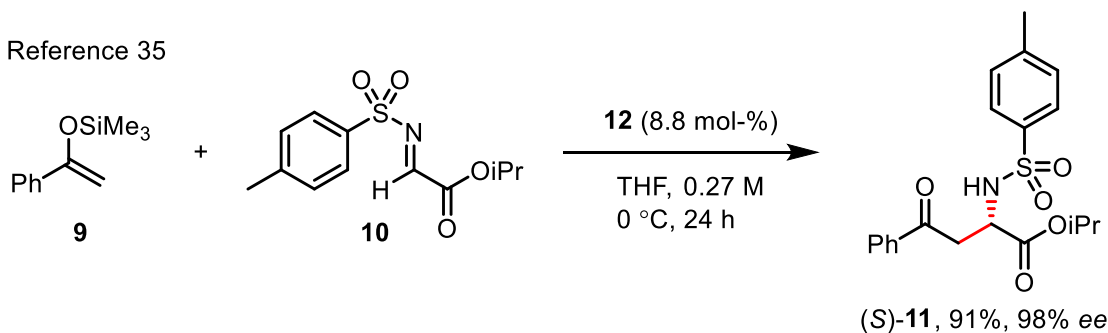
SCHEME 3. First Mannich reaction reported in 1917.

In contrast to the report by Mannich, the focus throughout this thesis is in catalytic asymmetric two-component transformations of aldehyde derived imines. Such imines, also known as aldimines, form a stereocenter on the  $\beta$ -carbon adjacent to the amine in a Mannich reaction.<sup>29</sup> The generation of these stereocenters in high fidelity through enantioselective Mannich reactions has been a goal for many research endeavors. The history, general principles, and development of Mannich reaction<sup>22</sup> and its enantioselective variants<sup>7,29</sup> have been well documented in the literature. In addition to catalytic approaches to induce chirality, the use of chiral auxiliaries in Mannich reactions is also described.<sup>30,31</sup>

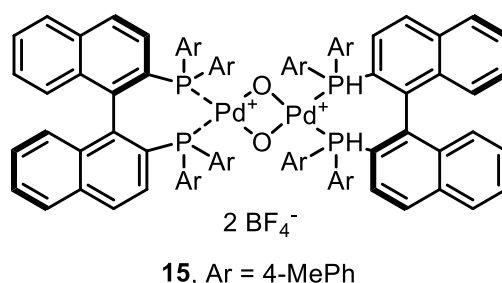
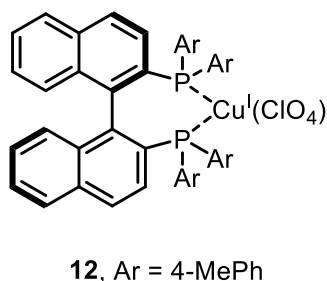
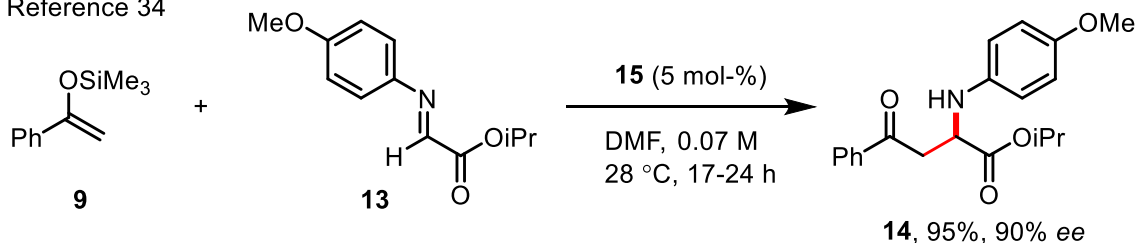
Since the first reports of stoichiometric<sup>32</sup> and catalytic<sup>33</sup> enantioselective additions of enol or enolate nucleophiles to imines, several approaches have been developed to access a variety of chiral aminoketones and aminoesters.<sup>7</sup> Few of the most widely studied approaches include the use of enol silanes,<sup>34,35</sup> in situ formed enamines<sup>36,37</sup> and  $\beta$ -dicarbonyl compounds<sup>38,39,40</sup> as nucleophiles. These catalytic asymmetric approaches avoid the use of chiral auxiliaries from the chiral pool to induce chirality to the final product. Catalytic asymmetric approaches are considered to lead to better atom economy than chiral induction from auxiliaries.<sup>19</sup> However, even in catalytic reactions, selection of a suitable protecting group may be necessary.

In 1998 Sodeoka<sup>34</sup> and Lectka<sup>35</sup> groups published Lewis acid catalyzed enantioselective Mannich reactions between silyl enol ethers and glyoxalate derived imines (SCHEME 4). Silyl enol ethers react readily with electrophiles and Lectka proposes that catalytic activity and selectivity is achieved through bidentate coordination of glyoxalate derived imine to Lewis acidic metal.

Reference 35



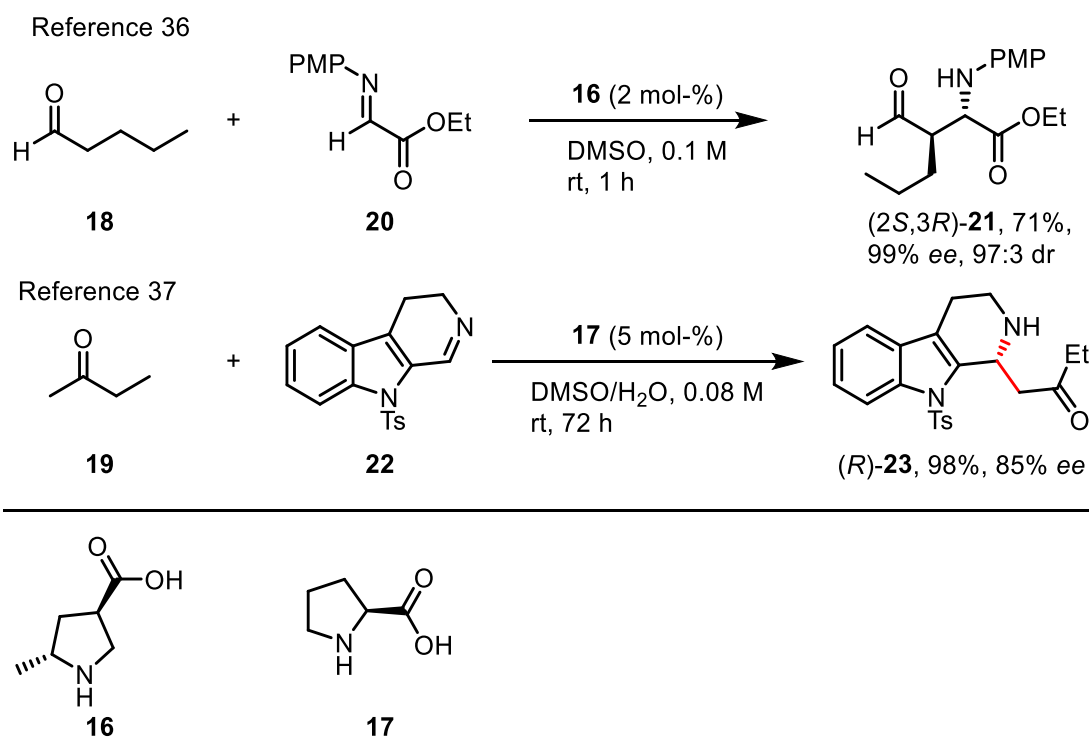
Reference 34



SCHEME 4. Selected examples of enantioselective catalytic Mannich-type reactions of Silyl enol ethers.

Secondary amine–carboxylic acid catalysts **16** and **17** are proposed to have additional interactions in the enantioselectivity determining C-C bond forming reaction. In these examples the amine functional group interacts with the aldehyde (**18**) or ketone (**19**) pronucleophile by covalently binding to the carbonyl functional group. The formed enamine is highly nucleophilic which contributes to rate acceleration and the high nucleophilicity of enamines is utilized in many catalytic applications.<sup>41</sup> Additionally, the carboxylic acid functional group can interact with mildly basic imine electrophiles activating it towards nucleophilic attack. Catalysts capable of activating both substrates synergistically through two distinct functional groups are known as bifunctional catalysts.<sup>42</sup>

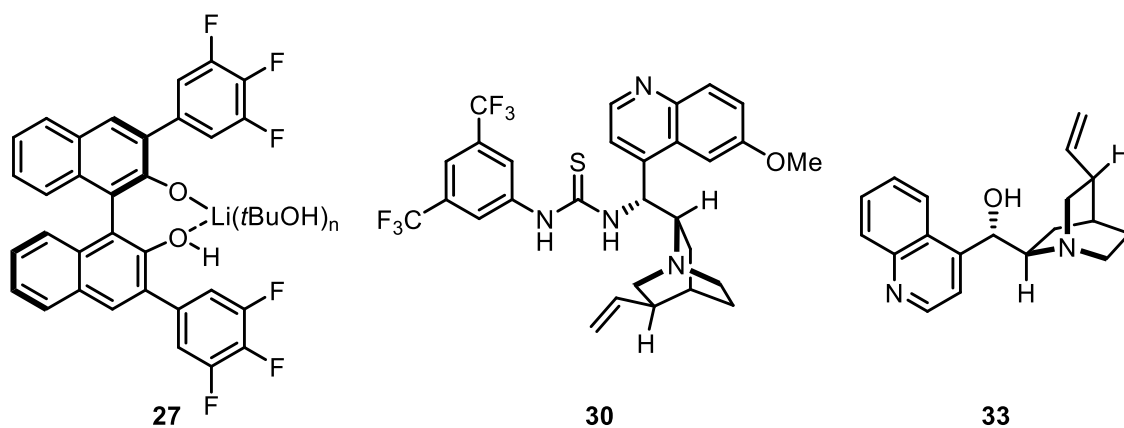
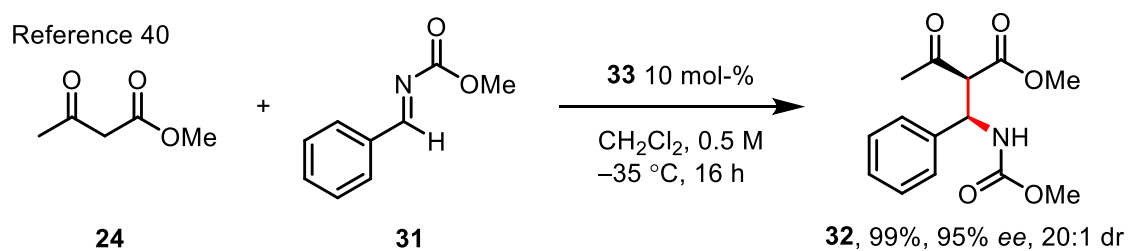
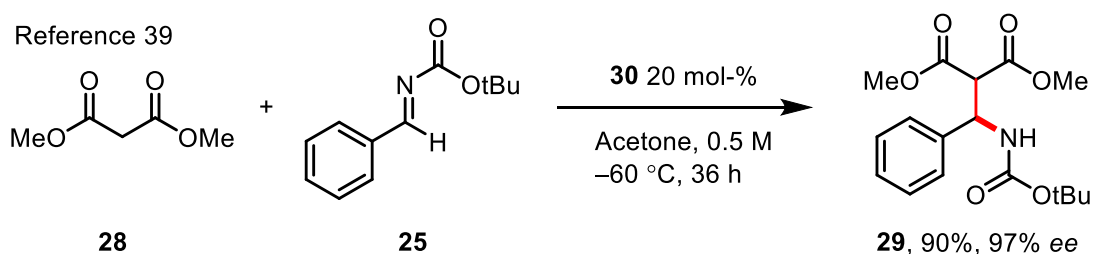
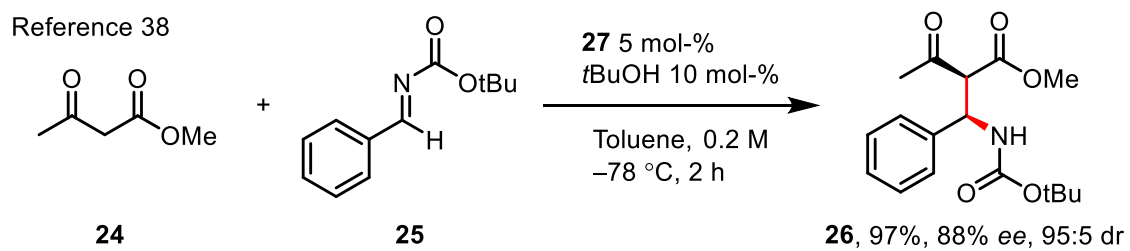
In contrast to the previous examples, enantioselective Mannich reactions in SCHEME 5 are catalyzed by small organic molecules. Asymmetric organocatalysis as a concept is used to describe catalysis with small organic molecules with asymmetric induction from the catalyst.<sup>43</sup> The various subclasses of asymmetric organocatalysis are discussed thoroughly in the book “Asymmetric Organocatalysis” by Berkessel and Gröger<sup>29</sup> and the utility of Asymmetric Organocatalysis has since been expanded to new reaction types.



SCHEME 5. Selected examples of Mannich-type reactions catalyzed by chiral secondary amines.

A third often used nucleophile type in Mannich reactions are  $\beta$ -Dicarbonyl compounds (SCHEME 6). These nucleophiles can be activated by Brønsted base catalysts and thus are highly potential substrates for asymmetric organocatalysis by organic bases. Ishihara and co-workers used a strong chiral base to deprotonate the pronucleophile.<sup>38</sup> They propose that the lithium cation activates also the imine towards nucleophilic attack and thus the catalyst system can be described as being bifunctional. The catalysts reported by Deng and co-workers<sup>39</sup> and Schaus and co-workers<sup>40</sup> include a Brønsted basic tertiary amine and a H-bond donor moiety in their structure. Similarly to Ishihara's report, the H-bond donor is proposed to activate the imine electrophile towards nucleophilic addition in an enantioselective fashion.





SCHEME 6. Selected examples of enantioselective Mannich reactions with  $\beta$ -dicarbonyl substrates.

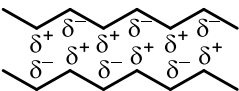
## 2 UNDERSTANDING CATALYTIC REACTIONS IN BIFUNCTIONAL ORGANOCATALYSIS

### 2.1 Non-covalent Interactions

Covalently bonded atoms interact mostly through shared electrons in a bonding molecular orbital. Bonding molecular orbitals have distinct geometries, spatial orientation and size, depending on hybridization of involved atoms.<sup>44</sup> In contrast, non-covalently interacting species are not limited in their relative orientation and the interaction occurs through space. Knowles and Jacobsen have summarized the distance dependency of non-covalent interaction energies which underlines the variety of these interactions (TABLE 1).<sup>45</sup>

At short intermolecular distances ( $<1,5\text{\AA}$ ) the orbital interactions are having a more profound effect on interaction energy. Biedermann and Schneider have compiled a comprehensive list of various experimental interaction energies. It is apparent that interaction energies should not be generalized based on interaction type but should rather be determined in the actual conditions.<sup>46</sup>

TABLE 1. Distance dependencies of idealized non-covalent interactions

Non-covalent interaction		Distance dependency of interaction energy
Ion-ion	$R-NH_3^+$ $O_2C^--R'$	$1/r$
Ion-dipole	$R-NH_3^+$ $\delta^- \begin{array}{c} H \delta^+ \\   \\ O \\   \\ H \delta^+ \end{array}$	$1/r^2$
Dipole-dipole	$\delta^- \begin{array}{c} H \delta^+ \\   \\ O \\   \\ H \delta^+ \end{array}$ $\delta^- \begin{array}{c} H \delta^+ \\   \\ O \\   \\ H \delta^+ \end{array}$	$1/r^3$
Ion-induced dipole	$R-CO_2^-$ $\delta^+ \text{---} \text{C}_6\text{H}_4 \text{---} \delta^- \text{---} R'$	$1/r^4$
Dipole-induced dipole	$\delta^- \begin{array}{c} H \delta^+ \\   \\ O \\   \\ H \delta^+ \end{array}$ $\delta^+ \text{---} \text{C}_6\text{H}_4 \text{---} \delta^- \text{---} R$	$1/r^5$
Dispersion		$1/r^6$
Hydrogen bond	$\begin{array}{c} R \\   \\ N-H \cdots O=C \\   \quad \quad   \\ \quad \quad \quad R' \\ \quad \quad \quad R'' \end{array}$	complex $\sim 1/r^2$
Steric repulsion	$R-CH_3 \text{---} \text{C} \text{---} H_3C-R'$	$1/r^{12}$

However, the table shown above does not consider the directionality of many of the weak interactions. For example, dipole moment is a vector variable and the dipolar interactions of polar compounds have an optimal direction. Thus magnitude of ion-dipole interaction depends on the direction of a dipole (FIGURE 4) with regards to a point charge and the Coulombic law which describes the interaction between two point charges ( $q_1$  and  $q_2$ , equation 6) is transformed into equation 7.<sup>47</sup>

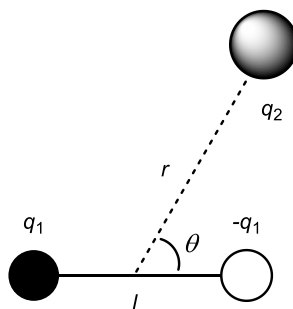


FIGURE 4. Factors affecting the strength of ion-dipole interaction

$$V = \frac{q_1 q_2}{4\pi\epsilon\epsilon_0 r} \quad (6)$$

$$V = \frac{\mu q_2 \cos \theta}{4\pi\epsilon\epsilon_0 r^2} \quad (7)$$

According to equation 7, the ion-dipole interaction energy  $V$  is proportional to the cosine of the angle between the dipole and the ion ( $\theta$ ). Additionally, the interaction energy is more sensitive to the distance as it is inversely proportional to its square.

The dipole-dipole interaction energy between two parallel stationary dipoles is proportional to the cubical of the distance. Also, in this case the angle between the dipoles ( $\theta$ , FIGURE 5) has a great influence on the interaction energy  $V$  that follows equation 8.

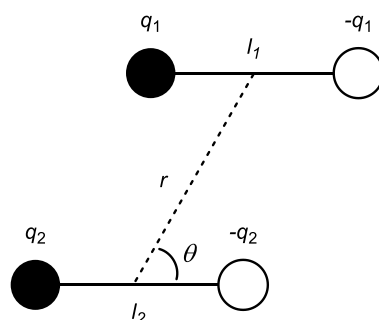


FIGURE 5. Factors affecting the interaction energy between two stationary dipoles

$$V = \frac{\mu_1 \mu_2 (1 - 3\cos^2 \theta)}{4\pi\epsilon\epsilon_0 r^3} \quad (8)$$

Non-covalent interactions are in the focus in the field of supramolecular chemistry.<sup>48</sup> Although supramolecular chemistry and catalysis are often studied and discussed separately, they share many common features.<sup>49</sup> The often relatively static molecular assemblies studied in supramolecular chemistry can give important insight to phenomena occurring in highly dynamic environment

of catalysis. One of these insights is that the directionality of H-bonding is higher than of any other weak interaction.<sup>50</sup>

The weakest of intermolecular interactions are the dispersion interactions. When ionic and dipolar interactions are present dispersion interactions can have an amplifying effect but seldom can overpower stronger interactions. However, when ionic and polar interactions are not present, the physical properties of substances are more dependent on dispersion interactions. Compared to ionic and dipole interactions dispersion interactions weaken rapidly as a function of distance.

Strength of hydrogen bonds is generally 20 kJ/mol but range between 0.2 and 40 kJ/mol.<sup>50</sup> Whereas ion-dipole, dipole-dipole and dispersion interactions are entirely coulombic interactions, in hydrogen bonds the governing interaction is dependent on the distance between the H-bond donor and the acceptor (TABLE 2). In extremely short H-bonds the interaction is mainly between two molecular orbitals and thus the fraction of coulombic interaction in the total interaction energy is small. In contrast, the longest H-bonds are close to dipole-dipole interactions since the orbital overlap is poor and most of the interaction energy is of coulombic origin. Thus, it can be stated that “H-bond” is often used as a general term for coulombic interactions in which part of the interaction energy comes from orbital overlap between an X-H antibonding orbital and an electron-rich full molecular orbital.

TABLE 2. Strength and type of interaction in hydrogen bonds.

	<b>Strong</b>	<b>Medium</b>	<b>Weak</b>
<b>Type of interaction</b>	mainly covalent	mainly coulombic	coulombic
<b>Bond length (Å)</b>	1.2–1.5	1.5–2.2	2.2–3.2
<b>Bond angle (°)</b>	175–180	130–180	90–180
<b>Bond energy (kcal/mol)</b>	14–40	4–15	<4

## 2.2 Brønsted Acids and Hydrogen Bond Donors in Noncovalent Activation of Electrophiles

The capability of Brønsted acidic compounds to lower the LUMO of carbonyls (C=O), conjugated C-C double bonds (C=C),<sup>51,52</sup> and imines (C=N)<sup>53</sup> has led to a plethora of new catalytic reactions.<sup>54</sup> The relation between the  $pK_a$  of an H-bond donor and the  $pK_{aH}$  of an H-bond acceptor separates the concepts of Brønsted acid and H-bond catalysis. In Brønsted acid catalysis the  $pK_a$  of a catalyst is significantly lower than the  $pK_{aH}$  of a reactant or an intermediate leading to full dissociation of the acid catalyst. In contrast, in the H-bond catalysis the  $pK_a$  of a catalyst is higher than  $pK_{aH}$  of a reactant or an intermediate, and catalyst stabilizes negative charges along the reaction coordinate without full dissociation.<sup>2</sup>

Brønsted acid catalysis can be further divided into two subgroups called general and specific acid catalysis. In general acid catalysis a proton is transferred from a catalyst to a reactant in a TOF determining transition state whereas in the specific acid catalysis a reactant is covalently bound to a proton before a TOF determining transition state. Thus, in specific acid catalysis the acid concentration affects the reaction rate only by increasing the equilibrium concentration of protonated intermediate and the acid catalyst performance cannot be observed through kinetic measurements.

In contrast to Brønsted acid catalysis, in the H-bond catalysis an H-bond stabilized anionic product is protonated only after a rate determining transition state by a non-catalytic proton source. Since the activity of H-bond catalysts does not rely on proton transfer, they are not, by definition, acid catalysts. The H-bond catalytic moiety may have ion-dipole or dipole-dipole interactions with the substrate in different states along the reaction coordinate, especially during complexation. However, the activation of substrate(s) towards the desired reaction should have orbital interactions between an occupied molecular orbital of the H-bond acceptor and  $\sigma^*$  of H-X bond in the H-bond donor.

Similarly to Lewis acid and Brønsted acid catalysts, H-bond catalysts are not limited to a single functional group and thus can be tuned to obtain optimal  $pK_a$ <sup>55</sup> and binding geometry (FIGURE 6) for the targeted reaction.<sup>56,57</sup> Examples of H-bond donors used in catalytic applications include ureas,<sup>58</sup> thioureas,<sup>59</sup> squaramides,<sup>60,61,62</sup> and chiral diols such as TADDOLs<sup>63</sup> and BAMOLs<sup>64</sup>. To explain and predict the catalytic activity of H-bond donors, spectrophotometric measurements have been used to analyze H-bonding and anion binding and to correlate interactions against catalyst structure.<sup>65,66</sup>

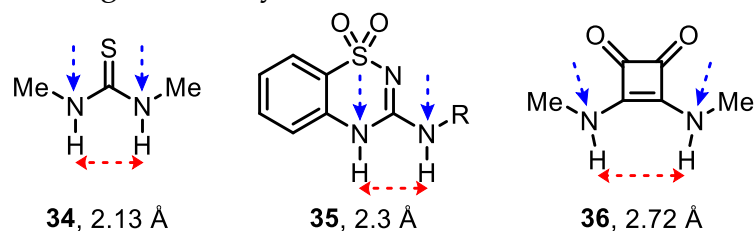


FIGURE 6. Directions of dipoles and distance of H-bond donors in reported H-bond catalytic moieties.<sup>57</sup>

Also, in the field of asymmetric Brønsted acid catalysis a major focus point has been on developing more acidic organic Brønsted acids capable of catalyzing reaction beyond the capabilities of previously available catalysts.<sup>54</sup>

H-bond catalysts have been found effective in many transformations where catalyst does not directly interact with the electrophile but instead stabilizes an anion formed during the catalyst cycle<sup>67,68,69</sup> or generates a chiral environment around nucleophile through solvation<sup>70</sup> (FIGURE 7). The Jacobsen group has developed several enantioselective catalytic systems relying on formation of oxocarbenium species through anion abstraction.<sup>71,72,73</sup> Similarly Mattson and co-workers have developed chiral silanediols as anion binding catalysts.<sup>74</sup>

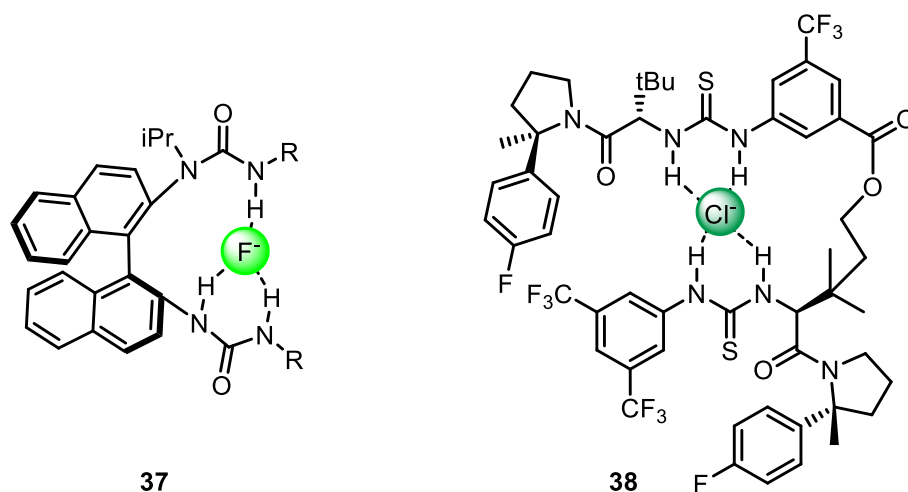


FIGURE 7. Examples of H-bonding in anion binding catalysis.

## 2.3 Basic Design Concepts of Catalysts for Enantioselective Reactions

### 2.3.1 Conceptualization of Catalyst Design

Often for communication purposes it is beneficial to conceptualize certain common features. Ways to describe homogeneous chiral catalyst structure have become established over the history of catalyst development. Typically, structure of catalysts for enantioselective transformations can be described with three distinct parts. The basic design remains the same in transition metal catalysts, Lewis-acid catalysts and organocatalysts. 1) Site for *primary interaction* with substrate facilitating the desired reaction. In the case of bifunctional catalysis two interactions activate substrates in conjunction. 2) *Chiral backbone* (also chiral scaffold or chiral platform are used) that creates asymmetry around the site of primary interaction with substrate. 3) Parts of catalyst that have *secondary weak interactions* with substrates to enhance enantioselectivity and preferably also reactivity.

### 2.3.2 Primary Interactions Between Catalyst and Substrates

Catalytic activity of a catalyst can be mostly attributed to the *primary interactions* that also define the nomenclature related to the catalyst. Examples of primary interactions include H-bonding,<sup>51</sup> deprotonation by a Brønsted base, coordination of  $\pi$  and non-bonding orbitals to Lewis acids,<sup>75</sup> and transition metal activation of C-H bonds.<sup>76</sup> Many electrostatic factors influencing behind binding of substrate to catalyst were discussed in chapter 2.1.

In the context of chemical catalysis, bifunctionality is used to describe simultaneous activation and spatial positioning of two substrates, such as a

nucleophile and an electrophile or diene and dienophile. Bifunctional catalysts have two functionalities that act in conjunction to activate substrates undergoing a chemical reaction.<sup>29,75</sup> Since the reactants need to be in a specific orientation at a specific distance for a reaction to occur, the design of the catalyst must promote such an orientation. High control over transition states through a preorganized electrostatic environment results in high chemo and enantioselectivity.<sup>77</sup> Although this organization of the reacting substrates has an entropic cost it reduces the free energy of the turnover determining transition state (TDTS).<sup>78</sup>

Since the first reports from the group of Takemoto,<sup>79</sup> bifunctional hydrogen bond (H-bond)-Brønsted base organocatalysis has gained significant attention among chemists. Due to its simple structure, easy synthesis, and general applicability, the original thiourea and tertiary amine-based catalyst is still an excellent benchmark for newly developed bifunctional H-bond organocatalysts. These features allow researchers to alter one or both functional groups to modulate the activity of bifunctional catalysts. Functions of the two moieties in Takemoto catalyst (**39**, FIGURE 8) can be described in the following way:

1. *H-bond donor moiety* activates and positions the electrophile through interaction between a polar heteroatom-hydrogen bond of the H-bond donor (electrostatic or  $\sigma^*$  orbital overlap depending on distance) and a non-bonding lone electron pair of an unsaturated heteroatom in the H-bond acceptor.<sup>51</sup>
2. *Brønsted basic site* deprotonates completely the nucleophile before or concertedly with the bond forming nucleophilic attack. The basicity should be high enough to be able to deprotonate the nucleophile generating an ion pair of the deprotonated anionic nucleophile and the protonated cationic catalyst.<sup>80</sup>

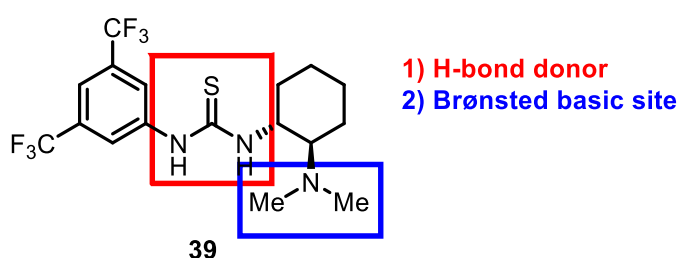


FIGURE 8. Activity of Takemoto catalyst **39** is results in simultaneous function of thiourea H-bond donor moiety and a tertiary amine Brønsted base.

### 2.3.3 Chiral Backbone in Enantioselective Catalysts

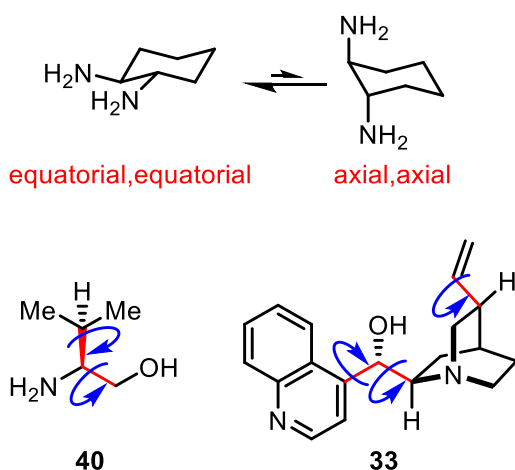
*Chiral backbone* generates the chiral environment around the primary interaction and together with the primary interaction allows the substrates to be correctly positioned for bond formation in the transition state. Catalysts containing rotatable bonds can in theory exist in an infinite number of conformations. However, certain well-established preferences exist which are based on steric



and electronic properties of the molecules. Below are listed most relevant for this study.

1. Allylic 1,3-strain is an interaction governing conformations in vicinity of double bonds in open-chain molecules<sup>81</sup> as well as in cyclic molecules.<sup>82</sup>
2. Substituents of saturate cyclic structures favor equatorial conformations over axial.<sup>44</sup>
3. Branched alkyl chains favor staggered conformations.<sup>83</sup>
4. Conformational preferences of  $\beta$ -peptoids can be engineered by side chain structure.<sup>84,85,86</sup>

Catalyst conformational robustness is essential for enantioselective catalysis. However, conformational predictability is not synonymous with rigidity. Predictability can be obtained through rigid cyclic structures or open-chain structures with high conformational preference. In cyclic structures the conformational changes through bond rotation are governed by energy differences between axial orientation of substituents versus equatorial orientation (SCHEME 7).



SCHEME 7. Conformational freedom of few common moieties in H-bond organocatalysts.

Additionally, conformations of flexible molecules can be stabilized by intramolecular attractive interactions such as H-bonds,<sup>87</sup> dispersion interactions,  $\pi$ - $\pi$  interactions and dipole-dipole interactions.<sup>88</sup> However, weakest of these attractive interactions can be easily overcome by torsional strain required for the attractive interaction.<sup>89</sup>

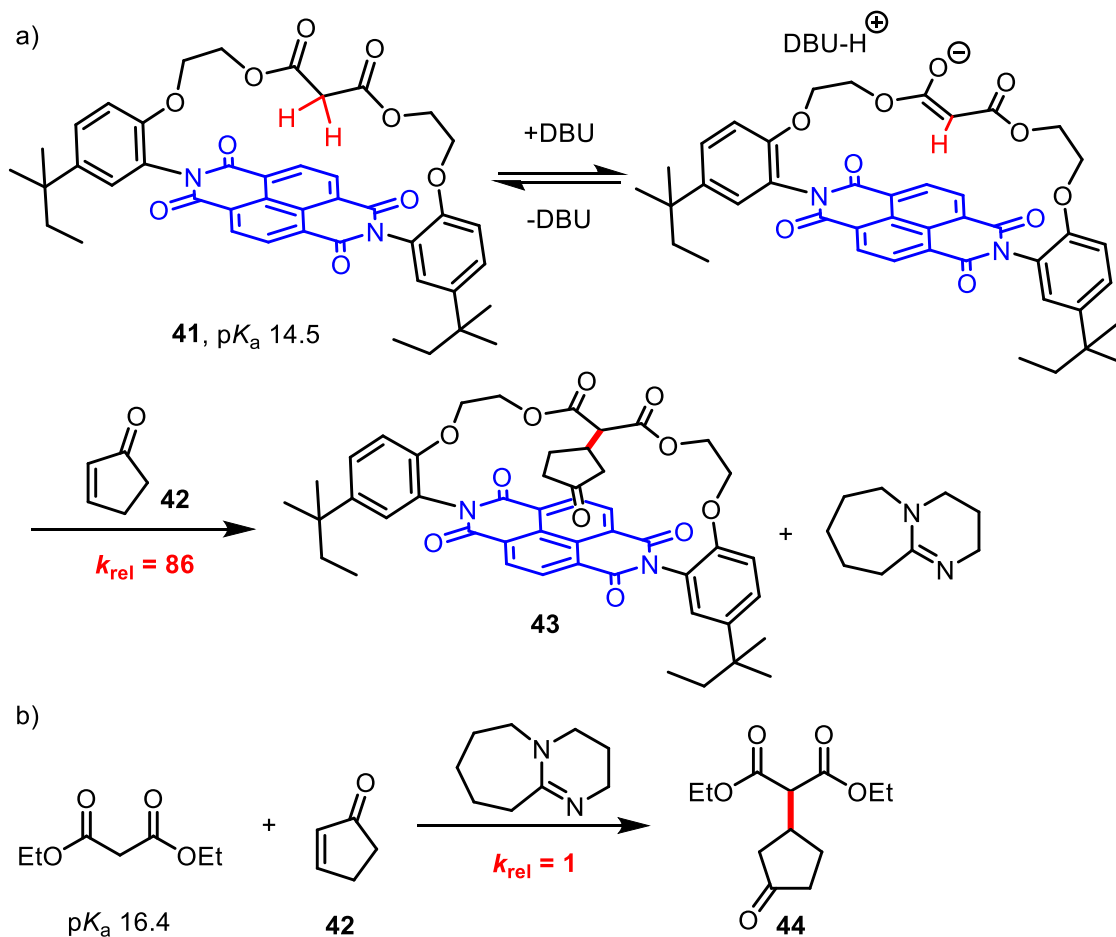
### 2.3.4 Secondary Interactions Between Catalyst and Substrates

*Secondary interactions* contribute to the binding of catalyst (ligand) and substrates in conjunction with the *primary interaction* leading to increased concentration of catalyst substrate complex. Additionally, the secondary interactions can lower the transition state energies by stabilization of partial charges formed in the reaction (FIGURE 3). In principle, distinction between primary and secondary interactions can be elusive if rate acceleration attributed to a single secondary

interaction is high. Many of the proposed secondary interactions are based on dispersion interactions and induced dipoles in aromatic groups. Such interactions include  $\pi$ - $\pi$ ,<sup>90,91</sup> cation- $\pi$ <sup>92,93</sup>, anion- $\pi$ <sup>94</sup> interactions and London dispersion<sup>95</sup>.

Wagner and Schreiner discuss in their article of London dispersion the fine balance between positive dispersion interactions and repulsive steric effects. As described in TABLE 1, the energy of dispersion interactions is highly distance dependent. For this reason, some degree of flexibility helps to maximize catalyst (ligand)-substrate dispersion interactions. Experimental quantification of individual attractive interactions is challenging but conformational preferences can be studied both experimentally and computationally.<sup>95</sup> Due to the challenging analysis of attractive interactions, simplified models, such as so called quadrant model for  $C_2$ -symmetric ligands, have been developed to explain observer selectivity trends.<sup>2</sup> However, more recently the focus has been devoted to the studies of steric bulk as a repulsive factor *versus* attractive dispersion interactions.<sup>96, 97</sup> As a result the crucial role of ligand-substrate attractive interactions in asymmetric transition metal catalysis has been discovered.<sup>98,99</sup>

Matile and co-workers have studied Brønsted base catalysis and anion- $\pi$  interaction in malonate anion stabilization (SCHEME 8) by a covalently bound malonate and polyaromatic  $\pi$ -system. They found that the stabilization of the deprotonated malonate anion by anion- $\pi$  interaction lowered the malonate  $pK_a$  by 1.9 units and increased the reaction rate 86-fold compared to diethylmalonate.<sup>91</sup> In a similar polyaromatic system, anion- $\pi$  interaction was found to be the enabling factor in a Kemp elimination reaction with a naphthalenediimide carboxylate catalyst.<sup>100, 101</sup> These reports highlight the potential of secondary interactions to increase the catalyst performance through the understanding of *secondary* substrate-catalyst *interactions*.



SCHEME 8. Rate acceleration by enolate and transition state stabilization in a Michael reaction.

When discussing electrostatic interactions, one must keep in mind that in practice these interactions are always susceptible to effects from surrounding functional groups, solvents<sup>102</sup>, and even external electric fields<sup>103</sup>. In systems consisting of even few atoms the complexity of intramolecular and intermolecular interactions, also including intramolecular orbitals interactions, become too high for human comprehension. With the advances in computation power and force fields, computational analysis has validated its role as a tool for quantification of the forces governing for example solution state conformations and catalyst substrate binding interactions.

## 2.4 Experimental Kinetic Methods Help to Reveal Reaction Mechanisms

### 2.4.1 General Considerations in Experimental Kinetic Measurements of Organocatalytic Reactions

Conducting experimental kinetic measurements requires significant amount of preparative thought and work. Before any experimental work is performed the purpose of kinetic experiments need to be clearly defined. Do we know what are the properties of substrates, solvent and catalyst, and the factors in reaction conditions that allow the reaction to take place? What do we already know from previous reports or general reactivity patterns which can be considered valid for the studied reaction? What information is missing and is considered essential? In many cases, different complementary approaches such as experimental kinetic measurements and computational methods can provide the missing data and support for rationalization of observed reactivity and selectivity.

Second, we need to find the best way to obtain the necessary data with good accuracy and acceptable effort with the available resources. We also need to secure access to the required substrates and equipment. It is often enough to use only few carefully selected methods to reveal missing details of the reaction mechanism. Moreover, often there is no individual experiment that could provide *all* required information in a single experiment and, on the other hand, many experiments can provide essentially the same information. In the worst case, wrong choice of experimental method can lead to vast amounts of useless data and lost time and money. Thus, the selection of most suitable experimental methods is of utmost importance.

We also need to confirm that the reaction is reproducible, robust, and selective. Poor selectivity of the studied reaction poses two major challenges in kinetic studies: 1) observed rate is a sum of the desired reaction and all side reactions with different kinetics consuming starting materials 2) the observed rate of product formation is the sum of all reaction pathways leading to the product. Thus, it is important to distinguish or eliminate competing reaction pathways and side reactions.<sup>2</sup>

### 2.4.2 Factors for Selecting Experimental Methods

A vast majority of organocatalytic reactions are addition reactions to double bonds. Typically, these reactions occur between two substrates mediated by the catalyst in solution phase and the initial concentrations of all components are known. This situation is a good foundation for kinetic measurements if a suitable measurement technique can be identified. A measurement technique capable of determining both substrate and product concentrations at any given time after initiation of reaction is essential for obtaining accurate kinetic data.<sup>104</sup> In addition to substrate and product concentrations, observation and identification of short-

lived intermediates and catalyst complexes can provide the missing clue in solving the reaction mechanism.<sup>105,106</sup>

Characteristics of the studied reaction can dictate which measurement techniques provide accurate and true results. Below are listed a few important considerations when selecting the measurement technique for a batch reaction. This list is not intended to be exhaustive but is rather intended to provide an overview of factors to be accounted in the selection.

1. *Reaction heat.* In highly exothermic reactions the main consideration is if the reactor setup can ensure sufficient heat transfer during reaction. As an example, the temperature control inside an NMR instrument is limited and the temperature of the reaction mixture cannot be controlled directly. Thus, the control of strongly exothermic reactions is poor in an NMR instrument. On the other hand, measurement techniques relying on probes that are introduced into bench scale reactions, such as ReactIR and other spectroscopic measurements, often provide excellent control over reaction temperature. Calorimetry excels in exothermic and highly selective reactions as the released reaction heat can often be directly converted into conversion by a calorimeter.
2. *Reaction temperature.* Very high and very low reaction temperature also present limitations to suitable measurement techniques. Especially reactions conducted in reflux require sufficient scale to be performed. The same limitations apply for high and low temperatures as for highly exothermic reactions. Additional challenge for spectrometric measurements in reflux conditions comes from inhomogeneity of reaction mixture due to boiling.
3. *Viscosity of reaction media.* Highly viscous reaction mixtures require efficient mixing to ensure adequate mass and heat transfer during the reaction. In many cases proper mixing can be achieved only by mechanical stirring which is available for reactions in >20 mL scale.
4. *Heterogeneity of the reaction mixture.* Similarly to highly viscous reaction mixtures, heterogeneity presents a challenge of sufficient mass transfer to ensure that it does not limit the reaction rate. In addition, homogeneity can cause challenges in spectroscopic measurement techniques due to fouling of the probe.
5. *Detection and identification of intermediates.* When kinetic measurements are performed the identity of main product is known. However, the reaction may proceed via an unknown intermediate that has remained undetected. Measurement techniques capable of detecting and more importantly identifying unknown intermediates include <sup>1</sup>H NMR and GC-MS. <sup>1</sup>H NMR has proven to be a superior method by allowing the identification of unexpected intermediates.<sup>105,106</sup>
6. *Pressure reactions.* In the case of highly selective reactions progressing through well documented intermediates, such as heterogeneous

hydrogenation of nitroaromatics, reaction progress can often be adequately monitored by indirect phenomena, such as hydrogen consumption in an autoclave or heat formation in a calorimeter.

7. *Reaction time and resolution of data.* In fast reactions the measurement frequency must be sufficient to provide several datapoints during the reaction. In such cases, on-line measurement is mandatory to obtain high resolution data. On the other hand, if the studied reaction is slow and reaction conditions do not allow direct observation of product and substrates, reaction rates can be measured by taking aliquots from reaction mixture for off-line analyses such as GC, HPLC and NMR.
8. *Reaction Scale.* Certain measurement techniques are available only for small-scale or gram-scale reactions. If only small amounts of starting material available, such as for deuterated substrates, or catalyst not available for large scale reactions on-line  $^1\text{H}$  NMR and off-line measurements such as GC and HPLC are best options. Use of on-line probes often requires >20 mL of reaction mixture volume and thus are not compatible with small scale reactions.

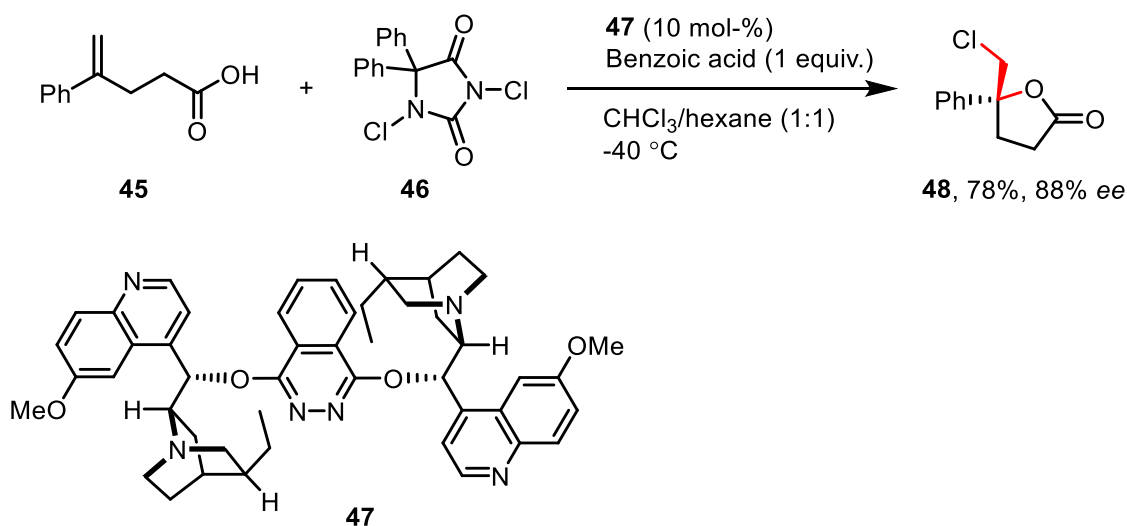
### 2.4.3 Reaction Order

The determination of reaction order and the use of reaction progress kinetic analysis (RPKA) in the research of small-molecule catalysis has been promoted by the Blackmond group. Reaction rate dependency from initial substrate and catalyst concentrations is a powerful way to analyze reaction kinetics as it can reveal catalyst saturation and other deviations from ideal reaction kinetics. Indeed, such approaches have been systematically and successfully used in enzymatic catalysis studies.<sup>104</sup> In an ideal case, first order kinetics in a two component organocatalytic reaction would result in equation 9.

$$\text{rate} = k[S1]^1[S2]^1[\text{catalyst}]^1 \quad (9)$$

The RPKA affords a practical view of the limiting factors in the overall reaction rate but it fails to give detailed information on individual events in a catalytic cycle. Examples of successful use of a simplified RPKA in reactions catalyzed by small molecules include an organocatalytic chlorolactonization revealing a catalyst-substrate ion pair as the catalyst resting state (SCHEME 9).<sup>107</sup> In this case the carboxylic acid starting material fully saturates the catalyst by forming an ion pair. The RPKA methodology was able to show that acid-base reaction is fast and precedes the TDTS by the indication that rate is zeroth order for the carboxylic acid **45** (Equation 10). However, it was not able to show which transition state is TOF determining. The key indication was obtained through other kinetic measurements such as linear free-energy relationships and kinetic isotope effects.

$$\text{rate}(\text{chlorolactonization}) = k_{\text{obs}}[\mathbf{45}]^0[\mathbf{46}]^1[\mathbf{X}]^1 \quad (10)$$



Scheme 9. Organocatalytic enantioselective chlorolactonization reaction studied with RPKA.

#### 2.4.4 Kinetic Isotope Effects

Although focusing only on organometallic transformations, an excellent review from Gómez-Gallego and Sierra describes the theory and ways to exploit kinetic isotope effects (KIEs) in study of reaction mechanisms.<sup>108</sup> Kinetic isotope effects can be divided into four classes, *primary* and *secondary kinetic isotope effects*, *equilibrium isotope effect* and *solvent isotope effect*. The classes differ in the information they provide and the magnitude of the observed kinetic isotope effect. The most studied isotope effects are those of H/D which have the largest relative mass change, as the weight of the atom is doubled from 1.000 to 2.000 g/mol. Weight difference of an atom in a covalent bond affects the zero-point energy of the bond which affects the energy profile of a reaction involving that bond or occurs in its vicinity. Kinetic isotope effects can be measured also for heavier atoms such as <sup>13</sup>C but the magnitude of KIEs are small. This weakness can be overcome by exploiting the natural abundance of <sup>13</sup>C.<sup>109</sup> Successful examples can be found also in enantioselective organocatalysis.<sup>110</sup>

1° KIE reveals if the atom is transferred in the TDTS or product determining transition state, in other words, if bonds to H/D are broken or formed. The two origins of KIE can be separated by experiment design. Intra- and intermolecular competition experiments should be avoided if the obtained KIE is used solely in determining the TDTS of the studied reaction.<sup>111</sup> In FIGURE 9 the zero-point energy of the deuterated compound ( $ZpE_D$ ) is lower than the zero-point energy of non-deuterated compound ( $ZpE_H$ ). Another variable affecting the kinetic isotope effect is the difference between transition state energies of TOF determining steps  $\Delta G_{ZpE}(\text{TS})$ . If the activation energy  $\Delta G_{ZpE}(\text{TS})$  of deuterated compound is larger than activation energy of non-deuterated, the reaction rate

( $k_D$ ) of deuterated product is lower than rate of non-deuterated product ( $k_H$ ), resulting in  $KIE > 1$ . In the opposite case, when reaction of deuterated substrate is faster than of non-deuterated substrate, an inverse kinetic isotope effect ( $KIE < 1$ ) is observed.

$$KIE = \frac{k_H}{k_D} \quad (11)$$

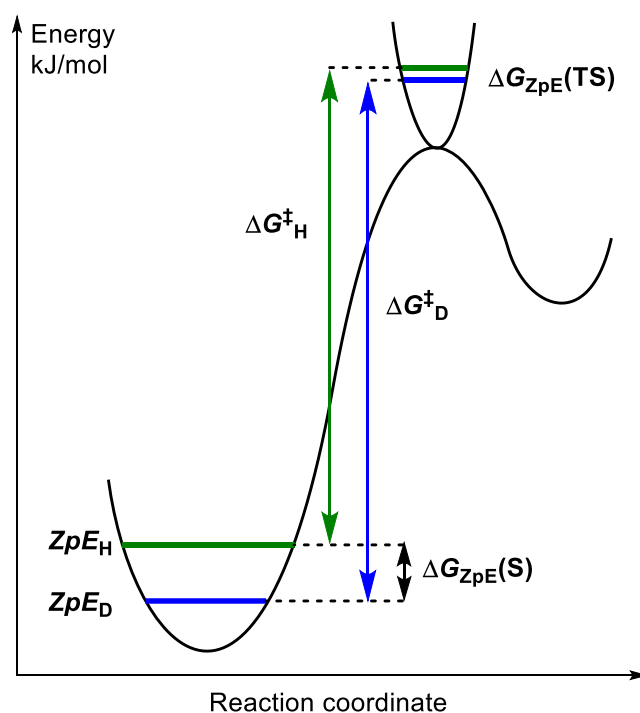
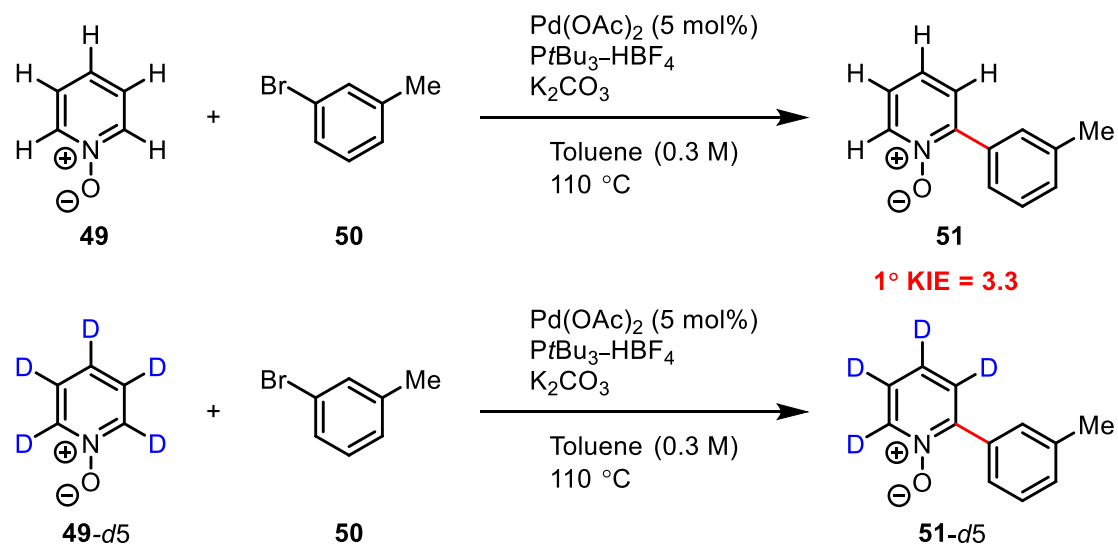


FIGURE 9. Energy diagram of a normal primary kinetic isotope effect.

The magnitude of normal  $1^\circ$  KIEs can vary from 1 to  $>10$  depending on several factors through the reaction coordinate. The simplified concept of transition state  $ZpE$  difference in KIE quantification has been recently challenged and more consideration of the effect of all intermediates on KIE is suggested.<sup>112</sup> Moreover, the importance on events preceding the TDTS, such as substrate catalyst coordination, have been recognized early in the research of enzymatic mechanisms by kinetic isotope effects.<sup>113,114</sup>  $1^\circ$  KIEs have been most notably utilized in mechanistic studies of several C-H activation reactions, such as palladium(II) acetate catalyzed coupling of pyridine *N*-oxides and aryl bromides (SCHEME 10).<sup>108,115</sup>





SCHEME 10. Selected example of primary kinetic isotope effect in catalytic reaction.

$2^\circ$  KIE is based on hybridization change in the heavy atom to which H/D is bonded and, in contrast to  $1^\circ$  KIE, bond to H or D is not broken. Thus,  $2^\circ$  KIE reveals if hybridization of adjacent atom is changed.  $2^\circ$  KIE has been proven helpful in determining mechanisms of addition reactions to double bonds. In double bonds the atoms are  $sp^2$  hybridized and during the addition reaction the double bond transforms to a single bond. In this process the hybridization changes to from  $sp^2$  to  $sp^3$  and the bond geometry from trigonal planar to tetrahedral. This change results in a negative secondary kinetic isotope effect if it occurs in the TDTS of the reaction (FIGURE 10). Reaction to the opposite direction, an elimination reaction, would result in a positive secondary kinetic isotope effect as the hybridization changes from  $sp^3$  to  $sp^2$ .

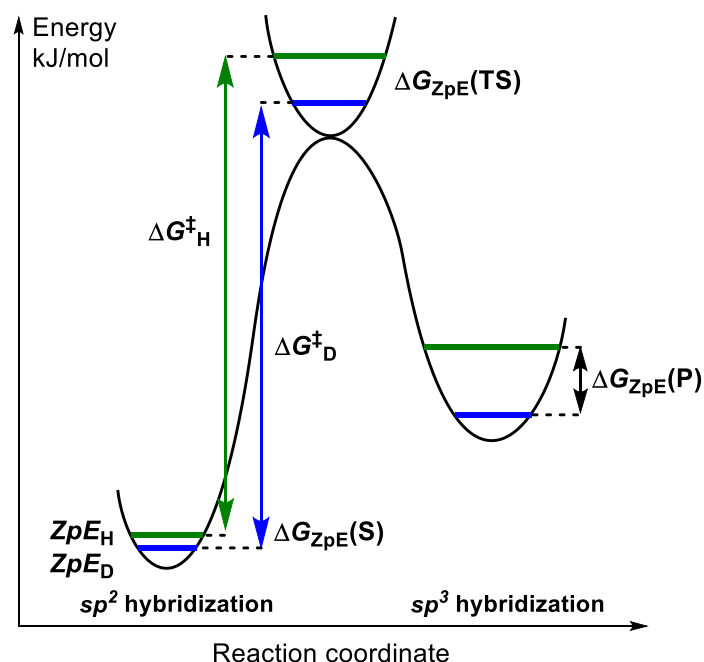


FIGURE 10. Energy diagram of an inverse secondary kinetic isotope effect.

Equilibrium isotope effect in turn affects the rates of reversible reactions resulting in altered equilibrium constant  $K_{eq}$ .

$$K_{eq} = \frac{k_H^{RP} / k_D^{RP}}{k_H^{PR} / k_D^{PR}} \quad (12)$$

Solvent isotope effect is observed when deuteration, for example protic solvent, affects the reaction rate. When studying solvent isotope effects in protic solvents, the H/D scrambling of solvent and substrate can result in an apparent solvent isotope effect although a deuterated substrate is generated in situ. Other solvent isotope effects arise from differences in solvation of substrates affecting relative energies of TDS and TDI. In all studies involving kinetic isotope effects, unwanted H/D scrambling must be avoided since conclusive interpretation of obtained data becomes extremely complex.

#### 2.4.5 Linear Free Energy Relationships

Linear free energy relationships (LFER) can be used to correlate observed reactivity or selectivity against structure related parameters that have been determined from a model reaction.<sup>116</sup> In case such correlation is not observed the factor likely does not influence the reaction performance. One of the most widely used, easily conducted, and best understood LFERs is *Hammett relationship*. It reveals how electronic substituent effects change the reaction rate of aromatic substrates. Hammett constants have been derived from 39 reaction types in which reaction rates were monitored.<sup>117</sup> Also more specific variations of Hammett, such as Taft equation, have been developed.<sup>118</sup>

## 2.4.6 Computational Methods Complement Experimental Results

Although this thesis focuses on experimental methods, often experimental methods are not enough to solve the fine details of a reaction mechanism. In many occasions, computational methods, especially DFT calculations, have provided additional insight to reaction mechanisms that are beyond the limitations of experimental measurements.<sup>119</sup> With sufficient initial information of reaction mechanism the transition states and intermediates can be identified with computational methods and their relative energies quantified. The challenge with computational studies of asymmetric catalysis is the often relatively small energy differences between competing pathways ( $\Delta G$ , FIGURE 3) leading to different enantiomers. At 0 °C, a  $\Delta G$  of 7.5 kJ/mol affords the product in 93% *ee*, whereas a  $\Delta G$  of 12.6 kJ/mol would afford the product in a much more impressive *ee* of 99.2%.<sup>2</sup> This difference in  $\Delta G$  can be explained by only one amide-amide H-bond or anion- $\pi$  interaction in polar organic solvent.<sup>46</sup>

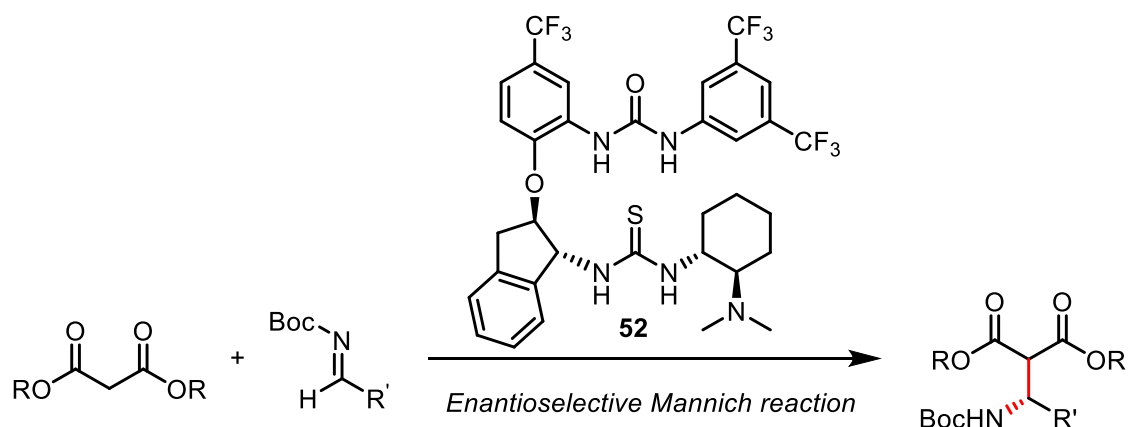
If the number of clearly identified non-covalent interactions is the same between two competing pathways, several weak interactions, such as dispersion interactions between alkyl groups, can provide an explanation for the observed selectivity. Cheong *et al.* describe in their 2011 review the deficiencies of DFT calculation with commonly used functionals especially for quantifying weak interactions. However, more recently weak interactions, such as dispersion interaction between substrate and ligand, have been proposed to explain observed trends in selectivity.<sup>120</sup>

## 3 RESULTS AND DISCUSSION

### 3.1 Aim of the Work

Although enantioselective addition reactions to C-N double bonds<sup>53</sup> and activation of  $\beta$ -dicarbonyl nucleophiles<sup>80,121</sup> are well documented, and first mechanistic studies of uncatalyzed three-component Mannich reactions were performed in 1960 by Cummings and Shelton,<sup>122</sup> to our knowledge mechanisms of organocatalytic asymmetric Mannich reactions have not been studied experimentally with  $\beta$ -dicarbonyl nucleophiles. Additionally, experimental kinetic studies for reactions catalyzed by bifunctional H-bond catalysts are scarce and thus suitable experimental procedures for organocatalysis needed to be established.

The first report of a catalyst capable of promoting Mannich reaction of aliphatic imines in high enantioselectivity with low catalyst loading was published by the Pihko group in 2012.<sup>123</sup> In this report the factor allowing the use of aliphatic imines as electrophiles was not found. The work described in this dissertation is built on the work of Dr. Nicholas Probst, partly published in reference 123 (SCHEME 11), while studying ways to improve H-bonding ability of bifunctional catalysts. The structure of catalyst **52** drew inspiration from the research done in the group of Martin Smith on protein-mimicking H-bond networks in asymmetric catalysis<sup>124</sup> and partly on the previously published bifunctional thiourea Brønsted base catalysts in malonic ester activation.<sup>125,126</sup> Many catalytic methods in Mannich reactions are limited to using non-enolizable imines as substrates (SCHEMES 4-6) or require high catalyst loading.<sup>127</sup> This limitation is likely caused by a rapid isomerization of imines to enamides in acidic conditions.



SCHEME 11. General scheme of enantioselective Mannich reaction studied in reference 123.

The research described in Publications I and II was aimed at expanding the utility of the discovered catalyst family that is compatible with enolizable imines in Mannich reactions. Publication I focuses on the exploring the limits of nucleophile activation while maintaining excellent selectivity observed with malonic esters.

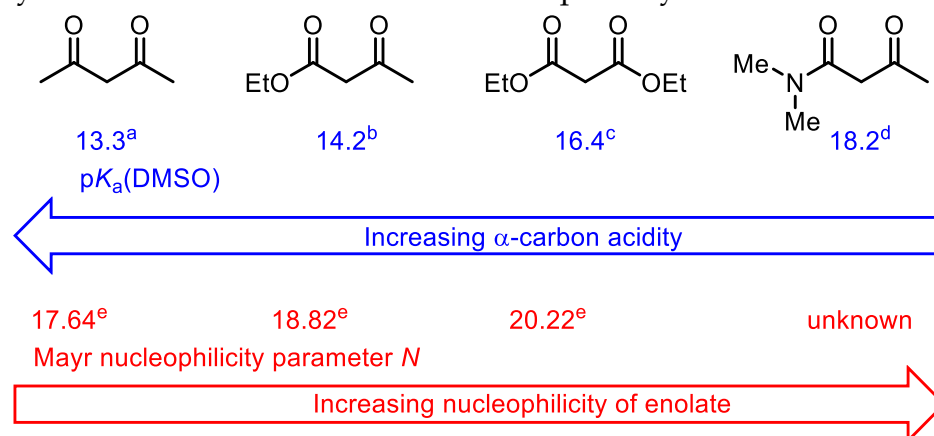
Publication II also explores ways to experimentally study the reaction mechanism of the reported Mannich reaction catalyzed by the developed catalyst family. However, the main objective of this publication was to find an explanation for observed distinctive reactivity with aliphatic imines compared to other, superficially similar, catalysts. In this publication the author contribution was limited to the experimental work and manuscript preparation so only most essential discussion on computational results is covered in this thesis.

Publication III focuses on determining catalyst folding as salts of selected organic and inorganic acids. This information is essential in creating a foundation for potential future work in asymmetric anion binding catalysis by increasing the understanding of catalyst conformational preferences relative to anion shape and size. In this publication the author contribution was mainly on solid state structure elucidation by solving 8 out of 14 published structures and manuscript writing. Thus, detailed discussion about solution-state structures and computational analysis is omitted.

### 3.2 Expanding the Scope of Enantioselective Organocatalytic Mannich Reactions<sup>1</sup>

The use of various structurally diverse aliphatic imines in organocatalytic asymmetric Mannich reactions with malonate esters was demonstrated in Pihko group already in 2012.<sup>123</sup> However, in this paper only malonate esters were used as nucleophiles and there was no proof of the generality of the catalyst with other nucleophiles. The reaction depicted in SCHEME 11 was chosen as a starting point for expanding the scope of compatible nucleophiles.

A hypothesis of reactivity was formulated from previous observations of notable reactivity differences between  $\beta$ -dicarbonyl compounds and the correlation with the  $pK_a$  (SCHEME 12) at the  $\alpha$ -carbon in  $\alpha$ -unsubstituted  $\beta$ -dicarbonyl and related compounds.<sup>128, 129</sup> It was expected that reactivity,  $pK_a$ <sup>130,131,132</sup> and Lewis basicity correlate also in this case as depicted in SCHEME 12. Previous reports have established that  $\alpha$ -substitution increases the  $\alpha$ -proton  $pK_a$  by *circa* two units in DMSO<sup>133</sup> and increases the nucleophilicity by 3-5 fold.<sup>134</sup> Additionally, from the study of cyclic structures, it is known that strain from an endocyclic double bond increases the nucleophilicity of the enolate.



SCHEME 12. Properties of  $\beta$ -dicarbonyl compounds. a) see ref. 133, b) see ref. 132, c) see ref. 130 d) see ref. 131, e) see ref. 129.

During the preparation of Publication I, it was quickly observed that  $\alpha$ -unsubstituted  $\beta$ -ketoesters are excellent nucleophiles with regards to reaction rate. On the other hand, reactions with catalysts **52** and **53** afforded poorer enantioselectivities than with less reactive malonate esters. High reaction rate but unacceptable enantioselectivity gave us an excellent starting point for catalyst modification to improve enantioselectivity. From prior published work from other research groups it is known that Lewis acid complexes<sup>135,136</sup> and Brønsted acids<sup>137</sup> activate imines sufficiently towards nucleophilic additions even without nucleophile activation. However, increased Brønsted acidity of the H-bond donor could jeopardize the stability of the aliphatic imines which are stable in basic conditions but readily isomerize to enamines in acidic conditions. With these aspects in mind we decided to focus on varying the Brønsted basic tertiary amine. The modular design of the catalyst allowed us to quickly obtain a modified catalyst **54** (FIGURE 11) with bulkier Brønsted base which was hypothesized to improve enantioselectivity without causing significant rate deterioration.

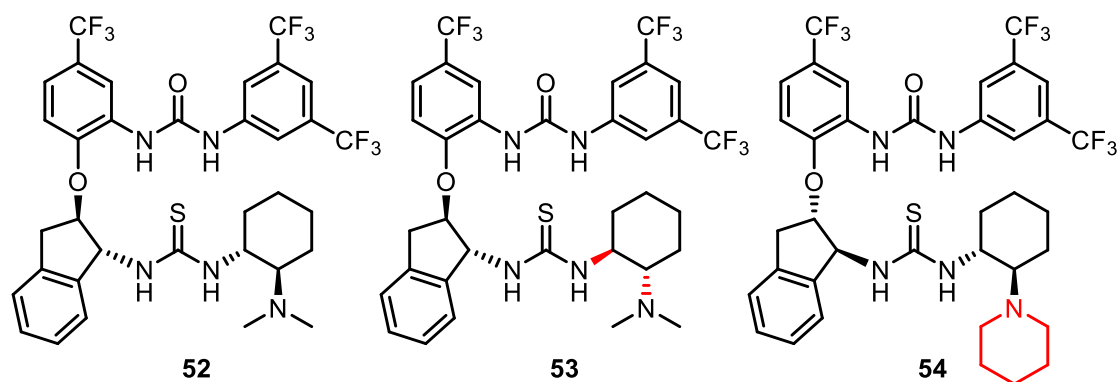


FIGURE 11. Catalysts studied in enantioselective Mannich reactions with  $\beta$ -ketoesters.

In addition to the published results, various ways to improve the basicity of the catalyst were studied. Inspired by Dixon and co-workers,<sup>138</sup> Feng and co-workers,<sup>139</sup> and Lambert and Bandar<sup>140</sup>, especially guanidine bases were identified as potential targets. However, all attempts to incorporate so called superbases, such as tetramethyl or tetracyclohexyl guanidine, into the catalyst design failed. The incorporation of a superbase was expected to result in a zwitterionic catalyst molecule by the deprotonation of the thiourea and favoring the nucleophile binding and deprotonation.

Nearly all screened  $\beta$ -ketoesters (**55**) provided good yields and selectivity with an acceptable reaction rate (TABLE 3) when using catalyst **54**. We were even able to reduce the catalyst loading to 1 mol-% when aromatic  $\beta$ -ketoesters were used and reduce imine excess by 50%. However, these conditions were not suitable for all substrates and an outlier was identified that did not afford any Mannich product. When *t*Bu-acetoacetate (**55b**) was subjected to the standard reaction conditions, only unreacted starting materials were observed. Since the electronic properties of the *t*Bu-acetoacetate are similar to other  $\alpha$ -unsubstituted aliphatic  $\beta$ -ketoesters, the only plausible hypothesis is that steric factors inhibit formation of ternary complex and simultaneous activation of both substrates. Additionally, distinct reactivity was observed when cyclic  $\beta$ -ketoester was used (**55f**). Two  $pK_a$  units lower acidity and higher nucleophilicity of  $\alpha$ -substituted  $\beta$ -ketoesters compared to  $\alpha$ -unsubstituted  $\beta$ -ketoesters, steric hindrance at  $\alpha$ -carbon and the observation of poor selectivity might suggest that a loose binary complex of catalyst and  $\beta$ -ketoester is formed and the C-C bond formation occurs without strong imine activation.

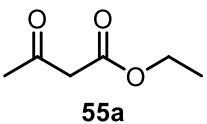
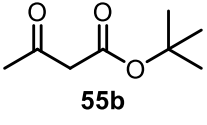
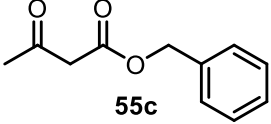
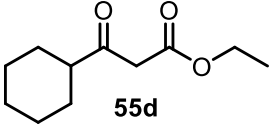
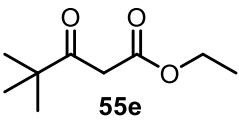
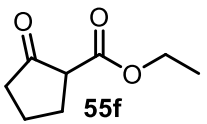
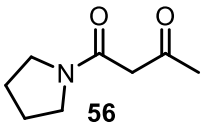
Tertiary  $\beta$ -ketoamides, such as **56**, are known to be more difficult to activate than  $\beta$ -ketoesters by Brønsted bases (SCHEME 12).<sup>141</sup> When pyrrolidine derived  $\beta$ -ketoamide was subjected to the reaction conditions no product was formed.<sup>142</sup> Constantineux and co-workers observed over 10-fold rate difference between tertiary amides and secondary amides in enantioselective conjugate addition reactions to nitroolefins catalyzed by bifunctional H-bond-Brønsted base catalysts.<sup>141</sup> Since the electronic properties do not explain the significant rate difference, allylic strain is more likely lowering the reactivity of tertiary  $\beta$ -ketoamides as well as  $\gamma$ -*t*Bu substituted  $\beta$ -ketoester **55e** (TABLE 3, Entry 5).

Constantineux and co-workers also demonstrated that  $\beta$ -ketoamides afford conjugate addition products in high distereoselectivity.<sup>141</sup> Unfortunately, these results were not available when conducting the experimental work for Publication I and we could not incorporate secondary  $\beta$ -ketoamides in this study. The use of  $\beta$ -ketoamides derived from primary amines could have afforded the Mannich reactions in higher diastereoselectivity than  $\beta$ -ketoesters. Due to the applicability of  $\beta$ -ketoamides derived from primary amines the explanation for failed reaction with pyrrolidine derived  $\beta$ -ketoamide can be a steric crowding upon enolization (FIGURE 12).



TABLE 3. Selected results from expanding nucleophile scope in asymmetric Mannich reaction.

Reaction scheme showing the asymmetric Mannich reaction of a chiral auxiliary (55 or 56) with an aldehyde (57) to form a chiral Mannich base (58a-f). The reaction conditions are Catalyst **54** (3 mol%), Na<sub>2</sub>SO<sub>4</sub>, CH<sub>2</sub>Cl<sub>2</sub> (0.3 M), 0 °C.

Entry	Substrate	Reaction time (h)	Yield (%)	Enantiomeric ratio ( <i>er</i> )
1	 <b>55a</b>	6	90	99:1
2	 <b>55b</b>	no reaction	-	-
3	 <b>55c</b>	4	94	98:2
4	 <b>55d</b>	10	92	99:1
5	 <b>55e</b>	36	82	91:9
6	 <b>55f</b>	8	97	74:26
7	 <b>56</b>	no reaction	-	-

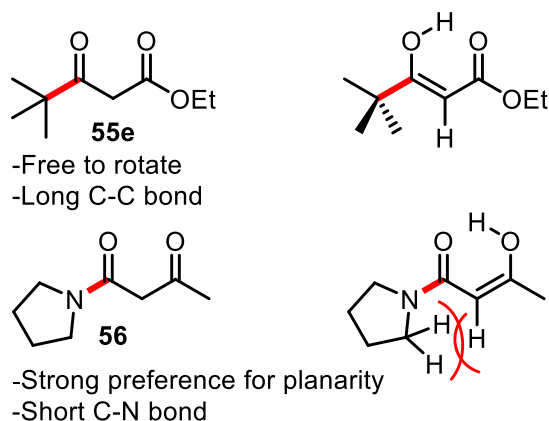
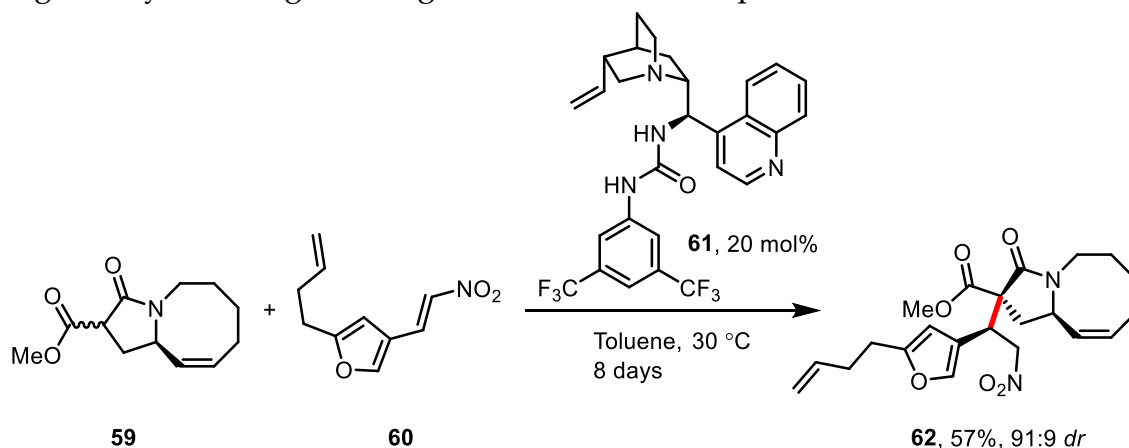


FIGURE 12. Hypothesis for failed application of pyrrolidine derived  $\beta$ -ketoamide **56** versus sterically challenging  $\beta$ -ketoester **55e**.

Despite the reactivity lowering effect of tertiary amides and  $\alpha$ -substitution, Dixon and co-workers were able to demonstrate the utility of bifunctional organocatalysis in the total synthesis of (-)-Nakadomarin A (SCHEME 13), albeit high catalyst loading and long reaction time was required.<sup>143</sup>



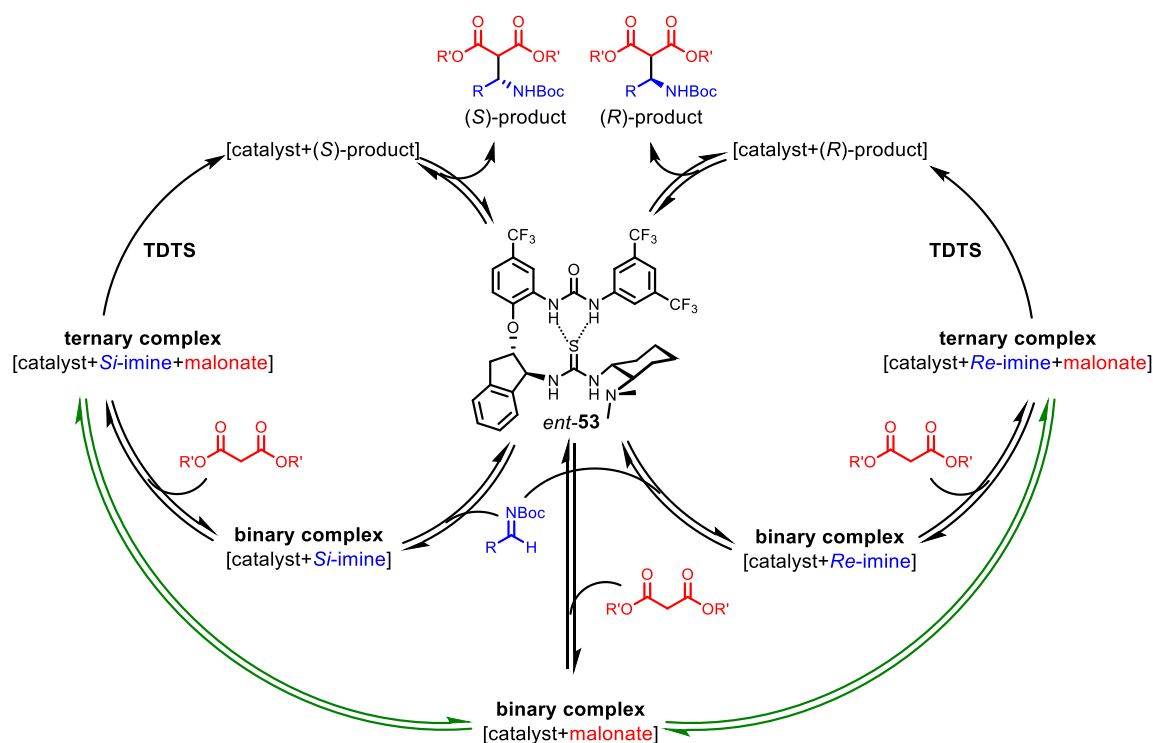
SCHEME 13. Diastereoselective organocatalytic generation of the key quaternary stereocenter in (-)-Nakadomarin A total synthesis.<sup>143</sup>

### 3.3 Understanding the Mechanism of Mannich Reactions Catalyzed by Bifunctional Organocatalysts<sup>II</sup>

#### 3.3.1 The Approach

Based on our previous studies and reports of reaction mechanisms catalyzed by bifunctional organocatalysts, a hypothetical reaction mechanism was formalized (SCHEME 14). However, we were missing definitive evidence of substrate binding and C-C bond formation, and the main factors behind observed high enantioselectivity. The hypothetical catalytic cycle consists of sequential

reversible binding of substrates (malonate and imine) to form first a binary complex of catalyst and one substrate which would form a ternary complex of catalyst and both substrates. Very rapid C-C bond formation after ternary complex formation would essentially mean that the ternary complex formation is irreversible.



SCHEME 14. Initial hypothesis for catalytic cycles of enantioselective Mannich reaction leading to both enantiomers.

Several experimental methods to provide evidence to support reaction mechanism hypotheses are described in Chapter 2.4. Most of the methods can provide insight into formation or breaking of covalent bonds but formation and breaking of non-covalent bonds such as H-bonds are more difficult to observe. At the beginning of the studies we were not able to say if the formation of the ternary complex or the C-C bond formation limits the reaction rate. In the end, these steps can be influenced by the catalyst design and thus it is a key information in the process of developing more efficient catalysts. We expected to see a clear Hammett relationship if the C-C bond formation limits the turnover rate. Additionally, results from other kinetic experiments, such as significant 2° KIE, could support C-C bond formation as the turnover rate limiting step.

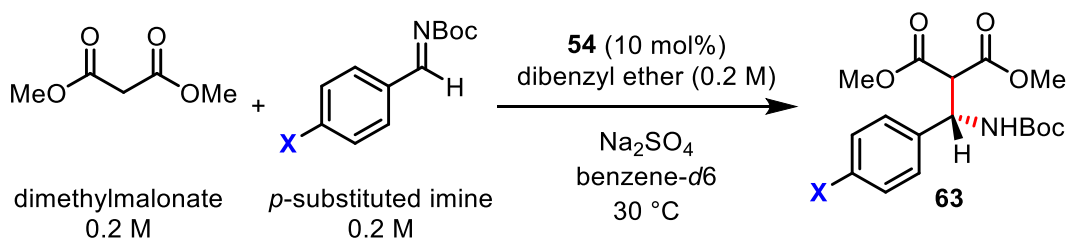
### 3.3.2 Key Findings of Kinetic Studies

First, to test the hypothesis of turnover rate limiting C-C bond formation in a model reaction (SCHEME 15), initial rates method was used for Hammett relationship determination. The observed positive Hammett relationship ( $\rho$ )

supports turnover rate limiting C-C bond formation after ternary complex formation. However, the relationship was found to have some non-linearity at  $\sigma = 0$  ( $\rho = 3.2$  for electron-rich,  $\rho = 0.88$  for electron-poor imines, FIGURE 13) and the explanation was not trivial. To complicate conclusions, in addition to TDTS energy, the *para*-substituent can affect the concentrations of intermediate complexes which in turn affect the overall reaction rate.

Ideally Hammett effect describes the direction of electron flow during TDTS. However, since the rate of C-C bond formation depends also on TDI energy, substituent effects before or after TDTS can affect the overall turnover frequency. Since coordination of imine to catalyst through H-bonding would lead to flow of electron density from the imine carbon, the Lewis basicity of imines and their strength as H-bond acceptors can be expected to have a Hammett relationship. In this scenario electron-donating substituents would increase the equilibrium concentration of the imine-catalyst binary complex as well as the stability of ternary complex leading to an increased reaction rate.

Substituent effects on secondary interactions between the catalyst and imine (Chapter 2.3.4) such as interactions between  $\pi$ -systems<sup>144,145</sup> could also contribute to the reaction rate through the binding energy of the imines. However, the strength and origin of the substituent effects on Ar-Ar binding interactions are still debated.<sup>91</sup> Although the reaction rate is susceptible to minor changes in substrate electronic effects, to a certain limit stronger binding of the substrates would result in a higher concentration of ternary complex, thus increasing the turnover rate.



SCHEME 15. Model reaction used in determination of Hammett relationship. X denotes the *para*-substituent.

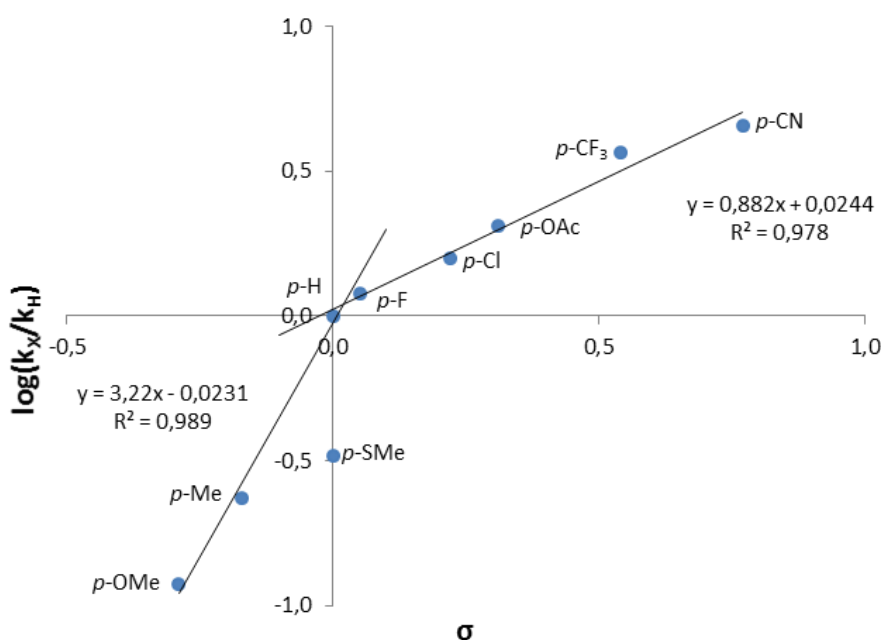
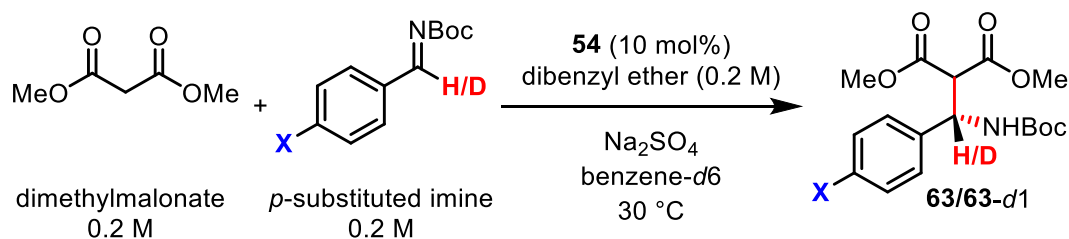


FIGURE 13. Relative reaction rate as a function of Hammett constant ( $\sigma$ ). Reprinted with permission from *ACS Catalysis*, **2017**, 7, 3284-3294. Copyright 2017 American Chemical Society.

The uncertainty caused by the possible Hammett relationship of imine coordination to the catalyst prompted us to study the mechanism further with complementary kinetic methods. Secondary kinetic isotope effect of the imine H/D was expected to be able to differentiate plausible causes for observed Hammett relationship (SCHEME 16). Since 2° KIE is a result of a hybridization change adjacent to deuterium atom, rate limiting H-bonding of imine to catalyst should not result in observable kinetic isotope effect. Furthermore, the 2° KIE was expected to be the same for electron deficient and electron-rich imines if the C-C bond formation is TDTS, although such substituent effects are not often determined and reported. The observed inverse 2° KIEs (0.90–0.93) were initially considered as further support for the rate limiting C-C bond formation with all tested imines. However, a thorough literature search brought to our attention an alternative explanation to the inverse isotope effect. A report from Gajewski and Ngerneesri demonstrated an inverse equilibrium isotope effect of 0.86 in coordination of aromatic aldehydes to a strong Lewis acid.<sup>146</sup> Thus it cannot be excluded that EIE also contributes to the observed isotope effect. Unfortunately, the error limits especially with the electron deficient *p*-CN aryl imine were too large for conclusions about minor changes in the energy profile of the reaction. Nevertheless, the explanation that 2° KIE results from C-C bond formation event is consistent with the observed substituent effects of the Hammett plot.



SCHEME 16. Model reaction used in determination of 2° KIE. X denotes the *para*-substituent.

The enantiomeric ratios of the isolated products from kinetic measurements were determined to confirm the reliability of the obtained results. In general, it is important to be able to verify that kinetics of the desired reaction is measured.<sup>2</sup> The results showed that the reactions proceeded in an enantioselective manner under the studied conditions. In a study leading to the work described in this thesis, a non-Arrhenius relationship on enantioselectivity was observed.<sup>123</sup> This result suggests that in this reaction and with this catalyst at temperatures above 0 °C a racemic or less selective mechanism contributes to the rate of product formation. This deviation from ideal can affect the magnitudes of Hammett reaction constant and isotope effects, but it would not produce false results of this magnitude. Despite the non-ideal measurement conditions, such as scale and reaction temperature, the methods used herein were considered suitable for obtaining enough data with the available resources and existing time constraints.

A combination of kinetic measurements and DFT calculations has been found useful in rationalization of observed reactivity and quantification of energy profiles in bifunctional organocatalysis.<sup>147</sup> Unfortunately, the kinetic experiments failed to answer is the relative orientations of substrates and catalyst in the ternary complex as the binding energies of ternary complexes did not show a significant difference. However, these complexes of similar energy result in the same enantiomer of the Mannich reaction product.

Taken together, the experimental kinetic studies supported by computational results were able to show that C-C bond formation is indeed the TDTS and thus plays a significant role in the turnover frequency. This important result still leaves open the question about the significance of ternary complex formation. To be able to answer this question, further experimental test focusing on events before C-C bond formation were required.

### 3.3.3 Inhibition Experiments as a Proxy for Complex Formation Studies

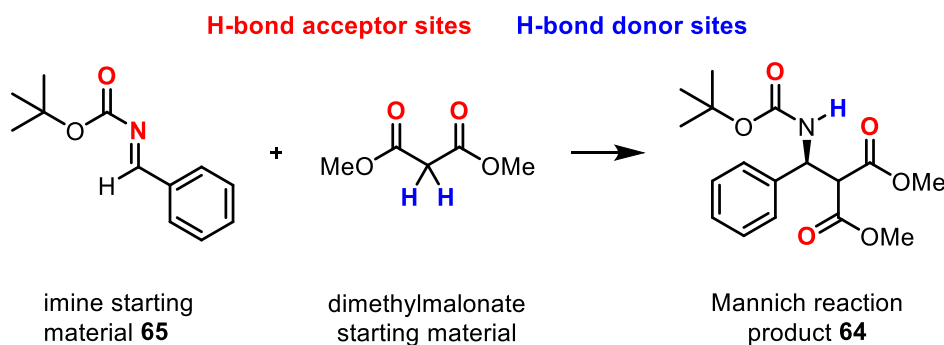
The most convenient way for studying catalyst-substrate complexation would be direct observation of a measurable change in either catalyst or substrate upon binding. Unfortunately, the substrates did not cause quantifiable changes in the substrates or catalyst by <sup>1</sup>H NMR spectroscopy. The small magnitude of observed changes even with high substrate loading is indicative of weak binding. Thus, we turned our attention to indirect methods to study the significance of catalyst-substrate complexation for turnover frequency.

We envisioned a slowly reacting electron-rich aromatic imine should competitively inhibit the reaction in the presence of a more reactive imine if the formation of catalyst-imine complex limits the turnover frequency. The observed significant reduction of reaction rate supports this conclusion.

According to the Energetic Span Model formulated by Kozuch and Shaik, also intermediates after the TDTS can influence the turnover frequency.<sup>21</sup> In the studied reaction, such an intermediate could be the catalyst-product complex. In enantioselective reactions one of the product enantiomers can bind more strongly than the other enantiomer, since diastereomeric complexes are formed. The initial rate of the model reaction was determined with added product to quantify the inhibitory effect of the product. This approach relates to RPKA discussed in Chapter 2.4.3 and the reaction rate should reduce in case of an inhibitory effect. Inhibition experiments indeed show that the reaction product has an inhibitory effect which is more pronounced as the product concentration increases. The observed inhibitory effect can be rationalized with the number and type of H-bond acceptors and donors in starting materials and Mannich reaction product shown in SCHEME 17.

Ideally, only the starting materials should bind to the catalyst active site and in a productive fashion while product and possible side products should have no or only weak interactions with the catalyst. In many H-bond catalyzed C-C bond forming reactions the starting materials and product contain the same functional groups, such as ketone, ester, and nitro groups. Although this similarity inevitably leads to some degree of inhibition and lowered TOF especially at high conversion, product inhibition of organocatalysts is rarely discussed in literature, despite being extensively studied in enzymatic processes which rely on H-bond catalysis. The practical outcome of significant product inhibition is incomplete conversion which can be overcome by increasing the catalyst loading.

In the Mannich reaction the only major change in H-bonding ability of the product **64** versus the substrates is the transformation of imine **65** H-bond acceptor into an H-bond donor (SCHEME 17). Additionally, the entropy of binding would likely disfavor the productive binding of two substrates over the binding of a single product molecule.<sup>78</sup>



SCHEME 17. H-bond acceptor (red) and donor (blue) sites in Mannich reaction substrates and product.

Catalysts **53** and **54** have an excellent pocket for binding urea. The same binding moiety with urea can be found in all Mannich reaction products studied in Publications I-III, namely a *syn*-carbamate. The observed H-bonds in solid state structure of catalyst **54**-urea complex (FIGURE 14) fill the criteria for a medium-strength H-bond (TABLE 2). On the other hand, steric factors likely prevent the adoption of the perfect binding geometry since the product is sterically more demanding than urea. Unfortunately, we were not able to obtain catalyst-product co-crystals for single crystal XRD measurement.

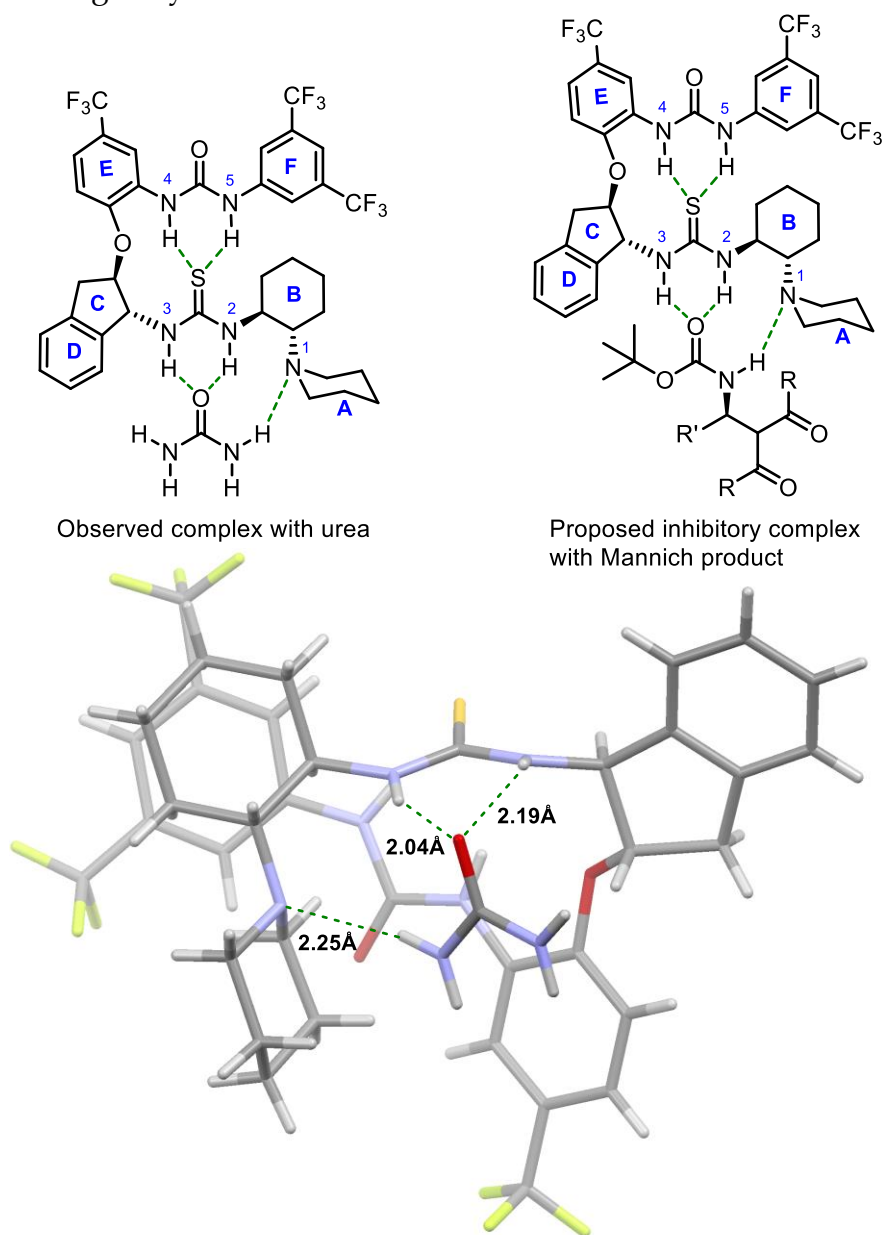


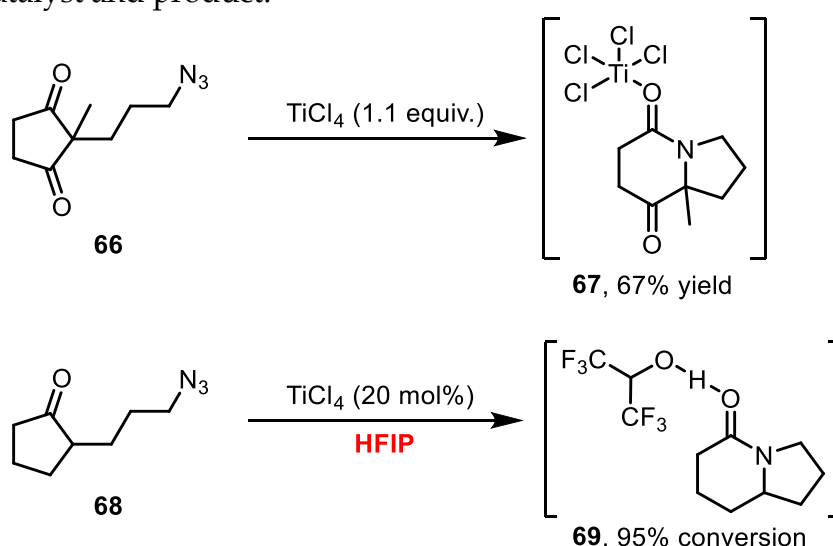
FIGURE 14. Hydrogen bond network of bifunctional catalyst **54** and urea.

The inhibition experiments discussed above suggest that the concentration of productive ternary complex of malonate, imine and catalyst is lowered by competitive complexation of the product by the catalyst. Thus, it can be stated



that the developed organocatalytic enantioselective Mannich reaction shows significant product inhibition which can explain why in some cases a high catalyst loading is required to reach full conversion.

In extreme cases of product inhibition, the catalyst binds the product much more strongly than to the starting material, leading to complete product inhibition (TON  $\leq 1$ ). Intramolecular Lewis acid mediated Schmidt reaction is a good example of this effect.<sup>148</sup> In this case, an equimolar amount of Lewis acid was required to reach full conversion because the amide formed in the reaction is a stronger Lewis base than the starting material ketone (SCHEME 18). This problem was overcome, and reaction rendered Lewis acid catalyzed, by using a Brønsted acidic solvent hexafluoroisopropanol (HFIP) to break the complex between the Lewis acid catalyst and product.<sup>149</sup>



SCHEME 18. An example of extreme product inhibition in a Lewis acid catalyzed Schmidt reaction.

### 3.4 Weak Interactions and Enhanced Activity in H-bond Catalysis

One of the main aims of the study leading to Publication II was to find an explanation for the exceptionally good performance of the catalyst family with aliphatic imines in Mannich reactions. The kinetic experiments described in the previous chapter did not unfortunately bring any insight to this matter. An interesting distinction between the catalyst **54** and Takemoto catalyst **39** was found in the computational analysis of the transition state. Whereas the Takemoto catalyst **39** shows only little dispersion interactions between the substrates and the catalyst, catalyst **54** shows in contrast tight secondary interactions between substrates and catalyst C and D rings (FIGURE 15). As described in Chapter 2.1, the interaction energy is highly dependent on the

distance and relative orientation of the interacting components which in the transition state with catalyst **54** appear beneficial for ternary complex stability.

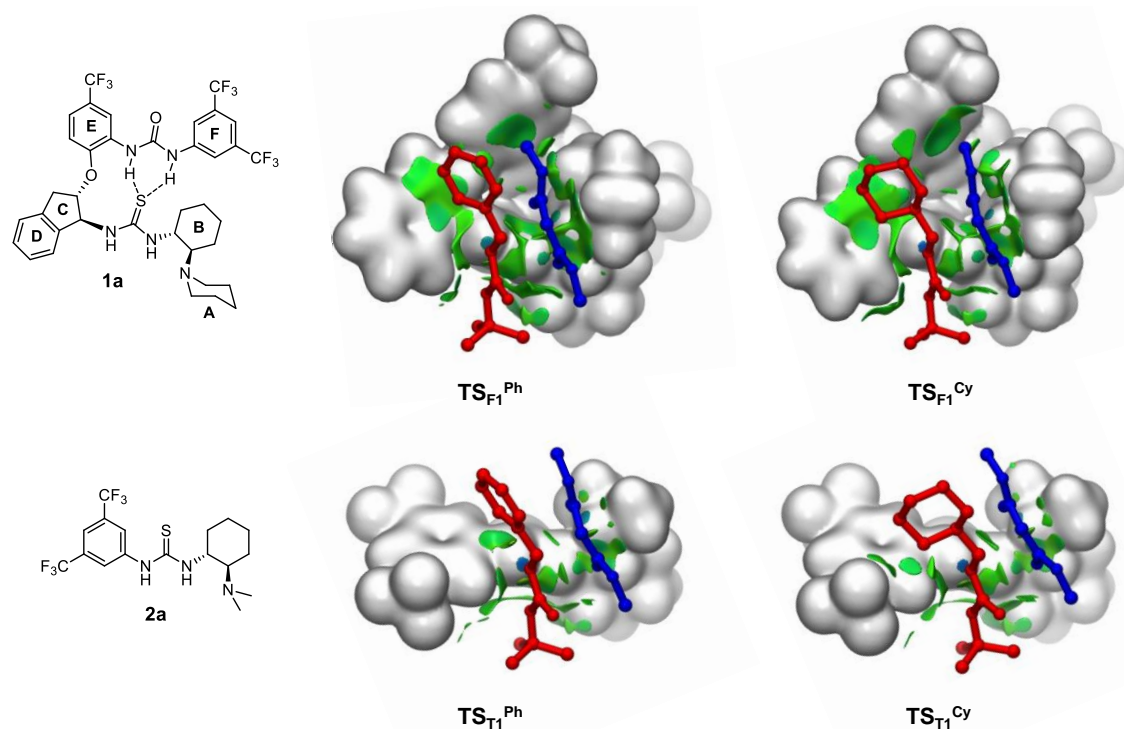


FIGURE 15. Computational comparison of plausible dispersion interactions with urea-thiourea catalyst **54** (**1a** in figure) and Takemoto catalyst **39** (**2a** in figure). Phenyl and cyclohexyl imines = red, dimethylmalonate = blue. Dispersion interactions = green, catalyst = light grey. Reprinted with permission from *ACS Catalysis*, **2017**, *7*, 3284-3294. Copyright 2017 American Chemical Society.

These interactions may contribute to the applicability of aliphatic imines as substrates with the folding catalysts such as **52–54**. However, based on the competition experiments between the aliphatic and aromatic imines in Publication II, the additional secondary interactions in the catalyst **54** compared to Takemoto catalyst **39** are beneficial with aliphatic *and* aromatic imines. To the authors' knowledge, the secondary interactions have not been widely studied in bifunctional H-bond-Brønsted base catalysis. As an example, Soós and co-workers have studied edge-to-face interactions of dimeric Cinchona-thiourea bifunctional catalyst complexes in solution. However, no correlation in catalysis was presented.<sup>150</sup>

## 3.5 Solving the Active Catalyst and Catalyst Salt Conformations<sup>III</sup>

### 3.5.1 The Native Conformation of Free Catalyst

The data gathered from Smith and co-workers on related structures<sup>88,124</sup> and our prior work<sup>123</sup> supported the idea that the intramolecularly H-bonding fold is the major conformation of the free catalyst in solution. This fold was therefore called “native fold”. However, in solid state structures, we have encountered conformational changes in the thiourea moiety, resulting in alternative folds. In principle, *N,N'*-disubstituted thioureas can exist as four different conformers, assuming the two substituents are not identical (FIGURE 16a).

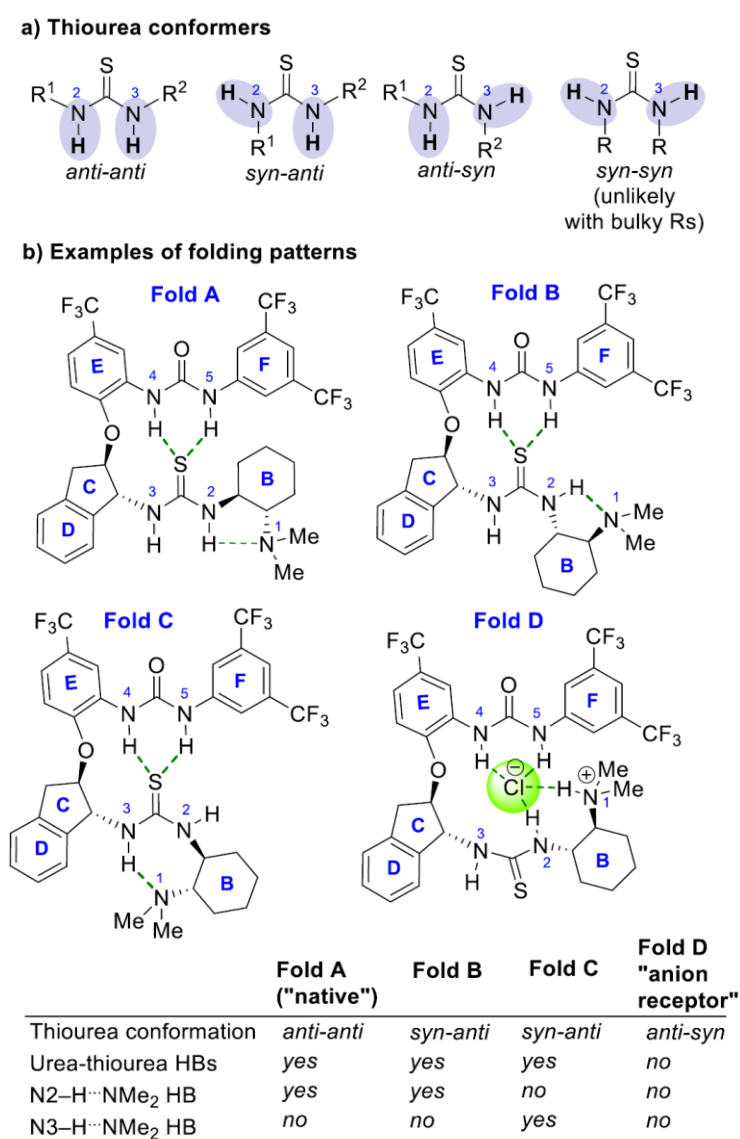


FIGURE 16. Observed catalyst **53** and catalyst **53** salt conformers in solid state. Reprinted with permission from *The Journal of Organic Chemistry*, **2019**, *84*, 15009–15019. Copyright 2019 American Chemical Society.

Two of these conformers had indeed been observed in solid state structures of free catalyst **53**, N2,N3 *anti* (Fold A) and N2 *syn*,N3 *anti* (Folds B and C, FIGURE 16b). We had previously obtained also an unexpected solid-state structure of catalyst hydrochloride salt with distinctive anion binding conformation (Fold D, N2 *anti*,N3 *syn*) and a structure of catalyst **52** hfacac salt where catalyst remained in its native fold (Fold A).<sup>123</sup> Of the four possible thiourea conformers, only N2,N3 *syn* has not been observed and it expected to be a high energy conformation due to unfavorable steric congestion. Prior to the work published in Publication III, we had obtained only the solid-state structures of **52** and **53** described above which do not provide sufficient data for generalization of anion binding modes of catalysts **52** and **53**.

The observations and computational analyses we have published previously provide conclusive evidence that the catalytically active catalyst conformation is indeed the intermolecularly H-bonded native fold. However, the exact stability of the catalyst conformations upon binding to various acids and the influence of the geometrical positioning of the anion H-bond acceptor sites were not known. Due to the number and type of possible simultaneous interactions, such as highly directional and distance dependent H-bonds, and less directional and less distance dependent ion-ion and ion-dipole interactions, we were not able to predict any catalyst salt conformations. An additional challenge in such a complex system is that individual interactions are cumulative. Also, cooperativity of interactions has been proposed to contribute significantly to overweighing the entropic cost of binding.<sup>78,151</sup>

### 3.5.2 Structure Elucidation of Catalyst Salts in Solid State and in Solution

Over the course of several years, we were very fortunate to obtain a complete set of solid-state structures from halide salts with both catalyst diastereomers **52** (diastereomer 2) and **53** (diastereomer 1, FIGURE 17). Painstaking screening of crystallization conditions finally allowed us to study these structures systematically and generalize the anion binding mode with hydrohalic acids. Additionally, we were able to obtain solid-state structures of few catalyst salts with structurally more complex organic acids. Availability of the solid-state structures provided us a solid starting point for computational analyses and to use them as reference for solution-state contact analyses, such as NOESY.

The striking similarity of the solid-state structures of catalyst halide salts across anion sizes suggests that anion size does not influence anion binding conformation significantly (FIGURE 17c). Such pincer-type binding is often highly dependent on anion size and binding affinity is low especially if large anions do not fit the binding pocket. However, a closer look at the binding reveals that the three H-bonds to anion are only on one face of the anion leaving the other face open. In the crystal lattice the other face of anions shows intermolecular coordination to thiourea *syn* N3-H.

The three-coordinate anion binding of **53** greatly resembles the anion binding mode observed by Gouverneur and co-workers in solid state of the fluoride binding phase-transfer catalyst. In their recent study *N*-alkylation of bis-

urea phase transfer catalyst was found to improve significantly the selectivity and yield of enantioselective fluorination of azetidinium salts.<sup>70</sup> The binding models of the *N*-alkylated urea show an *anti-syn* urea conformation with alkyl group pointing outwards and the three remaining urea hydrogens binding the fluoride from one face. This binding mode shows a clear preference for small anions such as fluoride over bromide (by 17 kJ/mol).<sup>152</sup>

The binding modes of diastereomeric catalysts **52** and **53** differ mainly in the direction of the dimethylammonium hydrogen. In catalyst **52** salts the ammonium hydrogen points towards the anion whereas in salts of **53** the hydrogen points away from the anion. Since ion-ion interactions are mostly non-directional the importance of this difference might not be significant. Perhaps more importantly, the distance between the ammonium N-H and the halide ion in salts of **52** (see FIGURE 17, a and b) is significantly shorter than in salts of catalyst **53**, suggesting that the nature of binding is more ionic than in salts of **53**.

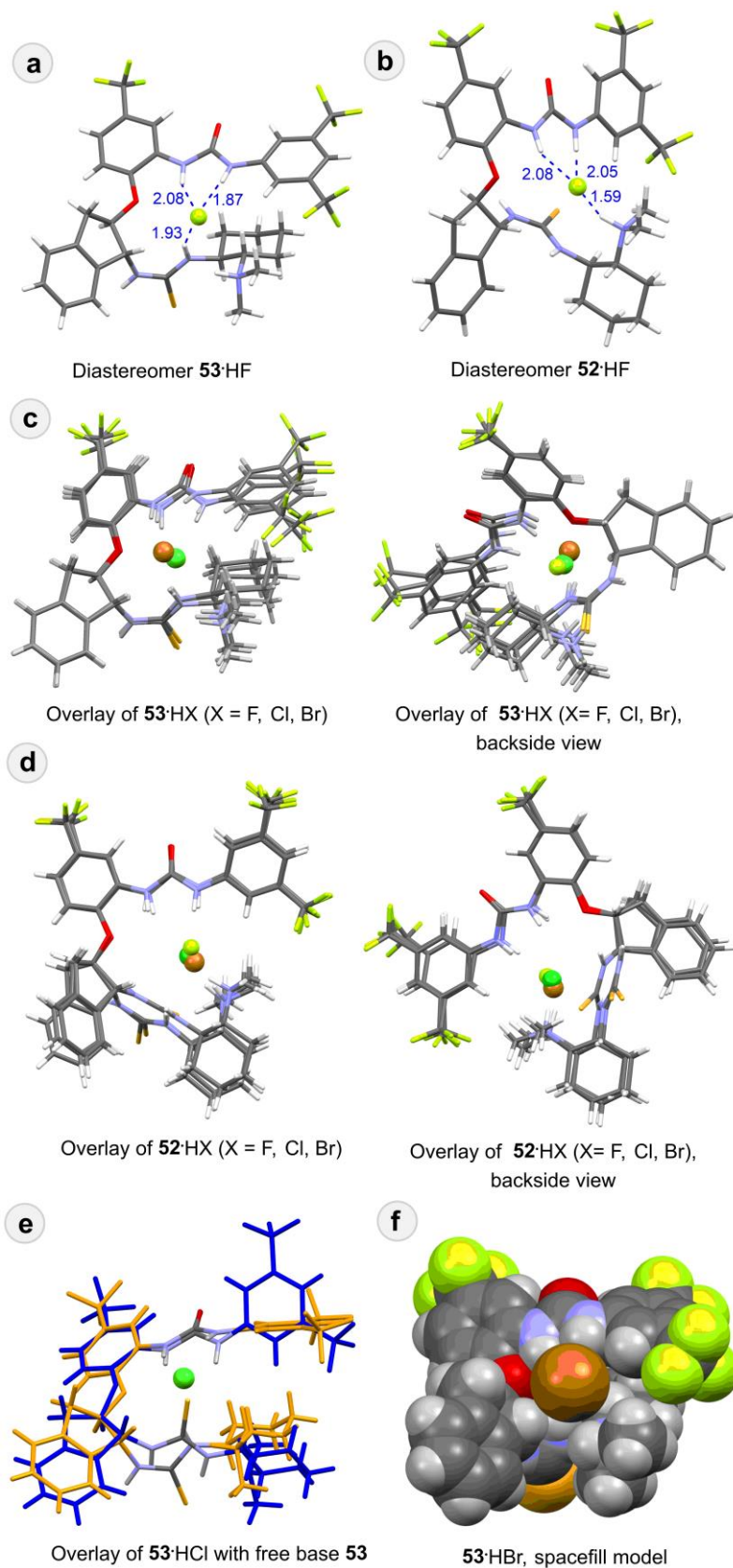


FIGURE 17. Solid state structures of catalyst **52** and **53** halide salts. Adapted with permission from *The Journal of Organic Chemistry*, **2019**, *84*, 15009–15019. Copyright 2019 American Chemical Society.

Thioureas are known to bind several types of anions and their anion binding modes have been summarized by Zhang and Schreiner.<sup>67</sup> High chloride binding affinity of conformationally flexible urea-thiourea H-bond organocatalysts have been demonstrated by Smith and co-workers. The authors propose the intramolecularly H-bonded ground-state conformation, similar to the native fold, as the anion binding conformation. However, they do not provide any evidence for this conclusion.<sup>124</sup> Gale, Davis and co-workers have demonstrated significant size discrimination in steroidal squaramide receptors with a rigid scaffold and five H-bond donors. While these receptors had extremely high affinities towards chloride and acetate ions, perchlorate and iodide showed hardly any affinity.<sup>153</sup> With similar structures, the clear trend in affinity (Cl>Br>I) was attributed mostly to anion size and the high selectivity to the number and positioning of H-bonds.<sup>154</sup>

We were able to obtain solid-state structures of catalyst **52** as salts with a few organic acids. However, catalyst **53** did not afford proper crystals for XRD measurements with the examined salts of organic acids. The only example of catalyst **53** salt structure was presented already in 2012 in the form of a hfacac salt. The hfacac structure was expected to mimic the binding of malonate anion in the catalyst. At the time, we were excited to obtain such a structure with the catalyst native fold that can be directly correlated with catalyst malonate ion pair, albeit being much more stable due to hfacac acidity.<sup>123</sup> In this work, we obtained a solid-state structure of **52** TFA salt (FIGURE 18), measured and solved by Filip Topić, that also exhibits the native fold. This trend was further demonstrated with diphenyl phosphate and 2,6-bis(trifluoromethyl)benzoic acetate salts of catalyst **52**.<sup>III</sup> These structures provided further support to the notion that native fold of the catalyst is retained with organic acids.

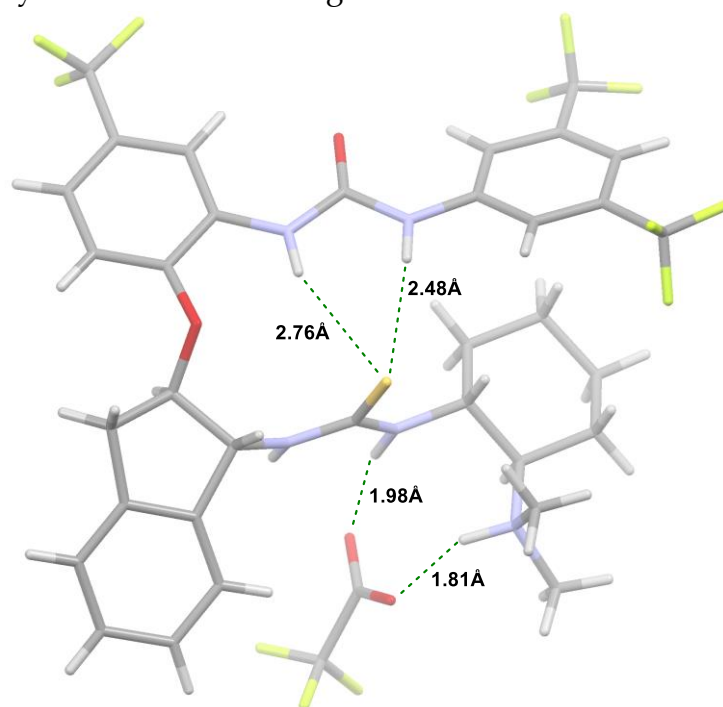


FIGURE 18. Solid-state structure of catalyst **52** TFA salt.

A general challenge in obtaining XRD quality single-crystals with this catalyst family was the high solubility of free catalyst and also its salts with organic acids in most common organic solvents, and the propensity to oil-out from non-polar solvents. To emphasize this difficulty, all attempts to crystallize piperidine catalyst **54** as free catalyst or as a salt failed. Interestingly, as a last resort, the author was able to obtain a highly crystalline  $C_2$ -symmetric 2:1:1 catalyst-urea-acetonitrile complex (FIGURE 19) with a *neutral* and strongly hydrogen bonding urea.<sup>II</sup>

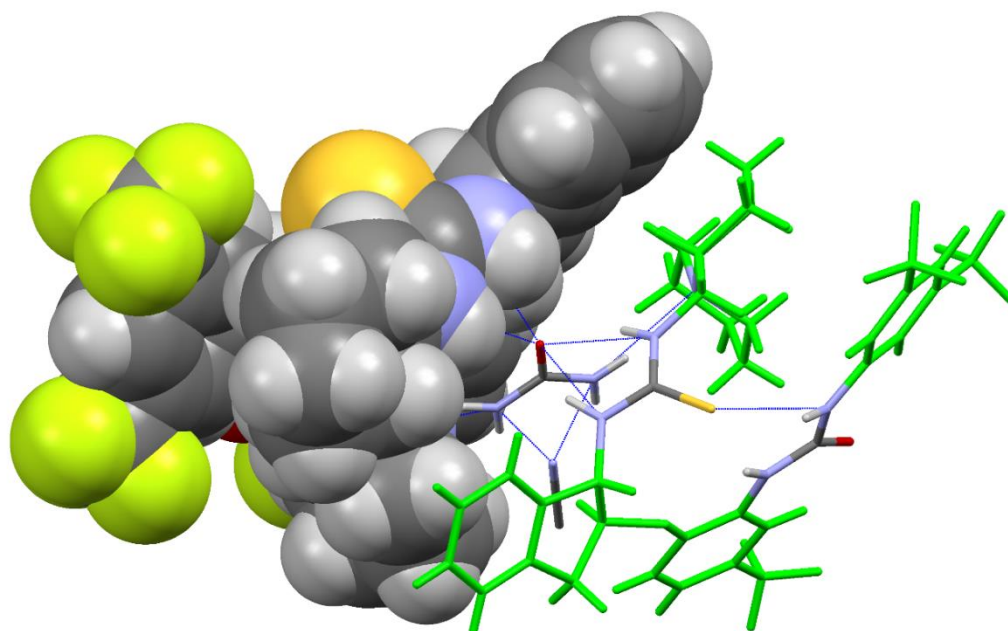


FIGURE 19. Solid-state structure of  $C_2$ -symmetric 2:1:1 catalyst-urea-acetonitrile complex.<sup>II</sup> One catalyst molecule is presented as space-fill model and urea, acetonitrile, and second catalyst molecule as wireframe model. H-Bonding moieties in second catalyst molecule are colored according to atom colors and the rest colored green for clarity.

With the solid-state structures at hand, we had an excellent starting point to compare the interactions observed in the crystal structures with the results obtained from DFT computations and solution state NMR measurements, such as expected NOESY peaks across the catalyst molecule. The NMR measurements highlight the dynamic nature of the free catalyst **52** as conflicting NOESY peaks were observed. The best explanation is that two similar-energy conformations (Folds A and C) are present that interconvert slowly enough to be observed in the  $^1\text{H}$  NMR timescale. However, NOESY peaks suggest that in the free catalyst **53**, only one conformation, the native fold, is present to a significant degree. The computational analyses were also well in line with the solid-state structures. Thus, it can be concluded that in this case the solid-state structures most likely are good representations of actual conformations present in future solution-state applications.



## 4 SUMMARY AND CONCLUSIONS

Through kinetic experiments we were able to fulfill one of the main aims of this thesis. Factors influencing the turnover frequency of enantioselective Mannich reactions were qualitatively defined although quantification of the catalyst substrate and catalyst product interactions was not successful. Studies of rate determining factors in catalysis can help chemists to find ways to lower the turnover frequency determining transition state energies. With this research we were able to demonstrate the importance of lowering the transition state energy of C-C bond forming step and the equally important effects governing catalyst substrate complexation. However, a definite answer to the excellent performance of this catalyst family with aliphatic imines was still not found.

Another aim of the studies behind this thesis was to study and find an explanation to conformational preferences of the developed catalyst family. As a result of this study, a clear correlation of catalyst conformation and counter anion shape was found. Whereas spherical halide anions facilitate a conformational change, organic anions allow catalyst to maintain its native fold. Since the anion transfer processes are also biologically and technologically important, the results presented in this thesis can be utilized in these fields to build a better understanding of the underlying phenomena. Thus, the results lay a foundation for potential anion binding related catalytic applications and applications in biological anion transport.

We were also able to define the limits of  $\beta$ -dicarbonyl nucleophiles both in terms of highly reactive and less selective  $\beta$ -ketoesters and non-reactive  $\beta$ -ketoamides of secondary amines. The catalyst structure was successfully modified to improve the enantioselectivity of Mannich reactions with  $\beta$ -ketoesters.

Through multidisciplinary collaboration we have obtained and shared with the chemical community detailed, systematic, and hopefully useful studies of anion binding, catalytic enantioselective Mannich reactions and the factors governing H-bonding catalysis beyond Mannich reactions.

## REFERENCES

- <sup>1</sup> Hagen, J. *Industrial Catalysis: A Practical Approach*, WILEY-VCH Verlag GmbH & Co, Weinheim, **2005**.
- <sup>2</sup> Walsh, P. J.; Kozlowski, M. C. *Fundamentals of Asymmetric Catalysis*, University Science Books, Sausalito, California, **2009**.
- <sup>3</sup> Barbaro, P.; Bianchini, C. *Catalysis for Sustainable Energy Production*, Wiley-VCH Verlag GmbH & Co. KGaA, Weinheim, **2009**.
- <sup>4</sup> Appl, M. *Ammonia, 2. Production Processes* in *Ullmann's Encyclopedia of Industrial Chemistry*, Wiley-VCH Verlag GmbH & Co. KGaA, Weinheim, **2012**.
- <sup>5</sup> Blaser, H. U.; Spindler, F.; Studer, M. Enantioselective catalysis in fine chemicals production. *Applied Catalysis A: General*, **2001**, 221, 119–143.
- <sup>6</sup> Jeschke, P. Current status of chirality in agrochemicals. *Pest. Manag. Sci.* **2018**, 74, 2389–2404.
- <sup>7</sup> Corey, E. J.; Kürti, L. *Enantioselective Chemical Synthesis*, Direct Book Publishing LLC, Dallas, Texas, **2010**.
- <sup>8</sup> Tan, J.; Yasuda, N. Contemporary Asymmetric Phase Transfer Catalysis: Large-Scale Industrial Applications. *Org. Process Res. Dev.* **2015**, 19, 1731–1746.
- <sup>9</sup> Dunkel, R.; Elbe, H.-L.; Rieck, H.; Hartmann, B.; Greul, J. N. Wachendorff-Neumann, U.; Dahmen, P.; Kuck, K.-H.; Suty-Heinze, A. Optically active carboxamides and use thereof to combat undesirable microorganisms, Patent: WO2005/058839 A1.
- <sup>10</sup> Vargesson, N. Thalidomide-Induced Teratogenesis: History and Mechanisms. *Birth Defects Research (Part C)*, **2015**, 105, 140–156.
- <sup>11</sup> Zahrt, A. F.; Athavale, S. V.; Denmark, S. E. Quantitative Structure-Selectivity Relationships in Enantioselective Catalysis: Past, Present, and Future. *Chem. Rev.* **2020**, 120, 1620–1689.
- <sup>12</sup> Lipkowitz, K. B.; Kozlowski, M. C. Understanding Stereoinduction in Catalysis via Computer: New Tools for Asymmetric Synthesis. *Synlett*, **2003**, 10, 1547–1565.
- <sup>13</sup> Ess, D.; Gagliardi, L.; Hammes-Schiffer, S. Introduction: Computational Design of Catalysts from Molecules to Materials. *Chem. Rev.* **2019**, 119, 6507–6508.

- <sup>14</sup> Ahn, S.; Hong, M.; Sundararajan, M.; Ess, D. H.; Baik, M.-H. Design and Optimization of Catalysts Based on Mechanistic Insights Derived from Quantum Chemical Reaction Modeling. *Chem. Rev.* **2019**, *119*, 6509–6560.
- <sup>15</sup> Freeze, J. G.; Kelly, H. R.; Batista, V. S. Search for Catalysts by Inverse Design: Artificial Intelligence, Mountain Climbers, and Alchemists. *Chem. Rev.* **2019**, *119*, 6595–6612.
- <sup>16</sup> EU's Roadmap to Resource Efficiency:  
[https://ec.europa.eu/environment/resource\\_efficiency/about/roadmap/index\\_en.htm](https://ec.europa.eu/environment/resource_efficiency/about/roadmap/index_en.htm), retrieved on August 4, 2020.
- <sup>17</sup> UN Sustainable Development Goals:  
<https://www.un.org/sustainabledevelopment/sustainable-development-goals>, retrieved on August 4, 2020.
- <sup>18</sup> Technology Roadmap - Energy and GHG Reductions in the Chemical Industry via Catalytic Processes - IEA, ICCA, DECHEMA (2015)  
[www.americanchemistry.com/Catalysis-Roadmap](http://www.americanchemistry.com/Catalysis-Roadmap), retrieved on August 4, 2020.
- <sup>19</sup> Trost, B. M. Atom Economy - A Challenge for Organic Synthesis: Homogeneous Catalysis Leads the Way. *Angew. Chem. Int. Ed.* **1995**, *34*, 159–281.
- <sup>20</sup> Vogel, P.; Lam, Y.-h.; Simon, A.; Houk, K. N. Organocatalysis: Fundamentals and Comparisons to Metal and Enzyme Catalysis. *Catalysts*, **2016**, *6*, 128.
- <sup>21</sup> Kozuch, S.; Shaik, S. How to Conceptualize Catalytic Cycles? The Energetic Span Model. *Acc. Chem. Res.* **2011**, *44*, 101–110.
- <sup>22</sup> Kürti, L.; Czakó, B. *Strategic Applications of Named Reactions in Organic Synthesis*, Elsevier Academic Press, Burlington, **2005**.
- <sup>23</sup> Definition of stereoisomers from IUPAC Gold Book: "Isomers that possess identical constitution, but which differ in the arrangement of their atoms in space."  
<http://goldbook.iupac.org/terms/view/S05984>, retrieved on August 9, 2020.
- <sup>24</sup> Definition of an enantiomer from IUPAC Gold Book: "One of a pair of molecular entities which are mirror images of each other and non-superposable."  
<http://goldbook.iupac.org/terms/view/E02069>, retrieved on August 9, 2020.
- <sup>25</sup> Brands, K. M. J.; Davies, A. J. Crystallization-Induced Diastereomer Transformations. *Chem. Rev.* **2006**, *106*, 2711–2733.
- <sup>26</sup> Anderson, N. G. Developing Processes for Crystallization-Induced Asymmetric Transformation. *Org. Process Res. Dev.* **2005**, *9*, 800–813.

- <sup>27</sup> Ward, R. S. Dynamic Kinetic Resolution. *Tetrahedron: Asymmetry* **1995**, *6*, 1475–1490.
- <sup>28</sup> Mannich, C. Synthesis of  $\beta$ -Ketonic Bases. *J. Chem. Soc., Abstr.* **1917**, *112*, 634–635. (*Arch. Pharm.* **1917**, *255*, 261–276)
- <sup>29</sup> Berkessel, A.; Gröger, H. *Asymmetric Organocatalysis*, WILEY-WCH Verlag GmbH & Co, Weinheim, **2005**.
- <sup>30</sup> Kunz, H.; Schanzenbach, D. Carbohydrates as Chiral Templates: Stereoselective Synthesis of  $\beta$ -Amino Acids. *Angew. Chem. Int. Ed* **1989**, *28*, 1068–1069.
- <sup>31</sup> Matsumura, Y.; Tomita, T. First synthesis of optically pure  $\alpha$ -amino amine as asymmetric amino transfer reagent and its use in asymmetric Mannich reaction. *Tetrahedron Lett.* **1994**, *35*, 3737–3740.
- <sup>32</sup> Corey, E. J.; Decicco, C. P., Newbold, R. C. Highly enantioselective and diastereoselective synthesis of  $\beta$ -amino acid esters and  $\beta$ -lactams from achiral esters and imines. *Tetrahedron Lett.* **1991**, *39*, 5287–5290.
- <sup>33</sup> Ishitani, H.; Ueno, M.; Kobayashi, S. Catalytic Enantioselective Mannich-Type Reactions Using Novel Chiral Zirconium Catalyst. *J. Am. Chem. Soc.* **1997**, *119*, 7153–7154.
- <sup>34</sup> Hagiwara, E.; Fujii, A.; Sodeoka, M. Enantioselective Addition of Enol Silyl Ethers to Imines Catalyzed by Palladium Complexes: A Novel Way to Optically Active Acylalanine Derivatives. *J. Am. Chem. Soc.* **1998**, *120*, 2474–2475.
- <sup>35</sup> Ferraris, D.; Young, B.; Dudding, T.; Lectka, T. Catalytic, Enantioselective Alkylation of  $\alpha$ -Imino Esters Using Late Transition Metal Phosphine Complexes as Catalysts. *J. Am. Chem. Soc.* **1998**, *120*, 4548–4549.
- <sup>36</sup> Mitsumori, S.; Zhang, H.; Cheong, P. H.-Y.; Houk, K. N.; Tanaka, F.; Barbas, C. F. III Direct Asymmetric *anti*-Mannich-Type Reactions Catalyzed by a Designed Amino Acid. *J. Am. Chem. Soc.* **2006**, *128*, 1040–1041.
- <sup>37</sup> Itoh, T.; Yokoya, M.; Miyauchi, K.; Nagata, K.; Ohsawa, A. Proline-Catalyzed Asymmetric Addition Reaction of 9-Tosyl-3,4-dihydro- $\beta$ -carboline with Ketones. *Org. Lett.* **2003**, *5*, 4301–4304.
- <sup>38</sup> Hatano, M.; Horibe, T.; Ishihara, K. Chiral Lithium(I) Binaphtholate Salts for the Enantioselective Direct Mannich-Type Reaction with a Change of Syn/Anti and Absolute Stereochemistry. *J. Am. Chem. Soc.* **2010**, *132*, 56–57.

- <sup>39</sup> Song, J.; Wang, Y.; Deng, L. The Mannich Reaction of Malonates with Simple Imines Catalyzed by Bifunctional Cinchona Alkaloids: Enantioselective Synthesis of  $\beta$ -Amino Acids. *J. Am. Chem. Soc.* **2006**, *128*, 6048–6049.
- <sup>40</sup> Lou, S.; Taoka, B. M.; Ting, A.; Schaus, S. E. Asymmetric Mannich Reactions of  $\beta$ -Keto Esters with Acyl Imines Catalyzed by Cinchona Alkaloids. *J. Am. Chem. Soc.* **2005**, *127*, 11256–11257.
- <sup>41</sup> Mukherjee, S.; Yang, J. W.; Hoffmann, S.; List, B. Asymmetric Enamine Catalysis. *Chem. Rev.* **2007**, *12*, 5471–5569.
- <sup>42</sup> Ma, J.-A.; Cahard, D. Towards Perfect Catalytic Asymmetric Synthesis: Dual Activation of the Electrophile and the Nucleophile. *Angew. Chem. Int. Ed.* **2004**, *43*, 4566–4583.
- <sup>43</sup> MacMillan, D. W. C. The Advent and Development of Organocatalysis. *Nature*, **2008**, *445*, 304–308.
- <sup>44</sup> Clayden, J.; Greeves, N.; Warren, S.; Wothers, P. *Organic Chemistry*, Oxford University Press, Oxford, **2001**, pp. 82–110.
- <sup>45</sup> Knowles, R. R.; Jacobsen, E. N. Attractive noncovalent interactions in asymmetric catalysis: Links between enzymes and small molecule catalysts. *Proc. Acad. Nat. Sci.* **2010**, *107*, 20678–20685.
- <sup>46</sup> Biedermann, F.; Schneider, H.-J. Experimental Binding Energies in Supramolecular Complexes *Chem. Rev.* **2016**, *116*, 5216–5300.
- <sup>47</sup> Anslyn, E. V., Dougherty, D. A. *Modern Physical Organic Chemistry*, University Science Books, Sausalito, **2006**.
- <sup>48</sup> Schneider, H. J. Binding Mechanisms in Supramolecular Catalysis *Angew. Chem. Int. Ed.* **2009**, *48*, 3924–3977.
- <sup>49</sup> Raynal, M.; Ballester, P.; Vidal-Ferran, A.; Leeuwen, P. W. N. M. Supramolecular catalysis. Part 1: non-covalent interactions as a tool for building and modifying homogeneous catalysis *Chem. Soc. Rev.* **2014**, *43*, 1660–1733.
- <sup>50</sup> Steiner, T. The Hydrogen Bond in the Solid State *Angew. Chem. Int. Ed.* **2002**, *41*, 48–76.
- <sup>51</sup> Doyle, A. G.; Jacobsen, E. N. Small-Molecule H-Bond Donors in Asymmetric Catalysis *Chem. Rev.* **2007**, *107*, 5713–5743.

- <sup>52</sup> Pihko, P. M. Activation of Carbonyl Compounds by Double Hydrogen Bonding: An Emerging Tool in Asymmetric Catalysis *Angew. Chem Int Ed.* **2004**, *43*, 2062–2064.
- <sup>53</sup> Kobayashi, S.; Mori, Y.; Fossey, J. S.; Salter, M. M. Catalytic Enantioselective Formation of C-C Bonds by Addition to Imines and Hydrazones: A Ten-Year Update *Chem. Rev.* **2011**, *111*, 2626–2704.
- <sup>54</sup> Akiyama, T.; Mori, K. Stronger Brønsted Acids: Recent Progress *Chem. Rev.* **2015**, *115*, 9277–9306.
- <sup>55</sup> Jakab, G.; Tancon, C.; Zhang, Z.; Lippert, K. M.; Schreiner, P. R. (Thio)urea Organocatalyst Equilibrium Acidities in DMSO. *Org. Lett.* **2012**, *14*, 1724–1727.
- <sup>56</sup> Malerich, J. P.; Hagihara, K.; Rawal, V. H. Chiral Squaramide Derivatives are Excellent Hydrogen Bond Donor Catalysts *J. Am. Chem. Soc.* **2008**, *130*, 14416–14417.
- <sup>57</sup> Auvil, T. J.; Schafer, A. G.; Mattson, A. E. Design Strategies for Enhanced Hydrogen-Bond Donor Catalysts *Eur. J. Org. Chem.* **2014**, 2633–2646.
- <sup>58</sup> Curran, D. P.; Kuo, L. H. Altering the Stereochemistry of Allylation Reactions of Cyclic  $\alpha$ -Sulfinyl Radicals with Diarylureas. *J. Org. Chem.* **1994**, *59*, 3259–3261.
- <sup>59</sup> Curran, D. P.; Kuo, L. H. Acceleration of a Dipolar Claisen Rearrangement by Hydrogen Bonding to a Soluble Diaryl Urea. *Tetrahedron Letters*, **1995**, *36*, 6647–6650.
- <sup>60</sup> Malerich, J. P.; Hagihara, K.; Rawal, V. H. Chiral Squaramide Derivatives are Excellent Hydrogen Bond Donor Catalysts. *J. Am. Chem. Soc.* **2008**, *130*, 14416–14417.
- <sup>61</sup> Storer, R. I.; Aciro, C.; Jones, L. H. Squaramides: physical properties, synthesis and applications. *Chem. Soc. Rev.* **2011**, *40*, 2330–2346.
- <sup>62</sup> Chauchan, P.; Mahajan, S.; Kaya, U.; Peuronen, A.; Rissanen, K.; Enders, D. Asymmetric Synthesis of Amino-Bis-Pyrazolone Derivatives via an Organocatalytic Mannich Reaction *J. Org. Chem.* **2017**, *82*, 7050–7058.
- <sup>63</sup> Huang, Y.; Unni, A. K.; Thadani, A. N.; Rawal, V. H. Single enantiomers from a chiral-alcohol catalyst. *Nature*, **2003**, *424*, 146.
- <sup>64</sup> Unni, A. K.; Takenaka, N.; Yamamoto, H.; Rawal, V. H. Axially Chiral Biaryl Diols Catalyze Highly Enantioselective Hetero-Diels–Alder Reactions through Hydrogen Bonding. *J. Am. Chem. Soc.* **2005**, *127*, 1336–1337.

- <sup>65</sup> Inokuma, T.; Furukawa, M.; Uno, T.; Suzuki, Y.; Yoshida, K.; Yano, Y.; Matsuzaki, K.; Takemoto, Y. Bifunctional Hydrogen-Bond Donors That Bear a Quinazoline or Benzothiadiazine Skeleton for Asymmetric Organocatalysis *Chem. Eur. J.* **2011**, *17*, 10470–10477.
- <sup>66</sup> Walvoord, R. R.; Huynh, P. N. H.; Kozlowski, M. C. Quantification of Electrophilic Activation by Hydrogen-Bonding Organocatalysts. *J. Am. Chem. Soc.* **2014**, *136*, 45, 16055–16065.
- <sup>67</sup> Zhang, Z.; Schreiner, P. R. (Thio)urea organocatalysis – What Can be Learnt from Anion Recognition. *Chem. Soc. Rev.* **2009**, *38*, 1187–1198.
- <sup>68</sup> Visco, M. D.; Attard, J.; Guan, Y.; Mattson, A. E. Anion-binding catalyst designs for enantioselective synthesis. *Tetrahedron Lett.* **2017**, *58*, 2623–2628.
- <sup>69</sup> Brak, K.; Jacobsen E. N. Asymmetric Ion-Pairing Catalysis. *Angew. Chem. Int. Ed.* **2012**, *51*, 2–30.
- <sup>70</sup> Roagna, G.; Ascough, D. M. H.; Ibba, F.; Chiara Vicini, A.; Fontana, A.; Christensen, K. E.; Peschiulli, A.; Oehrich, D.; Misale, A.; Trabanco, A. A.; Paton, R. S.; Pupo, G.; Gouveurneur, V. Hydrogen Bonding Phase-Transfer Catalysis with Ionic Reactants: Enantioselective Synthesis of  $\gamma$ -Fluoroamines. *J. Am. Chem. Soc.* **2020**, *142*, 14045–14051.
- <sup>71</sup> Ford, D. D.; Lehnerr, D.; Kennedy, C. R.; Jacobsen, E. N. Anion-Abstraction Catalysis: The Cooperative Mechanism of  $\alpha$ -Chloroether Activation by Dual Hydrogen-Bond Donors. *ACS Catal.* **2016**, *6*, 4616–4620.
- <sup>72</sup> Park, Y.; Harper, K. C.; Kuhl, N.; Kwan, E. E.; Liu, R. Y.; Jacobsen, E. N. Macrocyclic bis-thioureas catalyze stereospecific glycosylation reactions. *Science*, **2017**, *355*, 162–166.
- <sup>73</sup> Banik, S. M.; Levina, A.; Hyde, A. M.; Jacobsen, E. N. Lewis acid enhancement by hydrogen-bond donors for asymmetric catalysis. *Science*, **2017**, *358*, 761–764.
- <sup>74</sup> Schafer, A. G.; Wieting, J. M.; Fisher, T. J.; Mattson, A. E. Chiral Silanediols in Anion Binding Catalysis. *Angew. Chem. Int. Ed.* **2013**, *52*, 11321–11324.
- <sup>75</sup> Shibasaki, M.; Kumagai, N. *Lewis Acid-Brønsted Base Catalysis in Cooperative Catalysis: Designing Efficient Catalysts for Synthesis*, Ed. Peters, R. Wiley-VCH Verlag GmbH & Co. KGaA, Weinheim, **2015**.
- <sup>76</sup> Newton, C. G.; Wang, S.-G.; Oliveira, C. C.; Cramer, N. Catalytic Enantioselective Transformations Involving C–H Bond Cleavage by Transition-Metal Complexes. *Chem. Rev.* **2017**, *117*, 8908–8976.

- <sup>77</sup> Warshel, A.; Sharma, P. K.; Kato, M.; Xiang, Y.; Liu, H.; Olsson, H. M. Electrostatic Basis for Enzyme Catalysis. *Chem Rev.* **2006**, *106*, 3210–3235.
- <sup>78</sup> Calderone, C. T.; Williams, D. H. An Enthalpic Component in Cooperativity: The Relationship between Enthalpy, Entropy, and Noncovalent Structure in Weak Associations. *J. Am. Chem. Soc.* **2001**, *123*, 6262–6267.
- <sup>79</sup> Okino, T.; Hoashi, Y.; Furukawa, T.; Xu, X.; Takemoto, Y. Enantio- and Diastereoselective Michael Reaction of 1,3-Dicarbonyl Compounds to Nitroolefins Catalyzed by a Bifunctional Thiourea. *J. Am. Chem. Soc.* **2005**, *127*, 119–125.
- <sup>80</sup> Palomo, C.; Oiarbide, M.; López, R. Asymmetric organocatalysis by chiral Brønsted bases: implications and applications. *Chem. Soc. Rev.* **2009**, *38*, 632–635.
- <sup>81</sup> Hoffmann, R. W. Allylic 1,3-Strain as a Controlling Factor in Stereoselective Transformations. *Chem. Rev.* **1989**, *89*, 1841–1860.
- <sup>82</sup> Johnson, F. Allylic Strain in Six-Membered Rings. *Chem. Rev.* **1968**, *68*, 375–413.
- <sup>83</sup> Hoffmann, R. W. Conformation Design of Open-Chain Compounds. *Angew. Chem. Int. Ed.* **2000**, *39*, 2054–2070.
- <sup>84</sup> Dado, G. P.; Gellman, S. H. Intramolecular Hydrogen Bonding in Derivatives of  $\beta$ -alanine and  $\gamma$ -Amino Butyric Acid: Model Studies for the Folding of Unnatural Polypeptide Backbones. *J. Am. Chem. Soc.* **1994**, *116*, 1054–1062.
- <sup>85</sup> Appella, D. H.; Christianson, L. A.; Klein, D. A.; Powell, D. R.; Huang, X.; Barchi, J. J. Jr.; Gellman, S. H. Residue-based control of helix shape in  $\beta$ -peptide oligomers. *Nature*, **1997**, *387*, 381–384.
- <sup>86</sup> Morimoto, J.; Kim, J.; Kuroda, D.; Nagatoishi, S.; Tsumoto, K.; Sando, S. Per-Residue Program of Multiple Backbone Dihedral Angles of  $\beta$ -Peptoids via Backbone Substitutions. *J. Am. Chem. Soc.* **2020**, *142*, 2277–2284.
- <sup>87</sup> Miller, S. J.; Copeland, G. T.; Papaioannou, N.; Horstmann, T. E.; Ruel, E. M. Kinetic Resolution of Alcohols Catalyzed by Tripeptides Containing the *N*-Alkylimidazole Substructure. *J. Am. Chem. Soc.* **1998**, *120*, 1629–1630.
- <sup>88</sup> Driver, R. W.; Claridge, T. D. W.; Scheiner, S.; Smith, M. D. Torsional and Electronic Factors Control the C-H $\cdots$ O Interaction. *Chem. Eur. J.* **2016**, *22*, 16513–16521.
- <sup>89</sup> Gellman, S. H. Introduction: Molecular Recognition. *Chem. Rev.* **1997**, *97*, 1231–1232.



- <sup>90</sup> Krenske, E. H.; Houk, K. N. Aromatic Interactions as Control Elements in Stereoselective Organic Reactions. *Acc. Chem. Res.* **2013**, *46*, 979–989.
- <sup>91</sup> Neel, A. J.; Hilton, M. J.; Sigman, M. S.; Toste, F. D. Exploiting non-covalent  $\pi$  interactions for catalyst design. *Nature*, **2017**, *543*, 637–646.
- <sup>92</sup> Ma, J. C.; Dougherty, D. A. The Cation- $\pi$  Interaction. *Chem. Rev.* **1997**, *97*, 1303–1324.
- <sup>93</sup> Kennedy, C. R.; Lin, S.; Jacobsen, E. N. The Cation- $\pi$  Interaction in Small-Molecule Catalysis. *Angew. Chem. Int. Ed.* **2016**, *55*, 12596–12624.
- <sup>94</sup> Zhao, Y.; Sakai, N.; Matile, S. Enolate Chemistry with anion- $\pi$  interactions. *Nature Comm.* **2014**, *5*, 3991.
- <sup>95</sup> Wagner, J. P.; Schreiner, P. R.; London Dispersion in Molecular Chemistry – Reconsidering Steric Effects. *Angew. Chem. Int. Ed.* **2015**, *54*, 12274–12296.
- <sup>96</sup> Miller, J. J.; Sigman, M. S. Quantitatively Correlating the Effect of Ligand-Substituent Size in Asymmetric Catalysis Using Linear Free Energy Relationships. *Angew. Chem. Int. Ed.* **2008**, *47*, 771–774.
- <sup>97</sup> Yepes, D.; Neese, F.; List, B.; Bistoni, G. Unveiling the Delicate Balance of Steric and Dispersion Interactions in Organocatalysis Using High-Level Computational Methods. *J. Am. Chem. Soc.* **2020**, *142*, 3613–3625.
- <sup>98</sup> Seguin, T. J.; Wheeler, S. E. Competing Noncovalent Interactions Control the Stereoselectivity of Chiral Phosphoric Acid Catalyzed Ring Openings of 3-Substituted Oxetanes. *ACS Catal.* **2016**, *6*, 7222–7228.
- <sup>99</sup> Lu, G.; Liu, R. Y.; Yang, Y.; Fang, C.; Lambrecht, D. S.; Buchwald, S. L.; Liu, P. Ligand-Substrate Dispersion Facilitates the Copper-Catalyzed Hydroamination of Unactivated Olefins. *J. Am. Chem. Soc.* **2017**, *139*, 16548–16555.
- <sup>100</sup> Zhao, Y.; Domoto, Y.; Orentas, E.; Beuchat, C.; Emery, D.; Mareda, J.; Sakai, N.; Matile, S. Catalysis with Anion- $\pi$  Interactions. *Angew. Chem. Int. Ed.* **2013**, *52*, 9940–9943.
- <sup>101</sup> Zhao, Y.; Beuchat, C.; Domoto, Y.; Gajewy, J.; Wilson, A.; Mareda, J.; Sakai, N.; Matile, S. Anion- $\pi$  Catalysis. *J. Am. Chem. Soc.* **2014**, *136*, 2101–2111.
- <sup>102</sup> Hunter, C. A. Quantifying Intermolecular Interactions: Guidelines for the Molecular Recognition Toolbox. *Angew. Chem. Int. Ed.* **2004**, *43*, 5310–5324.
- <sup>103</sup> Shaik, S.; Danovich, D.; Joy, J.; Wang, Z.; Stuyver, T. Electric-Field Mediated Chemistry: Uncovering and Exploiting the Potential of (oriented) Electric Fields

to Exert Chemical Catalysis and Reaction Control. *J. Am. Chem. Soc.* **2020**, *142*, 12551–12562.

<sup>104</sup> Blackmond, D. G. Reaction Progress Kinetic Analysis: A Powerful Methodology for Mechanistic Studies of Complex Catalytic Reactions. *Angew. Chem. Int. Ed.* **2005**, *44*, 4302–4320.

<sup>105</sup> Sahoo, G.; Rahaman, H.; Madarász, Á.; Pápai, I.; Melarto, M.; Valkonen, A.; Pihko, P. M. Dihydrooxazine Oxides as Key Intermediates in Organic Michael Additions of Aldehydes to Nitroalkenes. *Angew. Chem. Int. Ed.* **2012**, *51*, 13144–13148.

<sup>106</sup> Leskinen, M. V.; Madarász, Á.; Yip, K.-T.; Vuorinen, A.; Pápai, I.; Neuvonen, A. J.; Pihko, P. M. Cross-Dehydrogenative Couplings between Indoles and  $\beta$ -Keto Esters: Ligand-Assisted Ligand Tautomerization and Dehydrogenation via a Proton-Assisted Electron Transfer to Pd(II). *J. Am. Chem. Soc.* **2014**, *136*, 6453–6462.

<sup>107</sup> Yousefi, R.; Sarkar, A.; Ashtekar, K. D.; Whitehead, D. C.; Kakeshpour, T.; Holmes, D.; Reed, P.; Jackson, J. E.; Borhan, B. Mechanistic Insights into the Origin of Stereoselectivity in an Asymmetric Chlorolactonization Catalyzed by (DHQD)2PHAL. *J. Am. Chem. Soc.* **2020**, *142*, 7179–7189.

<sup>108</sup> Gómez-Gallego, M.; Sierra, M. A. Kinetic Isotope Effects in the Study of Organometallic Reactions Mechanisms. *Chem. Rev.* **2011**, *111*, 4857–4963.

<sup>109</sup> Singleton, D. A.; Thomas, A. A. High-Precision Simultaneous Determination of Multiple Small Kinetic Isotope Effects at Natural Abundance. *J. Am. Chem. Soc.* **1995**, *117*, 9357–9358.

<sup>110</sup> Bandar, J. S.; Sauer, G. S.; Wulff, W. D.; Lambert, T. H.; Veticatt, M. J. Transition State Analysis of Enantioselective Brønsted Base Catalysis by Chiral Cyclopropenimines. *J. Am. Chem. Soc.* **2014**, *136*, 10700–10707.

<sup>111</sup> Simmons, E. M.; Hartwig, J. F. On the interpretation of Deuterium Kinetic Isotope Effects in C-H bond Functionalizations by Transition-Metal Complexes. *Angew. Chem. Int. Ed.* **2012**, *51*, 3066–3072.

<sup>112</sup> Mao, Z.; Campbell, C. T. Kinetic Isotope Effects: Interpretation and Prediction Using Degrees of Rate Control. *ACS Catal.* **2020**, *10*, 4181–4192.

<sup>113</sup> Northrop, D. B. Steady-State Analysis of Kinetic Isotope Effects in Enzymic Reactions. *Biochemistry*, **1975**, *14*, 2644–2651.

- <sup>114</sup> Northrop, D. B. Minimal Kinetic Mechanism and General Equation for Deuterium Isotope Effects on Enzymic Reactions: Uncertainty in Detecting a Rate-Limiting Step. *Biochemistry*, **1981**, *20*, 4056–4061.
- <sup>115</sup> Sun, H.-Y.; Gorelsky, S. I.; Stuart, D. R.; Campeau, L.-C.; Fagnou, K. Mechanistic Analysis of Azine *N*-Oxide Direct Arylation: Evidence for a Critical Role of Acetate in the Pd(OAc)<sub>2</sub> Precatalyst. *J. Org. Chem.* **2010**, *75*, 8180–8189.
- <sup>116</sup> Harper, K. C.; Sigman, M. S. Using Physical Organic Parameters To Correlate Asymmetric Catalyst Performance. *J. Org. Chem.* **2013**, *78*, 2813–2818.
- <sup>117</sup> Hammett, L. P. The Effect of Structure upon the Reactions of Organic Compounds. Benzene Derivatives. *J. Am. Chem. Soc.* **1937**, *59*, 96–103.
- <sup>118</sup> Taft, R. W. Jr. Linear Free Energy Relationships from Rates of Esterification and Hydrolysis of Aliphatic and Ortho-substituted Benzoate Esters. *J. Am. Chem. Soc.* **1952**, *74*, 2729–2732.
- <sup>119</sup> Cheong, P. H.-Y.; Legault, C. Y.; Um, J. M.; Çelebi-Ölçüm, N.; Houk, K. N. Quantum Mechanical Investigations of Organocatalysis: Mechanisms, Reactivities, and Selectivities. *Chem. Rev.* **2011**, *111*, 5042–5137.
- <sup>120</sup> Thomas, A. A.; Speck, K.; Kevlishvili, I.; Lu, Z.; Liu, P.; Buchwald, S. L. Mechanistically Guided Design of Ligands That Significantly Improve the Efficiency of CuH-Catalyzed Hydroamination Reactions. *J. Am. Chem. Soc.* **2018**, *140*, 13976–13984.
- <sup>121</sup> Govender, T.; Arvidson, P. I.; Maguire, G. E. M.; Kruger, H. G.; Naicker, T. Enantioselective Organocatalyzed Transformations of  $\beta$ -Ketoesters. *Chem. Rev.* **2016**, *116*, 9375–9437.
- <sup>122</sup> Cummings, T. F.; Shelton, J. R. Mannich Reaction Mechanisms. *J. Org. Chem.* **1960**, *25*, 419–423.
- <sup>123</sup> Probst, N.; Madarász, Á.; Valkonen, A.; Pápai, I.; Rissanen, K.; Neuvonen, A.; Pihko, P. M. Cooperative Assistance in Bifunctional Organocatalysis: Enantioselective Mannich Reactions with Aliphatic and Aromatic Imines. *Angew. Chem. Int. Ed.* **2012**, *51*, 8495–8499.
- <sup>124</sup> Jones, C. R.; Pantoş, G. D.; Morrison, A. J.; Smith, M. D. Plagiarizing Proteins: Enhancing Efficiency in Asymmetric Hydrogen-Bonding Catalysis through Positive Cooperativity. *Angew. Chem. Int. Ed.* **2009**, *48*, 7391–7394.
- <sup>125</sup> McCooney, S. H.; Connon, S. J. Urea- and Thiourea-Substituted Cinchona Alkaloid Derivatives as Highly Efficient Bifunctional Organocatalysts for the Asymmetric Addition of Malonate to Nitroalkenes: Inversion of Configuration at

C9 Dramatically Improves Catalyst Performance. *Angew. Chem. Int. Ed.* **2005**, *44*, 6367–6370.

<sup>126</sup> Tillman, A. L.; Ye, J.; Dixon, D. J. Direct enantio- and diastereoselective Mannich reactions of malonate and  $\beta$ -keto esters with *N*-Boc and *N*-Cbz aldimines catalysed by a bifunctional chinchonine derivative. *Chem. Commun.* **2006**, 1191–1193.

<sup>127</sup> Song, J.; Shih, H.-W.; Deng, L. Asymmetric Mannich Reactions with in Situ Generation of Carbamate-Protected Imines by an Organic Catalyst. *Org. Lett.* **2007**, *9*, 603–606.

<sup>128</sup> Lucius, R.; Mayr, H. Constant Selectivity Relationships of Addition Reactions of Carbanions. *Angew. Chem. Int. Ed.* **2000**, *39*, 1995–1997.

<sup>129</sup> Lucius, R.; Loos, R.; Mayr, H. Kinetic Studies of Carbocation–Carbanion Combinations: Key to a General Concept of Polar Organic Reactivity. *Angew. Chem. Int. Ed.* **2002**, *41*, 91–95.

<sup>130</sup> Olmstead, W. N.; Margolin, Z.; Borwell, F. G. Acidities of water and simple alcohols in dimethyl sulfoxide solution. *J. Org. Chem.* **1980**, *45*, 3295–3299.

<sup>131</sup> Bordwell, F. G.; Fried, H. E. Heterocyclic Aromatic Anions with  $4n + 2$   $\pi$ -Electrons. *J. Org. Chem.* **1991**, *56*, 4218–4223.

<sup>132</sup> Bordwell, F. G. Equilibrium Acidities in Dimethyl Sulfoxide Solution. *Acc. Chem. Res.* **1988**, *21*, 456–463.

<sup>133</sup> Bordwell, F. G.; Branca, J. C.; Hughes, D. L.; Olmstead, W. N. Equilibria Involving Organic Anions in Dimethyl Sulfoxide and *N*-Methylpyrrolidin-2-one: Acidities, Ion Pairing, and Hydrogen Bonding. *J. Org. Chem.* **1980**, *45*, 3305–3313.

<sup>134</sup> Corral-Bautista, F.; Mayr, H. Quantification of the Nucleophilic Reactivities of Cyclic  $\beta$ -Keto Ester Anions. *Eur. J. Org. Chem.* **2015**, 7594–7601.

<sup>135</sup> Karimi, B.; Jafari, E.; Enders, D. Highly Efficient Catalytic Enantioselective Mannich Reaction of Malonates with *N*-*tert*-Butoxycarbonyl Imines by Using Yb(OTf)<sub>3</sub>/Pybox Catalysts at Room Temperature. *Chem. Eur. J.* **2013**, *19*, 10142–10145.

<sup>136</sup> Marigo, M.; Kjærsgaard, A.; Juhl, K.; Gathergood, N.; Jørgensen, K. A. Direct Catalytic Asymmetric Mannich Reactions of Malonates and  $\beta$ -Keto Esters. *Chem. Eur. J.* **2003**, *9*, 2359–2367.

<sup>137</sup> Uraguchi, D.; Terada, M. Chiral Brønsted Acid-Catalyzed Direct Mannich Reactions via Electrophilic Activation. *J. Am. Chem. Soc.* **2004**, *126*, 5356–5357.

- <sup>138</sup> Núñez, M. G.; Farley, A. J. M.; Dixon, D. J. Bifunctional Iminophosphorane Organocatalysts for Enantioselective Synthesis: Application to the Ketimine Nitro-Mannich Reaction. *J. Am. Chem. Soc.* **2013**, *135*, 16348–16351.
- <sup>139</sup> Yu, Z.; Liu, X.; Zhou, L.; Lin, L.; Feng, X. Bifunctional Guanidine via an Amino Amide Skeleton for Asymmetric Michael Reactions of  $\beta$ -Ketoesters with Nitroolefins: A Concise Synthesis of Bicyclic  $\beta$ -Amino Acids. *Angew. Chem. Int. Ed.* **2019**, *48*, 5195–5198.
- <sup>140</sup> Lambert, T. H.; Bandar, J. S. Enantioselective Brønsted Base Catalysis with Chiral Cyclopropenimines. *J. Am. Chem. Soc.* **2012**, *134*, 5552–5555.
- <sup>141</sup> Du, H.; Rodriguez, J.; Bugaut, X.; Constantineux, T. Organocatalytic Enantio- and Diastereoselective Conjugate Addition to Nitroolefins: When  $\beta$ -Ketoamides Surpass  $\beta$ -Ketoesters. *Chem. Eur. J.* **2014**, *20*, 8458–8466.
- <sup>142</sup> Neuvonen, A. J. Unpublished results.
- <sup>143</sup> Jakubec, P.; Cockfield, D.; Dixon, D. J. Total Synthesis of (-)-Nakadomarin. *J. Am. Chem. Soc.* **2009**, *131*, 16632–16633.
- <sup>144</sup> Wheeler, S. E.; Houk, K. N. Substituent Effects in the Benzene Dimer are Due to Direct Interactions of the Substituents with the Unsubstituted Benzene. *J. Am. Chem. Soc.* **2008**, *130*, 10854–10855.
- <sup>145</sup> Wheeler, S. E. Local Nature of Substituent Effects in Stacking Interactions. *J. Am. Chem. Soc.* **2011**, *133*, 10262–10274.
- <sup>146</sup> Gajewski, J. J.; Ngernmeesri, P. Equilibrium Constants between Boron Trifluoride Etherate and Carbonyl Compounds in Chloroform Solution. *Org. Lett.* **2000**, *2*, 2813–2815.
- <sup>147</sup> Zhu, J.-L.; Zhang, Y.; Liu, C.; Zheng, A.-M.; Wang, W. Insights into the Dual Activation Mechanism Involving Bifunctional Cinchona Alkaloid Thiourea Organocatalysts: An NMR and DFT Study. *J. Org. Chem.* **2012**, *77*, 9813–9825.
- <sup>148</sup> Lertpibulpanya, D.; Marsden, S. P. Concise Access to Indolizidine and Pyrroloazepine Skeleta *via* Intramolecular Schmidt Reactions of Azido 1,3-Diketones. *Org. Biomol. Chem.* **2006**, *4*, 3498–3504.
- <sup>149</sup> Motiwala, H. F.; Fehl, C.; Li, S.-W.; Hirt, E.; Porubsky, P.; Aube, J. Overcoming Product Inhibition in Catalysis of the Intramolecular Schmidt Reaction. *J. Am. Chem. Soc.* **2013**, *135*, 9000–9009.

<sup>150</sup> Tárkányi, G.; Király, P.; Varga, S.; Vakulya, B.; Soós, T. Edge-to-Face CH/ $\pi$  Aromatic Interaction and Molecular Self Recognition in *epi*-Cinchona-Based Bifunctional Thiourea Organocatalysis. *Chem. Eur. J.* **2008**, *14*, 6078–6086.

<sup>151</sup> Mahadevi, A. S.; Sastry, G. N. Cooperativity in Noncovalent Interactions. *Chem. Rev.* **2016**, *116*, 2775–2825.

<sup>152</sup> Pupo, G.; Ibba, F.; Ascough, D. M. H.; Vicini, A. C., Ricci, P.; Christensen, K. E.; Pfeifer, L.; Morphy, J. R.; Brown, J. M.; Paton, R. S.; Gouverneur, V. Asymmetric nucleophilic fluorination under hydrogen bonding phase-transfer catalysis. *Science*, **2018**, *360*, 638–642.

<sup>153</sup> Edwards, S. J.; Valkenier, H.; Busschaert, N.; Gale, P. A.; Davis, A. P. High-Affinity Anion Binding by Steroidal Squaramide Receptors. *Angew. Chem. Int. Ed.* **2015**, *54*, 4592–4596.

<sup>154</sup> Clare, J. P.; Ayling, A. J.; Joos, J.-B.; Sisson, A. L.; Magro, G.; Pérez-Payán, M. N.; Lambert, T. N.; Shukla, R.; Smith, B. D.; Davis, A. P. Substrate Discrimination by Cholapod Anion Receptors: Geometric Effects and the “Affinity–Selectivity Principle”. *J. Am. Chem. Soc.* **2005**, *127*, 10739–10746.



## ORIGINAL PAPERS

### I

#### **ENANTIOSELECTIVE MANNICH REACTION OF $\beta$ -KETO ESTERS WITH AROMATIC AND ALIPHATIC IMINES USING A COOPERATIVELY ASSISTED BIFUNCTIONAL CATALYST**

by

Antti J. Neuvonen and Petri M. Pihko

*Organic Letters*, **2014**, *16*, 5152–5155.

DOI: 10.1021/ol5025025

Reprinted with permission  
from *Organic Letters*, **2014**, *16*, 5152–5155. Copyright 2014 American Chemical Society.

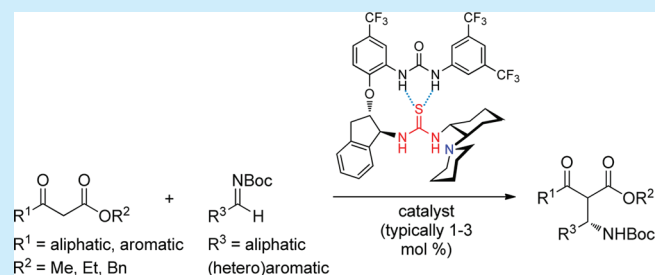
# Enantioselective Mannich Reaction of $\beta$ -Keto Esters with Aromatic and Aliphatic Imines Using a Cooperatively Assisted Bifunctional Catalyst

Antti J. Neuvonen and Petri M. Pihko\*

Department of Chemistry and NanoScience Center, University of Jyväskylä, Survantie 9B, 40520 Jyväskylä, Finland

**S** Supporting Information

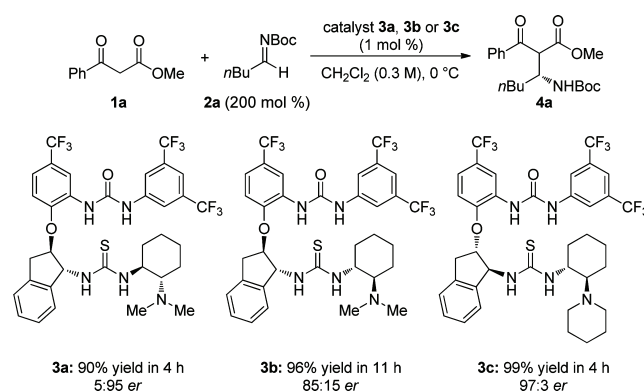
**ABSTRACT:** An efficient urea-enhanced thiourea catalyst enables the enantioselective Mannich reaction between  $\beta$ -keto esters and *N*-Boc-protected imines under mild conditions and minimal catalyst loading (1–3 mol %). Aliphatic and aromatic substituents are tolerated on both reaction partners, affording the products in good enantiomeric purity. The corresponding  $\beta$ -amino ketones can readily be accessed via decarboxylation without loss of enantiomeric purity.



$\beta$ -Amino ketones are highly valuable functionalities that can be found, typically in a protected form, in a large number of natural products and biologically active compounds.<sup>1</sup> A typical synthesis of the  $\beta$ -amino ketone subunit involves a classical Mannich-type reaction between enolates or enamines and imines.<sup>1,2</sup> With enamine catalysis, the reaction appears to be restricted to *N*-arylimines or aromatic *N*-Boc-protected imines.<sup>3</sup> With alternative enol equivalents such as enol silanes or  $\beta$ -dicarbonyl compounds, several enantioselective Mannich reactions with imines have been discovered,<sup>4,5</sup> especially with malonate esters. However, enantioselective reactions involving ketone and  $\beta$ -keto ester enolates are less common. Typically, Mannich reactions with  $\beta$ -keto esters and *N*-carbamoylimines are restricted to imines derived from aromatic aldehydes<sup>6</sup> or glyoxalates.<sup>7</sup> A third alternative to the  $\beta$ -amino ketone subunit involves Michael addition of nitrogen nucleophiles to enones.<sup>8</sup> Although the Michael addition strategy offers excellent enantioselectivities and wide substrate scope including aliphatic side chains, the methods still have practical limitations, such as the potentially hazardous use of azides under acidic conditions<sup>8c</sup> or high catalyst loadings (20 mol %).<sup>8d</sup> Herein, we report a practical protocol for a catalytic enantioselective Mannich reaction of both  $\beta$ -keto esters **1** with imines **2** using a highly efficient catalyst **3c**. Aliphatic and aromatic side chains are tolerated on both components, and the products can be readily converted to chiral  $\beta$ -amino ketones.

In our previous study,<sup>9</sup> we established the use of bifunctional, conformationally restricted urea–thiourea catalysts **3a** and **3b** (Scheme 1) for the organocatalytic Mannich reaction between malonates and both aliphatic and aromatic *N*-Boc imines.<sup>9,10</sup> Catalysts **3a** and **3b** were found to be profoundly more active in the Mannich reaction with aliphatic imines, which failed to react at all under catalytic conditions with the Takemoto<sup>11</sup> or the Chen–Dixon–Soós<sup>12</sup> catalysts lacking the extra urea group of **3a** or **3b**.

## Scheme 1. Cooperatively Assisted Bifunctional Organocatalysts



The  $\beta$ -keto ester derived enolates are less basic and, therefore, less reactive than the malonate enolates as substrates for reactions with less activated imines such as Boc-protected imines.<sup>13</sup> As such, we expected that the reaction might require even more active catalysts. Indeed, a preliminary screen with diastereomeric catalysts **3a** and **3b** revealed that the Mannich reaction with  $\beta$ -keto ester **1a** and imine **2a** afforded good enantioselectivity only with catalyst **3a**. Further optimization by replacing the dimethylamino group of catalyst **3a** with a slightly more basic and bulky piperidine unit afforded a more active and selective catalyst **3c** (Scheme 1). This catalyst was thus selected for further reaction optimization.

The optimization of conditions was started from toluene as the solvent at 0 °C (Table 1, entry 1) since these conditions were found to be optimal for the related Mannich reaction

Received: August 25, 2014

Published: September 17, 2014



Table 1. Optimization of Reaction Conditions<sup>a</sup>

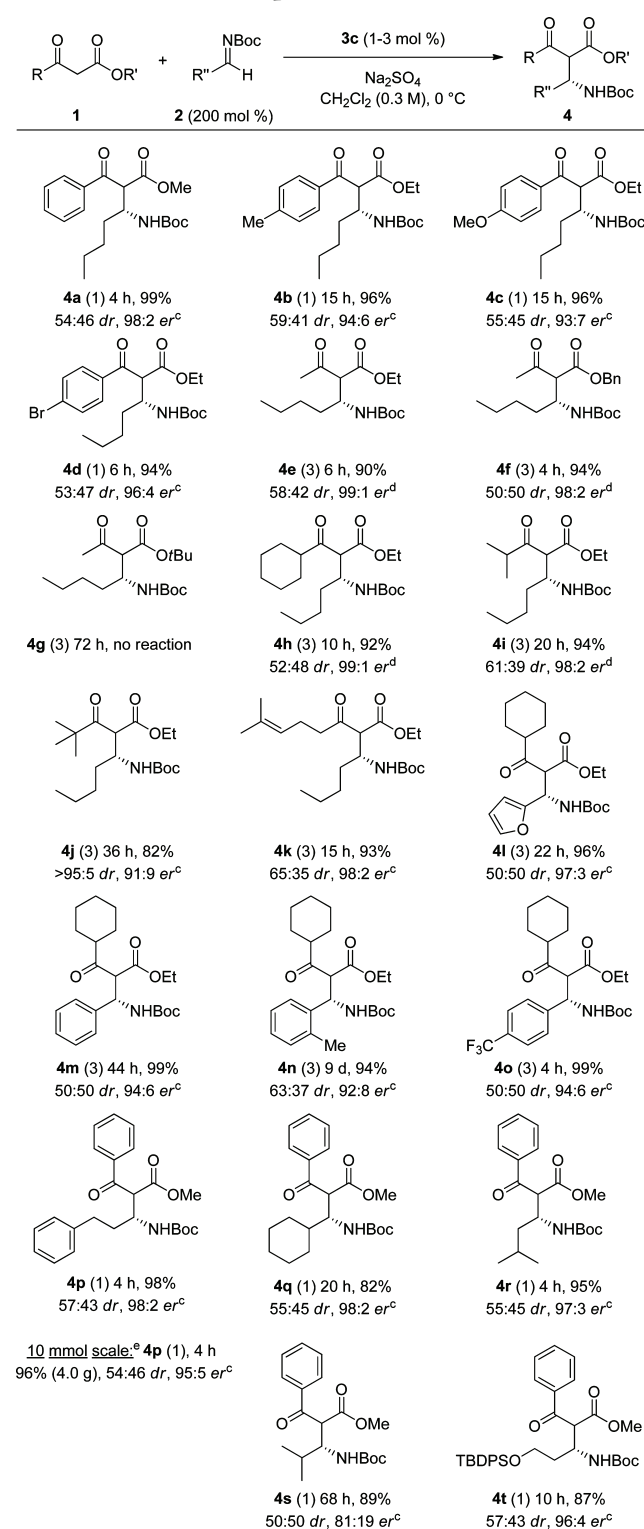
entry	<i>t</i> (°C)	solvent	additive	time (h)	yield <sup>b</sup> (%)	er <sup>c</sup>
1	0	toluene		1	98	89:11
2	0	mesitylene		1	95	93:7
3	-30	mesitylene		3	97	95:5
4	-30	mesitylene/ hexane (1:1)		3	95	96:4
5	28	CH <sub>2</sub> Cl <sub>2</sub>		3	98	81:19
6 <sup>d</sup>	0	CH <sub>2</sub> Cl <sub>2</sub>		3	94	91:9
					-99	-96:4
7	-30	CH <sub>2</sub> Cl <sub>2</sub>		3	98	97:3
8	0	CH <sub>2</sub> Cl <sub>2</sub>	granular 4 Å MS	3	97	88:12
9	0	CH <sub>2</sub> Cl <sub>2</sub>	Na <sub>2</sub> SO <sub>4</sub>	4	99	97:3
10	0	CH <sub>2</sub> Cl <sub>2</sub>	H <sub>2</sub> O	4	99	97:3

<sup>a</sup>Reactions were conducted with 0.2 mmol of **1a**, 0.4 mmol of **2a**, and 0.002 mmol of **3c** in 0.66 mL of indicated solvent. <sup>b</sup>Yields of isolated product. <sup>c</sup>Determined by chiral HPLC as a sum of diastereomers. <sup>d</sup>Results of three independent reactions.

between malonate esters and *N*-Boc-imines.<sup>9</sup> Surprisingly, under these conditions, the product (**4a**) was obtained in excellent yield but with only moderate enantioselectivity (89:11 er). We envisioned that reducing the polarity of the solvent and lowering the temperature (entries 2–4) should enhance the enantioselectivity by producing a tighter ion pair between the protonated catalyst and the enolate nucleophile. Although the enantioselectivity was improved significantly, the reaction mixtures became very heterogeneous. This problem was solved by returning to dichloromethane as the solvent (entries 5–7), and excellent yields and good enantioselectivities were obtained without any precipitate formation. Interestingly, the enantioselectivity dropped significantly when the reaction was performed at 28 °C instead of 0 and -30 °C. This type of non-Arrhenius behavior was also observed previously in the Mannich reaction using malonate esters.<sup>9</sup>

Even with dichloromethane as the solvent, we found that the enantioselectivities were not fully reproducible while the yields remained excellent (entry 6). To examine the possibility of residual water affecting the enantioselectivity, we carried out control experiments by excluding the water with solid drying agents and alternatively adding water into the reaction mixture. Molecular sieves decreased the enantioselectivity (entry 8), presumably allowing competing racemic Lewis acid promoted reaction. A less Lewis acidic drying agent, Na<sub>2</sub>SO<sub>4</sub>, indeed improved both the enantioselectivity and the reproducibility of the reaction (entry 9). However, a control experiment with added water also improved the enantioselectivity (entry 10). Presumably, both water and Na<sub>2</sub>SO<sub>4</sub> can trap traces of inorganic impurities in the imine that lead to lower selectivities.<sup>14</sup> For maximum reproducibility, Na<sub>2</sub>SO<sub>4</sub> was selected as the additive for further screening.

The β-keto ester and the imine components were then varied (Scheme 2). Aromatic β-keto esters reacted smoothly with only 1 mol % of catalyst to give products **4a–d** and **4p–t**, and with aliphatic β-keto esters 3 mol % of catalyst was required to access products **4e–m,o** in a reasonable reaction time. Interestingly, electron-donating substituents in the aromatic

Scheme 2. Substrate Scope<sup>a,b</sup>

<sup>a</sup>Amount of catalyst (mol %) in parentheses. <sup>b</sup>Reaction times, yields of isolated products, diastereomeric ratios, and enantiomeric ratios are reported below each product. <sup>c</sup>Determined by chiral HPLC analysis as a sum of diastereomers. <sup>d</sup>Determined by chiral HPLC analysis after decarboxylation. <sup>e</sup>150 mol % of **2d** (R'' = CH<sub>2</sub>CH<sub>2</sub>Ph); see the Supporting Information. Boc = *tert*-butyloxycarbonyl, TBDPS = *tert*-butyldiphenylsilyl.

β-keto ester nucleophiles do not increase reactivity but instead result in lower reaction rates (**4a** vs **4c**). The catalytic process is

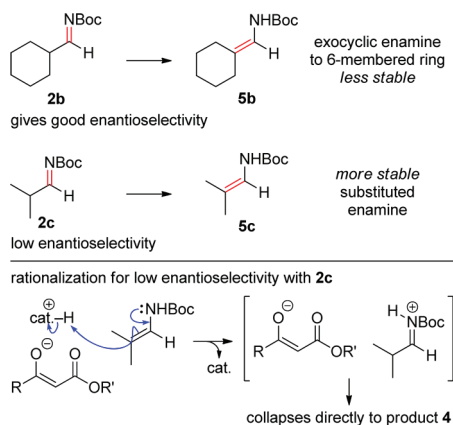
also fairly sensitive to steric properties of the  $\beta$ -keto ester, and while branched alkyl and cycloalkyl substituents are tolerated, *tert*-butyl esters are not (**4e** vs **4g**). Similarly, the quaternary substitution in the  $\gamma$ -position in ethyl pivaloylacetate lowers the rate and affords lower enantioselectivity but nevertheless affords excellent diastereocontrol (**4j**, dr > 95:5).<sup>15</sup> In all of the other cases, the diastereoselectivity was found to be below 2:1, and this ratio is likely to be thermodynamically controlled.

On the side of the imines, aliphatic and electron-poor aromatic imines were found to be highly reactive substrates for the Mannich reaction. In contrast, electron-neutral (**4m**) and electron-rich (**4n**) aromatic imines required longed reaction times. *o*-Methyl substitution in the arylimine was especially challenging for the present catalytic system. With 3 mol % of catalyst, product **4n** was obtained after 9 days in good to moderate yields and slightly lower enantioselectivity (catalyst **3c**, 9 days, 94% yield, 92:8 er; catalyst **3a**: 9 days, 74%, 91:9 er; catalyst **3b**: 9 days 94%, 88:12 er).

Finally, gram-scale synthesis of **4p** using 1 mol % of catalyst and only 1.5 equiv of imine **2d** proceeded smoothly, affording the desired Mannich adduct **4p** in 96% yield and 95:5 enantioselectivity.

An interesting reactivity difference between  $\alpha$ -branched aliphatic imines, leading to **4q** and **4s**, was observed. While the cyclohexanecarboxaldehyde-derived imine **2b** provided good enantioselectivity (giving **4q** in 98:2 er), the isobutyraldehyde-derived imine **2c** provided only modest enantioselectivity (**4s**, 81:19 er) (Scheme 3). To rationalize these

### Scheme 3. Rationalization for Observed Reactivity Difference between Imines **2b** and **2c**



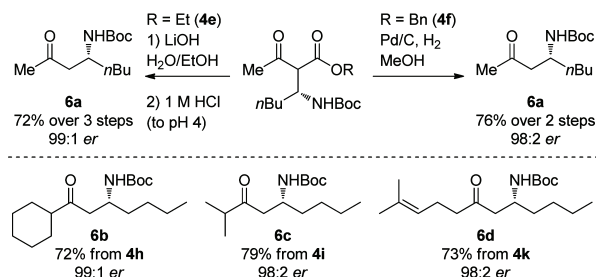
observations, we presume that the reactions proceed through a mechanism where the  $\beta$ -keto ester anion reacts with the imine or iminium ion.<sup>9</sup> In a control experiment in the absence of catalyst **3c**, imine **2c** does not provide product **4s**, suggesting that the catalyst is still involved in the racemic pathway. It should be noted that **2c** readily tautomerizes to the corresponding enecarbamate whereas **2b** does not.<sup>16</sup> Although the enecarbamates do not appear to react directly with  $\beta$ -keto esters, the catalyst  $\beta$ -keto ester salt could protonate the enecarbamate, leading to an enolate–iminium ion pair which should directly collapse to product **4**.<sup>17</sup>

This rationalization is consistent with previously proposed mechanisms for Brønsted<sup>18</sup> and Lewis<sup>19</sup> acid catalyzed enecarbamate to imine tautomerization–nucleophilic addition sequences. Although  $\alpha$ -unbranched imines could also tautomerize to the corresponding enecarbamates, these enecarba-

mates could readily dimerize or oligomerize with the imines and thus would not participate in further reactions. In contrast, **2b** and **2c** are more hindered and less likely to react with the corresponding enecarbamates.

As an application of the Mannich addition protocol, decarboxylation should directly afford enantioenriched  $\beta$ -amino ketones. Since the reaction tolerates both ethyl and benzyl  $\beta$ -keto esters (Scheme 4, **4e** and **4f**), the decarboxylation could be initiated either via saponification or hydrogenation, respectively. These unoptimized decarboxylative transformations (Scheme 4) result in over 70% overall yield of **6a** (form

### Scheme 4. Decarboxylation to Chiral $\beta$ -Amino Ketones<sup>a</sup>



<sup>a</sup>See the Supporting Information for experimental details.

ethyl and benzyl acetoacetate) without compromising the enantiomeric purity. The absolute stereochemistry of **6a** was determined to be *R* by correlation with the corresponding carboxylic acid.<sup>20</sup>

In conclusion, cooperatively assisted urea–thiourea catalyst **3c** catalyzes the Mannich reaction between  $\beta$ -keto esters and *N*-Boc-imines with high yields and enantioselectivities under very mild conditions. Both aliphatic and aromatic substrates are tolerated. A full account on the mechanistic implications of this study is forthcoming.

## ■ ASSOCIATED CONTENT

### Supporting Information

Experimental procedures, analytical data, and copies of NMR spectra and chromatograms for synthesized products. This material is available free of charge via the Internet at <http://pubs.acs.org>.

## ■ AUTHOR INFORMATION

### Corresponding Author

\*E-mail: [petri.pihko@jyu.fi](mailto:petri.pihko@jyu.fi)

### Notes

The authors declare no competing financial interest.

## ■ ACKNOWLEDGMENTS

Financial support from the University of Jyväskylä, Academy of Finland (Grant No. 259532), and Emil Aaltonen foundation (to A.J.N.) is gratefully acknowledged. We thank Dr. Elina Kalenius and Ms. Johanna Lind (University of Jyväskylä) for HRMS analyses and Mr. Esa Haapaniemi (University of Jyväskylä) for assistance with NMR spectroscopy.

## ■ REFERENCES

(1) For a recent review, see: Nguyen, N. H.; Hughes, A. B.; Sleebs, B. E. *Curr. Org. Chem.* **2014**, *18*, 260.

(2) For a review on enantioselective organocatalytic reactions with *N*-carbamoyl imines, see: Vesely, J.; Rios, R. *Chem. Soc. Rev.* **2014**, *43*, 611.

(3) For a review, see: (a) Benohoud, M.; Hayashi, Y. In *Science of Synthesis: Asymmetric Organocatalysis 1*; List, B., Ed.; Georg Thieme Verlag: Stuttgart, 2012; pp 73–134. Selected examples of enamine catalysis in Mannich reactions leading to ketones: (b) Córdova, A.; Notz, W.; Zhong, G.; Betancort, J. M.; Barbas, C. F. *J. Am. Chem. Soc.* **2002**, *124*, 1842. (c) Yang, J. W.; Stadler, M.; List, B. *Angew. Chem., Int. Ed.* **2007**, *46*, 609.

(4) Selected enantioselective Mannich reactions with enol silanes/ketene silyl acetals: (a) Hagiwara, E.; Fujii, A.; Sodeoka, M. *J. Am. Chem. Soc.* **1998**, *120*, 2474. (b) Ferraris, D.; Young, B.; Dudding, T.; Lectka, T. *J. Am. Chem. Soc.* **1998**, *120*, 4548. (c) Wenzel, A. G.; Jacobsen, E. N. *J. Am. Chem. Soc.* **2002**, *124*, 12964. (d) Nakamura, Y.; Matsubara, R.; Kiyohara, H.; Kobayashi, S. *Org. Lett.* **2003**, *5*, 2481. (e) Kobayashi, S.; Arai, K.; Shimizu, H.; Ichori, Y.; Ishitani, H.; Yamashita, Y. *Angew. Chem., Int. Ed.* **2005**, *44*, 761. (f) Wang, Q.; Leutzsch, M.; van Gemmeren, M.; List, B. *J. Am. Chem. Soc.* **2013**, *135*, 15334.

(5) Selected enantioselective Mannich reactions with malonate esters: (a) Song, J.; Wang, Y.; Deng, L. *J. Am. Chem. Soc.* **2006**, *128*, 6048. (b) Song, J.; Shih, H.-W.; Deng, L. *Org. Lett.* **2007**, *9*, 603. (c) Hatano, M.; Horibe, T.; Ishihara, K. *Org. Lett.* **2010**, *12*, 3502. See also ref 6b. For a review, see: (d) Verkade, J. M. M.; van Hemert, L. J. C.; Quaedflieg, P. J. L. M.; Rutjes, F. P. J. T. *Chem. Soc. Rev.* **2008**, *37*, 29.

(6) Enantioselective Mannich reactions of  $\beta$ -keto esters with aromatic imines: (a) Lou, S.; Taoka, B. M.; Ting, A.; Schaus, S. E. *J. Am. Chem. Soc.* **2005**, *127*, 11256. (b) Tillman, A. L.; Ye, J.; Dixon, D. J. *Chem. Commun.* **2006**, 1191. (c) Ting, A.; Lou, S.; Schaus, S. E. *Org. Lett.* **2006**, *8*, 2003. (d) Kang, Y. K.; Kim, D. Y. *J. Org. Chem.* **2009**, *74*, 5734. (e) Hatano, M.; Horibe, T.; Ishihara, K. *J. Am. Chem. Soc.* **2010**, *132*, 56.

(7) Enantioselective Mannich reaction of  $\beta$ -keto esters with glyoxalate derived imine: Hamashima, Y.; Sasamoto, N.; Hotta, D.; Somei, H.; Umeyayashi, N.; Sodeoka, M. *Angew. Chem., Int. Ed.* **2005**, *44*, 1525.

(8) For reviews, see: (a) Zhang, S.; Wang, W. In *Catalytic Asymmetric Conjugate Reactions*; Córdova, A., Ed.; Wiley: Weinheim, 2010; pp 295–299. (b) Xu, L.-W.; Xia, C.-G. *Eur. J. Org. Chem.* **2005**, 633. For selected examples of this approach, see: (c) Taylor, M. S.; Zalatan, D. N.; Lerchner, A. M.; Jacobsen, E. N. *J. Am. Chem. Soc.* **2005**, *127*, 1313. (d) Lu, X.; Deng, L. *Angew. Chem., Int. Ed.* **2008**, *47*, 7710. (e) Ma, S.; Wu, L.; Liu, M.; Xu, X.; Huang, Y.; Wang, Y. *RSC Adv.* **2013**, *3*, 11498.

(9) Probst, N.; Madarász, A.; Valkonen, A.; Pápai, I.; Rissanen, K.; Neuvonen, A.; Pihko, P. M. *Angew. Chem., Int. Ed.* **2012**, *51*, 8495. In this study, we also established that the urea moiety provides cooperative assistance to the thiourea through intramolecular hydrogen bonds.

(10) For the seminal paper on cooperatively assisted urea–thiourea catalysts, see: Jones, C. R.; Pantoş, G. D.; Morrison, A. J.; Smith, M. D. *Angew. Chem., Int. Ed.* **2009**, *48*, 7391. In contrast to the original design, our catalyst uses a more rigid *trans*-1,2-aminoindanol linker, resulting in a more active catalyst (see ref 9 for details).

(11) Okino, T.; Hoashi, Y.; Takemoto, Y. *J. Am. Chem. Soc.* **2003**, *125*, 12672.

(12) (a) Ye, J.; Dixon, D. J.; Hynes, P. S. *Chem. Commun.* **2005**, 4481. (b) Vakulya, B.; Varga, S.; Csámpai, A.; Soós, T. *Org. Lett.* **2005**, *7*, 1967. (c) Li, B.-J.; Jiang, L.; Liu, M.; Chen, Y.-C.; Ding, L.-S.; Wu, Y. *Synlett* **2005**, 603.

(13) For example, cinchona alkaloid derived bifunctional catalysts typically afford lower yields and enantioselectivities with  $\beta$ -keto esters compared to malonate esters. See ref 6b. The differential reactivity and selectivity of malonate esters and  $\beta$ -keto esters has also been noted with metal enolates; see ref 5c.

(14) Aliphatic imines such as **2a** are prone to decomposition, and they cannot typically be purified by chromatography. See the Supporting Information for a discussion on the effect of additives.

(15) With a cyclic  $\beta$ -keto ester, the Mannich reaction gave the product **4u** in excellent dr but only moderate enantioselectivity. As such, the present catalyst system appears to be optimal for  $\beta$ -keto esters without an  $\alpha$  substituent. See the Supporting Information for details.

(16) Presumably, **2b** is less likely to generate an enecarbamate **5b** due to the presence of an exocyclic double bond to a 6-membered ring in **5b**. For a discussion, see: Brown, H. C.; Brewster, J. H.; Shechter, H. *J. Am. Chem. Soc.* **1954**, *76*, 467.

(17) The catalyst– $\beta$ -keto ester ion pair is expected to be more acidic than the corresponding ion pair with malonate esters, thus rendering this problem more acute with  $\beta$ -keto ester substrates.

(18) Terada, M.; Sorimachi, K. *J. Am. Chem. Soc.* **2007**, *129*, 292.

(19) Lewis acid promoted tautomerization and dimerization of aliphatic imines and enecarbamates: Kobayashi, S.; Gustafsson, T.; Shimizu, Y.; Kiyohara, H.; Matsubara, R. *Org. Lett.* **2006**, *8*, 4923.

(20) The methyl ketone moiety was cleaved via the Lieben iodoform reaction. See the Supporting Information for experimental details. Moutevelis-Minakakis, P.; Sinanoglou, C.; Loukas, V.; Kokotos, G. *Synthesis* **2005**, 933.



## II

# ORGANOCATALYSTS FOLD TO GENERATE AN ACTIVE SITE POCKET FOR THE MANNICH REACTION

by

Antti J. Neuvonen, Tamás Földes, Ádam Madarász, Imre Pápai and Petri M. Pihko

*ACS Catalysis*, **2017**, 7, 3284-3294.

DOI: 10.1021/acscatal.7b00336

Reprinted with permission  
from *ACS Catalysis*, **2017**, 7, 3284-3294. Copyright 2017 American Chemical  
Society.

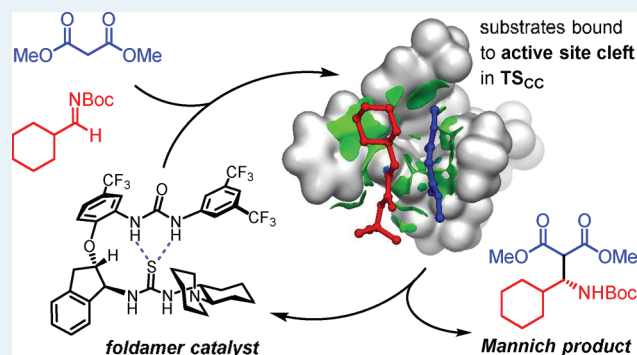
# Organocatalysts Fold To Generate an Active Site Pocket for the Mannich Reaction

Antti J. Neuvonen,<sup>†</sup> Tamás Földes,<sup>‡</sup> Ádám Madarász,<sup>‡</sup> Imre Pápai,<sup>\*,‡</sup> and Petri M. Pihko<sup>\*,†,‡</sup><sup>†</sup>Department of Chemistry and NanoScience Center, University of Jyväskylä, FI-40014 Jyväskylä yliopisto, Finland<sup>‡</sup>Research Center for Natural Sciences, Hungarian Academy of Sciences, Magyar tudósok körútja 2, H-1117 Budapest, Hungary

## Supporting Information

**ABSTRACT:** Catalysts containing urea, thiourea, and tertiary amine groups fold into a three-dimensional organized structure in solution both in the absence as well as in the presence of substrates or substrate analogues, as indicated by solution NMR and computational studies. These foldamer catalysts promote Mannich reactions with both aliphatic and aromatic imines and malonate esters. Hammett plot and secondary kinetic isotope effects provide evidence for the C–C bond forming event as the turnover-limiting step of the Mannich reaction. Computational studies suggest two viable pathways for the C–C bond formation step, differing in the activation modes of the malonate and imine substrates. The results show that the foldamer catalysts may promote C–C bond formation with an aliphatic substrate bearing a cyclohexyl group by enhanced binding of the substrates by dispersion interactions, but these interactions are largely absent with a simpler catalyst. Additional control experiments demonstrate the ability of simple thiourea catalysts to promote competing side reactions with aliphatic substrates, such as reversible covalent binding of the thiourea sulfur to the imine which deactivates the catalyst, and imine to enamine isomerization reactions. In foldamer catalysts, the nucleophilicity of sulfur is reduced, which prevents catalyst deactivation. The results indicate that the improved catalytic performance of foldamer catalysts in Mannich reactions may not be due to cooperative effects of intramolecular hydrogen bonds but simply due to the presence of the folded structure that provides an active site pocket, accommodating the substrate and at the same time impeding undesirable side reactions.

**KEYWORDS:** organocatalysis, bifunctional, cooperativity, mechanism, kinetics, computations, Mannich reaction



## INTRODUCTION

Enzymes bind their substrates into a characteristic active site cleft that contributes to binding and the remarkable degree of selectivity obtained in enzymatic catalysis.<sup>1</sup> In contrast, many organocatalysts are small molecules that do not appear to possess any folded active site cleft, yet they are often able to exhibit remarkable degrees of selectivity as well.<sup>2</sup>

We have previously described a family of urea–thiourea–tertiary amine catalysts (**1a–c** in Scheme 1) that appear to fold into a conformation with an active site pocket. These catalysts promote highly enantioselective Mannich reactions of malonates and  $\beta$ -keto esters with aromatic and aliphatic imines (Scheme 1).<sup>3</sup> In contrast to the prototype small-molecule bifunctional catalyst, Takemoto's thiourea–tertiary amine catalysts (**2a**),<sup>4</sup> these new catalysts readily accepted both aliphatic and aromatic imines as electrophiles in the Mannich reaction. The design of these catalysts was sparked by the seminal work of Smith, who showed that intramolecular hydrogen bonds between urea and thiourea groups lead to enhanced reactivity.<sup>5</sup> An alternative explanation for the higher activity of our catalysts is that the intramolecular hydrogen

bond generates a folded structure and an active site cleft in the catalyst. Such folding is not possible with catalyst **2a**.

Herein we show that these catalysts indeed form a well-defined folded structure in solution, even in the presence of substrates or substrate analogues. Furthermore, the most likely reason for the superiority of the new catalyst family is that the active site pocket, generated upon folding of the catalyst, allows additional stabilizing interactions with the substrates and facilitates the turnover-determining C–C bond formation step.

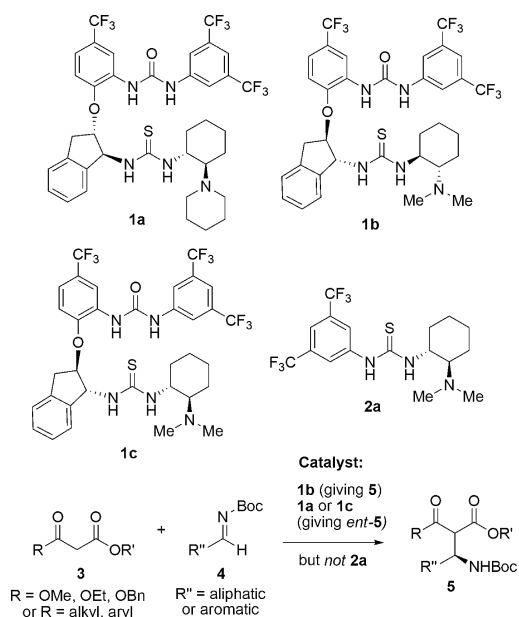
The dual activation modes of tertiary amine–thiourea bifunctional organocatalysts have previously been studied using both computational and experimental methods.<sup>6</sup> In addition, the H-bond donor ability of thioureas and other hydrogen-bonding catalysts have been studied by colorimetry by Kozłowski.<sup>7</sup> However, the folded, more complex nature of catalysts **1a–c** suggests that mechanistic lessons learned in previous studies should be complemented for these catalysts. To enable a more rational design of future catalysts, and to

Received: January 31, 2017

Revised: March 29, 2017

Published: March 30, 2017

### Scheme 1. Catalysts 1a–c and 2a and Their Contrasting Reactivity



expand the substrate scope, we undertook a combined experimental and computational mechanistic study of these new catalysts.

## RESULTS

### Conformational Analysis of Catalyst 1a in Solution.

We had previously established that catalyst 1b, or its diastereomer 1c, could fold into at least two completely different conformations with different anions (Figure 1).<sup>8</sup>

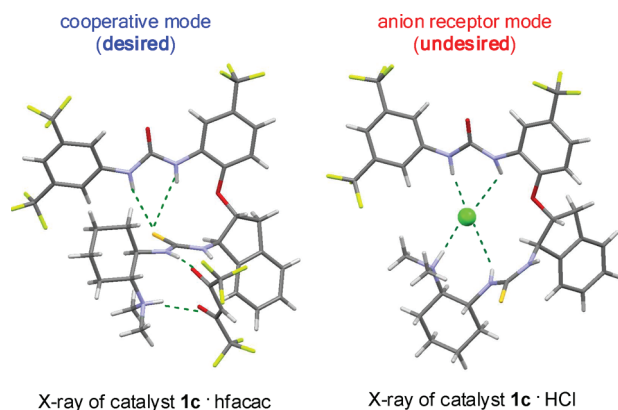


**Figure 1.** Comparison of X-ray structures of two different salts of catalyst 1c, showing that at least two possible folds are readily accessible.

The first conformation, corresponding to an intramolecularly hydrogen bonded structure, is observed when the catalyst forms a salt with a malonate surrogate, hexafluoroacetylacetonate (hfacac). The hfacac salt might be viewed as an analogue of the corresponding catalyst–malonate ion pair that likely forms in the Mannich reaction. The second conformation was observed in the HCl salt of 1c.<sup>3a</sup> These results, however, were obtained in the solid state.

To elucidate the major populated conformations in solution, a benzene-*d*<sub>6</sub> solution of catalyst 1a was studied by <sup>1</sup>H NMR

measurements. NOESY cross peaks in the free catalyst 1a in benzene (Figure 2) are consistent with the obtained crystal

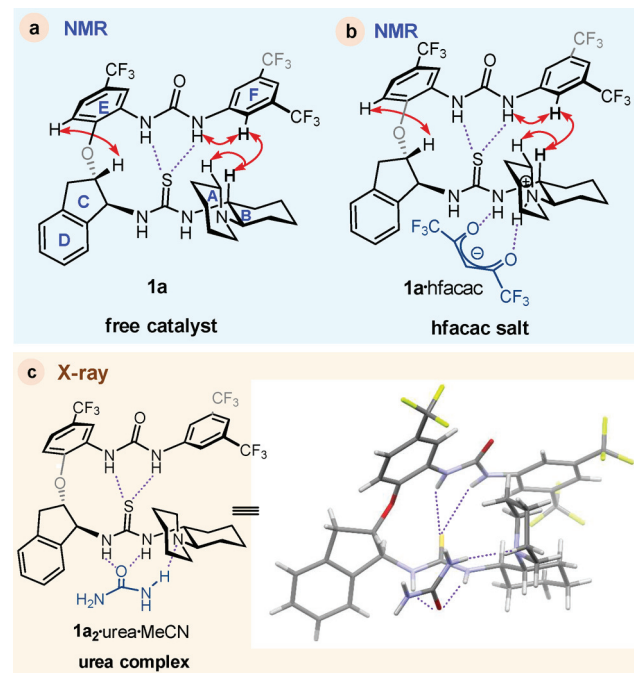


**Figure 2.** Structurally diagnostic 2D NOE cross peaks of (a) 1a and (b) 1a·hfacac in benzene-*d*<sub>6</sub> at 30 °C. (c) X-ray structure of 1a complexed with urea and MeCN (MeCN molecule omitted for clarity).

structure of the folded urea complex ((1a)<sub>2</sub>·urea·MeCN) of the catalyst (see the Supporting Information). Importantly, the same characteristic NOESY cross peaks were also observed in the spectrum of the hfacac salt of 1a in benzene. These NMR experiments thus established that the fold of the catalyst remains similar in both the free state and the catalytically relevant ion pair complex (assuming that the fold remains similar to the malonate salt and the hfacac salt). The presence of several close contacts in the structure indicates that the fold is tight, and the piperidine ring A as well as the indane (CD) and one of the aryl rings (E) can form the walls of a possible catalytic pocket (Figure 2).

Our computational analysis<sup>9</sup> provides further support for the preference of the folded structure of catalyst 1a. We find that the most stable form of 1a features an asymmetric double hydrogen bonding pattern between the urea and thiourea moieties with an additional intramolecular hydrogen bond formed between the tertiary amine and the adjacent NH group (see Figure 3). The unfolded structures (i.e., those without N–H···S hydrogen bonds) are all predicted to be at least 8 kcal/mol less stable than the most favored conformer.<sup>10</sup>

**Catalyst–Substrate Binary Complexes.** In the folded structure of catalyst 1a, the thiourea NH groups are easily accessible by the substrate molecules; therefore, the formation of binary complexes is expected. Computations were carried out for binary 1a–substrate systems relevant to our present mechanistic studies (Scheme 2).

Dimethyl malonate (3a) forms a multiply H bonded complex with 1a, as shown in Figure 4; however, the complexation is predicted to be slightly endergonic. In complex 1a·3a, one of the C–H bonds of the methylene group is oriented toward the

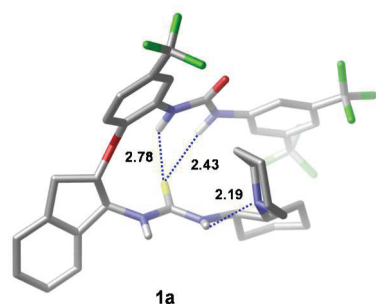


**Figure 3.** Most stable conformer of catalyst **1a** as predicted by DFT calculations. Internal hydrogen bonds are indicated by blue dotted lines (related distances are given in Å). Hydrogen atoms are omitted for clarity, except those of NH groups.

### Scheme 2. Substrates Used in the Computational Study of Binary Complexation

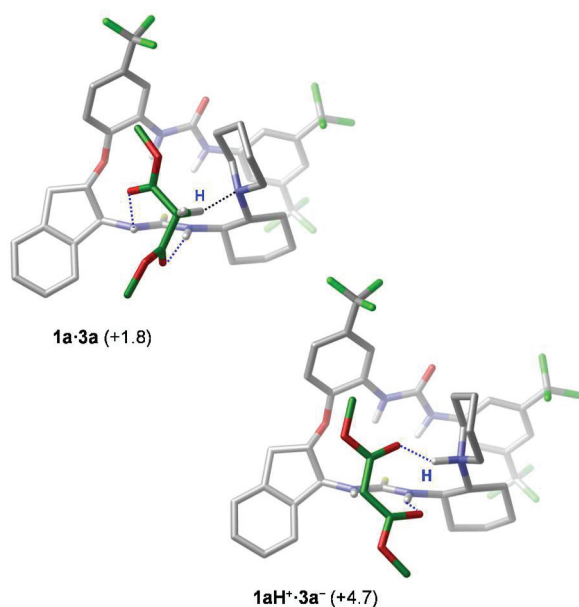
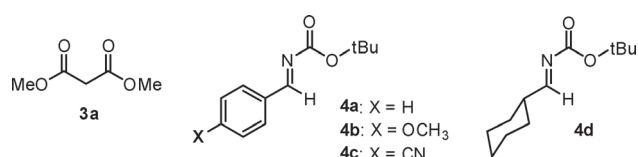


**Figure 4.** Binary complex **1a·3a** and the ion pair formed upon substrate deprotonation. Relative stabilities (in kcal/mol; with respect to **1a** + **3a**) are given in parentheses. For the sake of clarity, internal H bonds between urea and thiourea are not indicated. Most of the hydrogen atoms are not shown either (except those of NH groups and the  $\text{CH}_2$  of **3a** in **1a·3a**). Carbon atoms of the substrate are highlighted in dark green. The hydrogen involved in the proton shift is marked with a blue H.

basic center of the catalyst; thus, the malonate is structurally well prepared for deprotonation. The deprotonation occurs via a relatively low barrier (14.7 kcal/mol) and leads to an ion pair ( $1\text{aH}^+\cdot 3\text{a}^-$ ) lying at +4.7 kcal/mol in free energy.<sup>11</sup>

Various binding modes could be identified computationally for imine **4a**. In the most stable form, the imine binds via its N atom to thiourea (see Figure 5) and this **1a·4a** complex is practically isoenergetic with the dissociated state (**1a** + **4a**).<sup>12</sup> Para-substituted aromatic imines **4b,c** form very similar binary

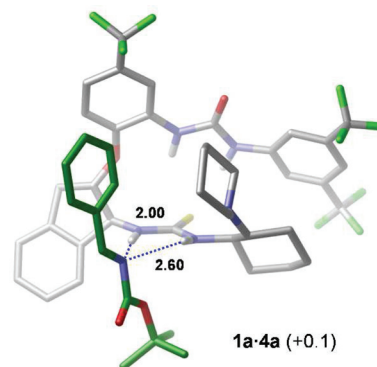


**Figure 5.** Most stable form of complex **1a·4a** and the ion pair formed upon substrate deprotonation. The relative stability (in kcal/mol; with respect to **1a** + **4a**) is given in parentheses.

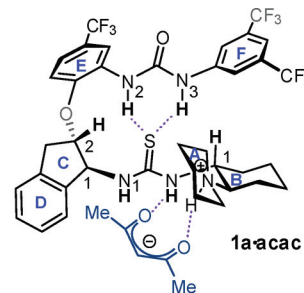
complexes with **1a**. The predicted stabilities (+0.3 and +1.9 kcal/mol, respectively) do not fully reflect the trend expected from the nature of the substituents, which is likely related to entropic effects.<sup>13</sup> An analogous binary complex formed with the aliphatic imine **4d** is found to be notably less stable (at +2.5 kcal/mol).

Our attempts to identify complexes with malonate **3a** and catalyst **1a** experimentally were not productive, which is in line with the computed thermodynamics. However, with acetylacetonate (acac), a more acidic  $\beta$ -dicarbonyl compound, small shifts were indeed observed in NMR titration experiments (Figure 6). More pronounced shifts were observed in NMR titrations with imine **4b**, indicating that the imine interacts with several key protons in the catalytic pocket of **1a** (see Figure 6).

**Competition Experiments.** To be able to directly compare the reactivity of aromatic and aliphatic *N*-Boc imines, we conducted a series of competition experiments using two foldamer bifunctional catalysts (**1a,b**), Takemoto catalyst (**2a**), and urea-Takemoto catalyst (**2b**) (Figure 7). In order to avoid problems associated with the imine isomerization, we selected

#### Shift at 5:1 ratio of acac:1a

$\text{H}_{\text{B}1}$  +0.04 ppm  
 $\text{H}_{\text{C}1}$  +0.02 ppm  
 $\text{H}_{\text{C}2}$  +0.08 ppm  
 $\text{H}_{\text{N}1}$  +0.32 ppm  
 $\text{H}_{\text{N}2}$  +0.05 ppm  
 $\text{H}_{\text{N}3}$  +0.04 ppm



#### Shift at 5:1 ratio of 4b:1a

$\text{H}_{\text{B}1}$  +0.14 ppm  
 $\text{H}_{\text{C}1}$  +0.11 ppm  
 $\text{H}_{\text{C}2}$  +0.19 ppm  
 $\text{H}_{\text{N}1}$  +~1.2 ppm  
 $\text{H}_{\text{N}2}$  +0.15 ppm  
 $\text{H}_{\text{N}3}$  +0.11 ppm

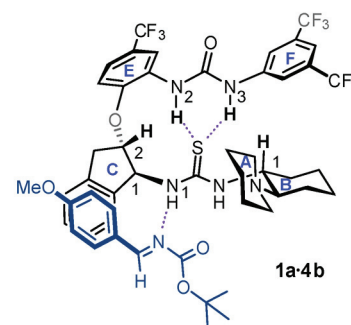


**Figure 6.** Summary of  $^1\text{H}$  NMR shifts observed when catalyst **1a** was titrated with (a) acetylacetonate (acac) or (b) imine **4b**.

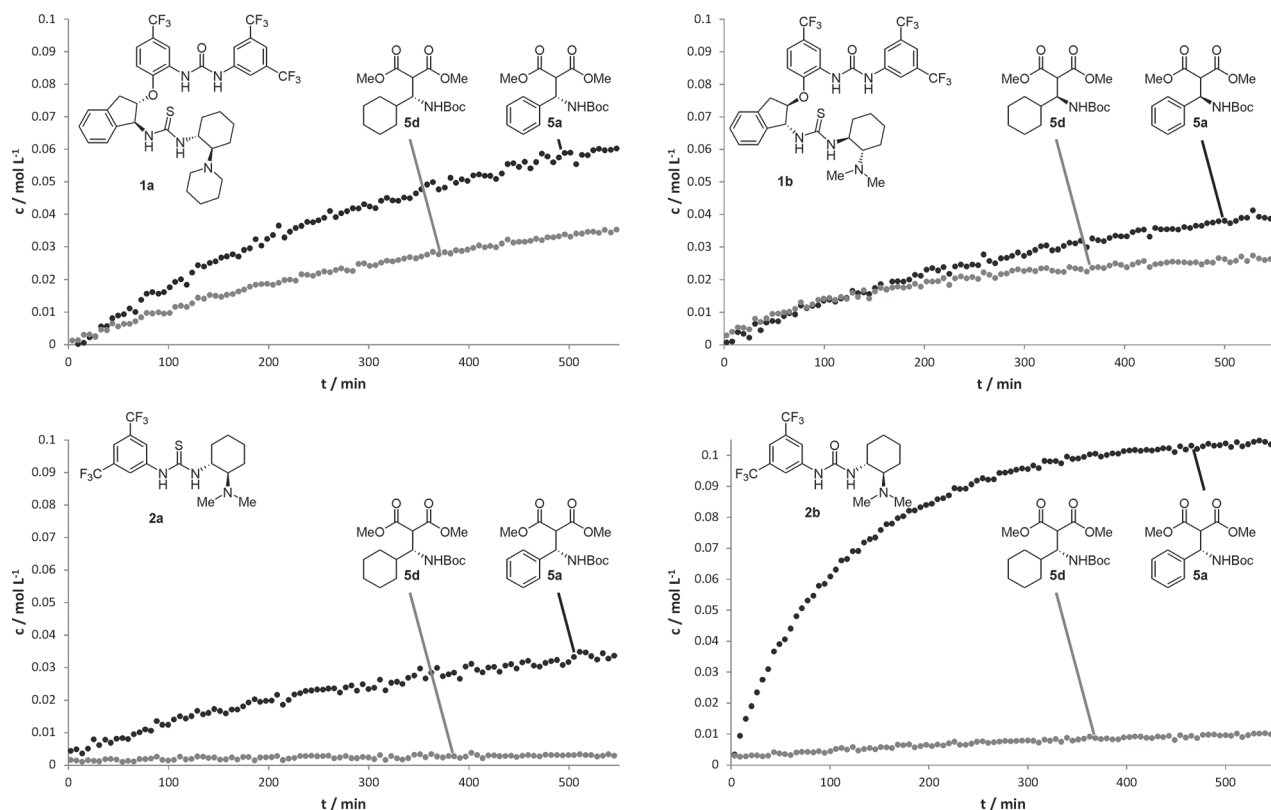


**Figure 7.** Mannich reaction progress curves in competition experiments between imines **4a** and **4d**. The product concentrations are plotted as a function of time relative to the internal standard. Reaction conditions: catalyst (10 mol %),  $[3a]_0 = 0.2$  M,  $[4a]_0 = 0.1$  M,  $[4d]_0 = 0.1$  M, [dibenzyl ether] = 0.2 M, benzene- $d_6$  at 30 °C.

the imine **4d** as the aliphatic imine since **4d** is less prone to isomerization side reactions than other aliphatic imines.<sup>14</sup> As expected, arylimine **4a** and aliphatic imine **4d** exhibited clearly different reactivities when Takemoto catalyst (**2a**) was used. Interestingly, the urea variant of **2a** (**2b**) displayed increased activity but maintained the clear reactivity difference between **4a** and **4d**. These graphs indicate that, for aromatic imine **4a**, the foldamer structure of the bifunctional catalysts **1a,b** provide only a slight rate acceleration in comparison to Takemoto catalyst; however, the reaction with aliphatic imine **4d** is catalyzed more efficiently by foldamer catalysts. Moreover, the foldamer catalyst **1b** gave similar initial rates for both aromatic and aliphatic imine.

We had already demonstrated the superiority of catalyst **1a** over **1b** in reactions with  $\beta$ -keto esters.<sup>3b</sup> Catalyst **1a** was also superior to catalyst **1b** in preparative experiments with dimethyl malonate (Table 1). Both catalysts provide excellent isolated

**Table 1.** Preparative Mannich Reaction Examples with Malonate using Foldamer Catalysts **1a,b**

catalyst	R	yield (%)	er
<b>1a</b>	Ph ( <b>4a</b> )	99	97.0:3.0
<b>1b</b>	Ph ( <b>4a</b> )	99	7.5:92.5
<b>1a</b>	c-hex ( <b>4d</b> )	99	>99.5:0.5
<b>1b</b>	c-hex ( <b>4d</b> )	95	1.0:99.0

yields regardless of the imine used. For both imines, catalyst **1a** gave better selectivity than catalyst **1b**. Especially in the case of aromatic imine **4a** the selectivity difference was significant.

**Kinetic Measurements.** We anticipated that a linear free-energy relationship, such as a Hammett plot (Figure 8), could clarify the rate-limiting step of the catalytic Mannich reaction. For example, if the rate is limited by the binding of the imine to

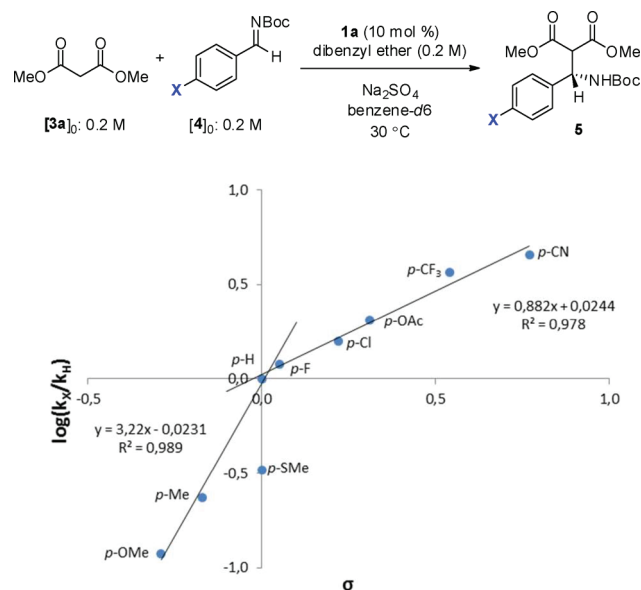


**Figure 8.** Hammett plot. *p*-SMe imine was omitted from the line fitting.



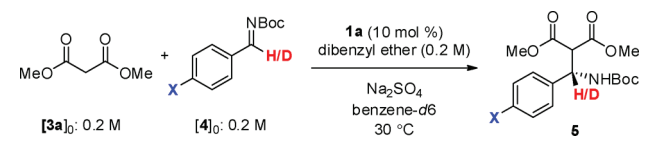
the catalyst, a negative reaction constant ( $\rho$ ) should be obtained. In contrast, with a rate-limiting C–C bond formation, the  $\rho$  value should be positive.

With nine para-substituted imines a clear positive Hammett correlation was observed; however, there was significant deviation from linearity.<sup>15</sup> In the Hammett plot, two subgroups were clearly distinguishable, the electron-rich and the electron-poor aromatic imines. For both the electron-donating ( $\rho = 3.22$ ;  $R^2 = 0.989$ ) and the electron-withdrawing ( $\rho = 0.882$ ;  $R^2 = 0.978$ ) substituents excellent correlations were obtained. This relatively small deviation from linearity does not support any profound change in the reaction mechanism but instead suggests a change in the energy profile of the reaction as the electronic properties of the imine are changed. With different imines, the relative stabilities of the complexes preceding the turnover-determining transition state may change, which would influence the reaction rate.

Nevertheless, the Hammett plot clearly suggests that the rate-determining step involves a transition state with increasing electron density at the imine carbon. Thus, initial binding of the imine, or final protonation of the intermediate, is unlikely to be rate-limiting. An internal rearrangement within the catalyst structure after the C–C bond formation event might, in theory, exhibit a positive  $\rho$  value. In order to rule out this possibility, a kinetic isotope effect study with deuterium-labeled imines was carried out.

KIE measurements were conducted by <sup>1</sup>H NMR reaction monitoring by comparing the reaction rates<sup>16</sup> with aromatic imines **4a–c** and **4a–c-d**<sub>1</sub> with dimethyl malonate in parallel experiments (Table 2). In all cases, a notable inverse secondary

Table 2. Kinetic Isotope Effect Measurements



X	rate <sub>0</sub> H (mM min <sup>-1</sup> )	rate <sub>0</sub> D (mM min <sup>-1</sup> )	KIE ( $k_H/k_D$ )
OMe ( <b>4b</b> )	0.0779	0.0865	0.90 ± 0.04
H ( <b>4a</b> )	0.499	0.552	0.90 ± 0.16
CN ( <b>4c</b> )	1.82	1.97	0.93 ± 0.07

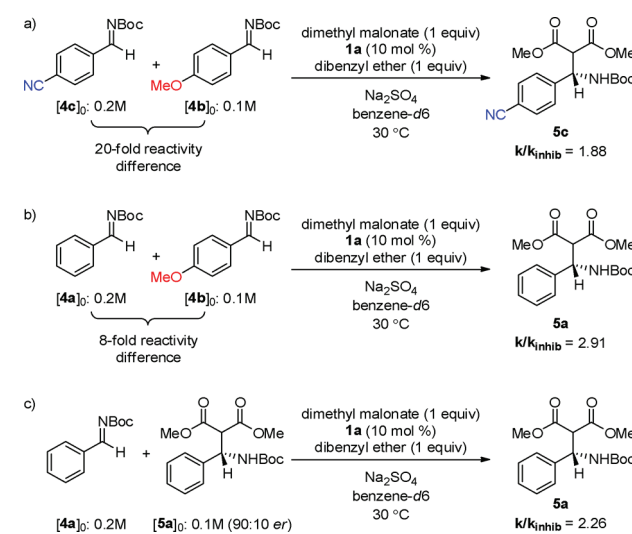
KIE (0.90–0.93) was observed. These KIEs are indicative of a change in the bonding environment (hybridization) of the imine carbon in the rate-determining step. Together with the Hammett plot data, these experiments strongly indicate that the C–C bond formation is rate-determining. An alternative rationalization for the KIEs, an inverse 2° equilibrium isotope effect<sup>17</sup> arising from the binding event of the imine, is not compatible with the results of the Hammett plot, which indicates that the rate-determining step involves an increase in the electron density of the imine carbon.

Further support for the C–C bond formation step as the rate-determining step could be obtained from a crossover experiment with the Mannich reaction product **5a** (0.2 M) and imine **4c** (0.2 M) in the presence of 10 mol % of catalyst **1a**. In this experiment, no crossover product was observed after 24 h, indicating that the C–C bond formation step is essentially irreversible.

**Inhibition and Complexation Experiments.** To clarify the importance of catalyst complexation with imines, we performed a kinetic experiment with *p*-CN benzaldimine (**4c**)

and a substoichiometric amount of *p*-OMe benzaldimine (**4b**) as a potent inhibitor (Scheme 3a). As the rate difference of

Scheme 3. Inhibition Experiments Carried Out with (a) **4c** and **4b**, (b) **4a** and **4b**, and (c) **4a** and **5a**



these imines in the Mannich reaction is over 20-fold, **4b** can be considered purely as an inhibitor. The presence of 50 mol % of **4b** retarded the Mannich reaction between *p*-CN benzaldimine (**4c**) and dimethyl malonate by a factor of 1.88. This inhibitory effect might result from a change in the turnover-determining intermediate (TDI) of the reaction.<sup>18</sup> With an electron-rich imine, such as **4b**, the complex with the catalyst could become the TDI.

In addition, **4b** (50 mol %) inhibited the Mannich reaction of **4a** by a factor of 2.91 (Scheme 3b). Although in this case the reactivity difference of the imines is only 8-fold, the Mannich reaction rate of **4b** was found to be negligible. These results further support the notion that competitive substrates retard the reaction by lowering the concentration of the productive complex, even if the interactions are weak (as evidenced by the NMR titration experiments).

Finally, product inhibition with product **5a** was also observed ( $k/k_{\text{inhib}} = 2.26$ , Scheme 3c), which justifies the need for an excess of imine to drive the reactions to completion.

**C–C Bond Formation Pathways.** The details of the C–C bond formation process in the present Mannich reactions were explored computationally for the reaction **3a** + **4a** promoted by foldamer catalyst **1a**. We considered several possible mechanistic scenarios for this step that involve different substrate activation modes, and we found two feasible reaction pathways as illustrated in Figure 9.

In route 1, the deprotonated dimethyl malonate is bound to the protonated amine and to the proximal NH group of thiourea, whereas the imine is activated via the distal NH group of the thiourea moiety of the catalyst. This type of substrate activation has already been described in our previous work,<sup>3a</sup> and it has also been identified as the most favored pathway for organocatalytic vinylogous Michael reaction of  $\alpha,\beta$ -unsaturated-butylolactam to chalcone.<sup>6e</sup> On the other pathway, in route 2, the deprotonated nucleophile is shifted to thiourea displaying double H-bonding interactions, and the electrophilic imine binds to the protonated amine unit via the carbonyl group of the Boc moiety.

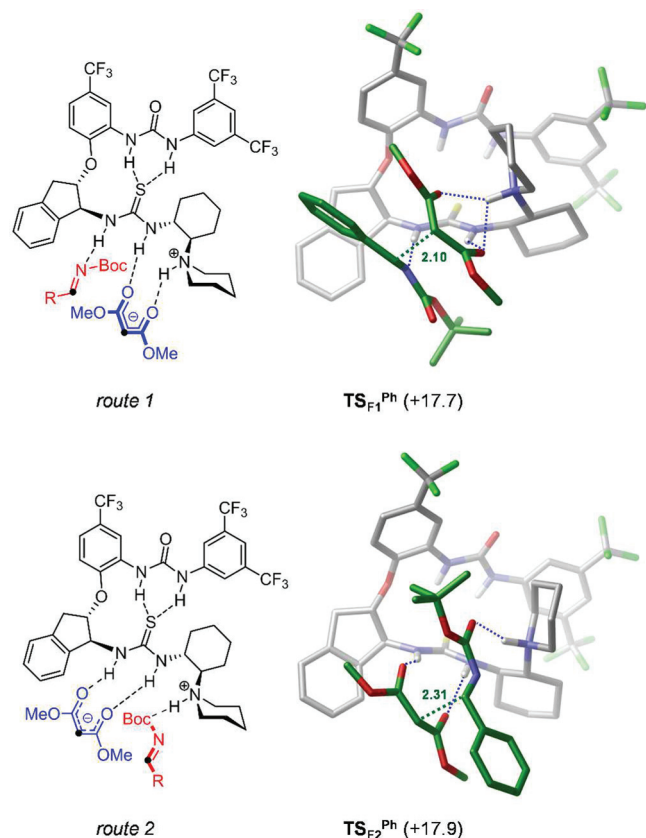


**Figure 9.** C–C bond formation pathways explored computationally for reaction **3a** + **4a** catalyzed by **1a**. In the schematic view, the carbon atoms involved in bond formation are labeled by black dots. Relative stabilities (solution phase Gibbs free energies with respect to reactant state **3a** + **4a** + **1a**; in kcal/mol) are given in parentheses. Hydrogen bonds formed between the substrates and the catalyst are indicated by blue dotted lines, whereas the developing C–C bond is illustrated by green dotted lines (related distances are given in Å). For clarity of images, hydrogen atoms are omitted, except those of NH groups.

The C–C bond formation transition states identified computationally on the two reaction pathways ( $\text{TS}_{\text{F1}}^{\text{Ph}}$  and  $\text{TS}_{\text{F2}}^{\text{Ph}}$  in Figure 9) represent very similar barriers with respect to the **3a** + **4a** + **1a** reactant state (17.7 and 17.9 kcal/mol, respectively), suggesting that both addition mechanisms might be operative in this particular reaction.<sup>19</sup> This finding may seem surprising, but it actually supports the view formulated recently in our previous work that the application of a single reactivity model might not always be sufficient to describe the mechanism of bifunctional noncovalent organocatalysis.<sup>20</sup>

To test the two mechanistic scenarios against experimental data, calculations were carried out for analogous reactions with para-substituted imines **4b,c** as well. We find that both C–C bond formation mechanisms account qualitatively for the observed reactivity trend. As shown in Table 3, the barriers predicted for the two pathways decrease gradually in the **4b**–**4a**–**4c** series, which is in line with the positive Hammett correlation. It is also apparent that computations predict nearly identical kinetic isotope effects for the two C–C bond formation pathways, all equal to or very close to 0.9, which are in reasonable agreement with the measured data (see Table 2). These results thus provide further support for the relevance of parallel reaction channels in this Mannich reaction.

**Table 3.** Computed Barriers ( $\Delta G^\ddagger$ ; in kcal/mol) and Kinetic Isotope Effects (KIE) for Reactions with Para-Substituted Aromatic Imines<sup>a</sup>

imine	R	route 1		route 2	
		$\Delta G^\ddagger$	KIE	$\Delta G^\ddagger$	KIE
<b>4b</b>	OMe	18.1	0.90	19.7	0.91
<b>4a</b>	H	17.7	0.90	17.9	0.90
<b>4c</b>	CN	15.5	0.92	17.5	0.92

<sup>a</sup>The barriers refer to reactions with nondeuterated imines.

**Comparative Analysis.** To gain insight into the origin of the unprecedented reactivity of foldamer catalysts in Mannich reactions with aliphatic aldimines, we performed a comparative computational analysis for reactions **3a** + **4a** and **3a** + **4d** catalyzed by bifunctional organocatalysts **1a** and **2a**. The computed barriers associated with the two C–C bond formation mechanisms are collected in Figure 10.

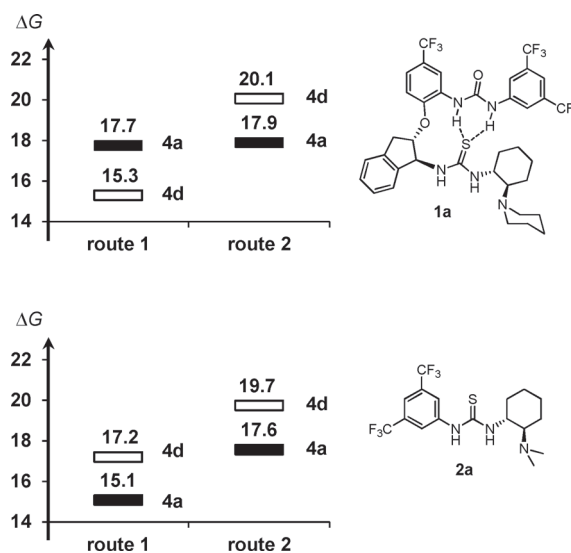


**Figure 10.** Computed C–C bond formation barriers (in kcal/mol) for reactions **3a** + **4a** (filled bars) and **3a** + **4d** (empty bars) promoted by catalysts **1a** and **2a**.

Note first that the foldamer catalyst **1a** offers a kinetically favored pathway for the reaction with aliphatic imine **4d** as well, since the barrier computed in route 1 is only 15.3 kcal/mol, which is actually lower than that computed for **4a**. On the other hand, route 2 becomes less accessible in this reaction, as expected from the increased barrier (20.1 kcal/mol). The free energy data obtained for analogous reactions catalyzed by the Takemoto catalyst **2a** reveal a different pattern in the diagram. The barriers in route 1 are found to be notably lower for both substrates, and the reaction with aromatic imine **4a** is predicted to be kinetically more favored in both reaction pathways.

Although these results corroborate the diverse catalytic effect of the two catalysts in the **3a** + **4a** and **3a** + **4d** reactions, and they point to an enhanced reactivity of **4d** with the foldamer catalyst, the computed barriers are not fully consistent with the results of competition experiments (Figure 2). The reactivity difference between **4a** and **4d** is reasonably well reproduced for the Takemoto catalyst, but computations seem to overestimate the reactivity of **4d** for the foldamer catalyst.<sup>21</sup> The quantitative discrepancy between the computed barriers and the observed

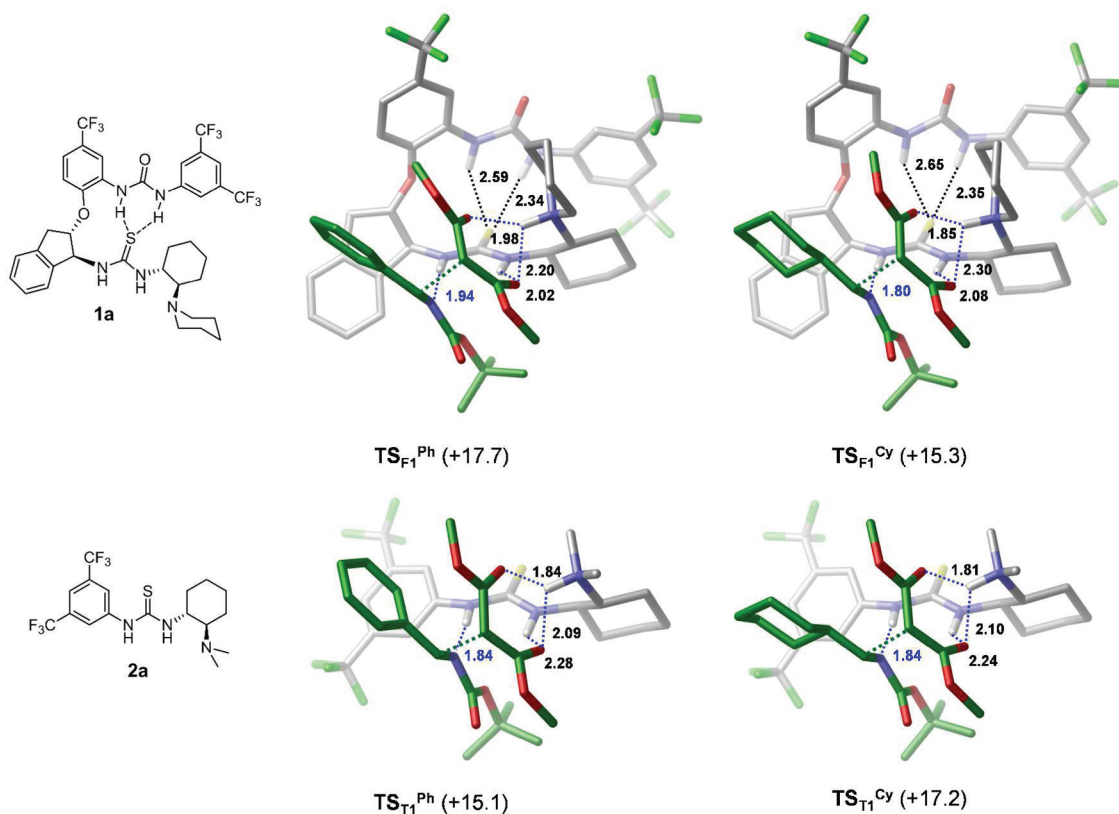


**Figure 11.** Bond distances (in Å) characteristic of H-bonding interactions in C–C bond formation transition states in route 1 in reactions 3a + 4a and 3a + 4d promoted by catalysts 1a (upper structures) and 2a (lower structures). Catalyst–substrate interactions are indicated in blue, and intramolecular urea–thiourea interactions are shown in black. Relative stabilities (in kcal/mol; with respect to reactants) are given in parentheses.

rates could be related to the inaccuracy of the applied computational method, which might be considerable, particularly for large molecular models involving the bulky catalyst 1a.<sup>22</sup>

In addition to computational errors, the apparent discrepancy might be due to mechanistic events beyond the C–C bond formation step; therefore, we examined the mechanism of reprotonation as well for the reaction 3a + 4a. This step involves a proton shift from the protonated amine unit of the catalyst to the N atom of the anionic adduct intermediate formed in the C–C bond formation step. We find that proton transfer occurs very easily in route 2 because the N atom of the adduct lies in close vicinity of the protonated amine (see TS<sub>F2</sub><sup>Ph</sup> in Figure 9).<sup>23</sup> In route 1, however, substantial structural rearrangement in the H-bonded network of this intermediate is required prior to proton transfer (see TS<sub>F1</sub><sup>Ph</sup> in Figure 9). This rearrangement and subsequent reprotonation is still facile with the Takemoto catalyst; however, it appears to be hindered with the bulky foldamer catalyst. The difference found for the two catalysts is clearly due to the presence of the urea side group in catalyst 1a, which imposes a restriction on intramolecular structural rearrangements needed for reprotonation. Potential energy scan calculations suggest that transition states of this multistep rearrangement process may lie above TS<sub>F1</sub><sup>Ph</sup>; thus, the 3a + 4a reaction may preferentially follow route 2 with catalyst 1a.<sup>24</sup> In the 3a + 4d reaction, the reprotonation step in route 1 is likely hindered as well, but this pathway could be still favored over route 2. It is therefore possible that the reactions with the two imines (4a and 4d) take place via two different pathways (route 2 and route 1, respectively) but with comparable rates. We recall that experimentally, in the reaction

with aromatic imines (4a–c), the C–C bond formation is clearly rate limiting, but the same may not hold true with aliphatic imine 4d. Unfortunately, a reliable KIE analysis could not be performed for imine 4d due to side reactions.

**Beneficial Role of the Foldamer Catalyst.** To provide further understanding of the beneficial effect of catalyst 1a on the C–C bond formation barrier for imine 4d, we analyzed the structures and the nature of interactions in transition states located in route 1 (see Figure 11).

We note first that the intramolecular hydrogen bonds between urea and thiourea in TS<sub>F1</sub><sup>Ph</sup> and TS<sub>F1</sub><sup>Cy</sup> are notably strengthened in comparison to the free foldamer catalyst (see Figure 3), which is evidence for the cooperativity, but these changes alone do not account for the improved reactivity for aliphatic imines. Cooperative effects amplify the acidity of the thiourea unit in foldamer catalysts,<sup>25</sup> which is likely beneficial for both aromatic and aliphatic imines; however, this does not translate to increased reactivity for aromatic imines, only for aliphatic imines.

In transition states involving the Takemoto catalyst (TS<sub>T1</sub><sup>Ph</sup> and TS<sub>T1</sub><sup>Cy</sup>) the binding of reacting partners is very similar, as indicated by the distances characteristic of H-bonding interactions (e.g., both imines form hydrogen bonds with a distance of 1.84 Å). In contrast, there are notable differences in these distances in transition states involving the foldamer catalyst 1a (TS<sub>F1</sub><sup>Ph</sup> and TS<sub>F1</sub><sup>Cy</sup>), and they show a more compact binding for aliphatic imine 4d. For instance, the N–H...N hydrogen bond associated with the activation of imine 4d is significantly elongated in TS<sub>F1</sub><sup>Ph</sup> and it is shorter in TS<sub>F1</sub><sup>Cy</sup> (1.94 and 1.80 Å, respectively). The longer N–H...N hydrogen bond in TS<sub>F1</sub><sup>Ph</sup> is consistent with the trend obtained for relative

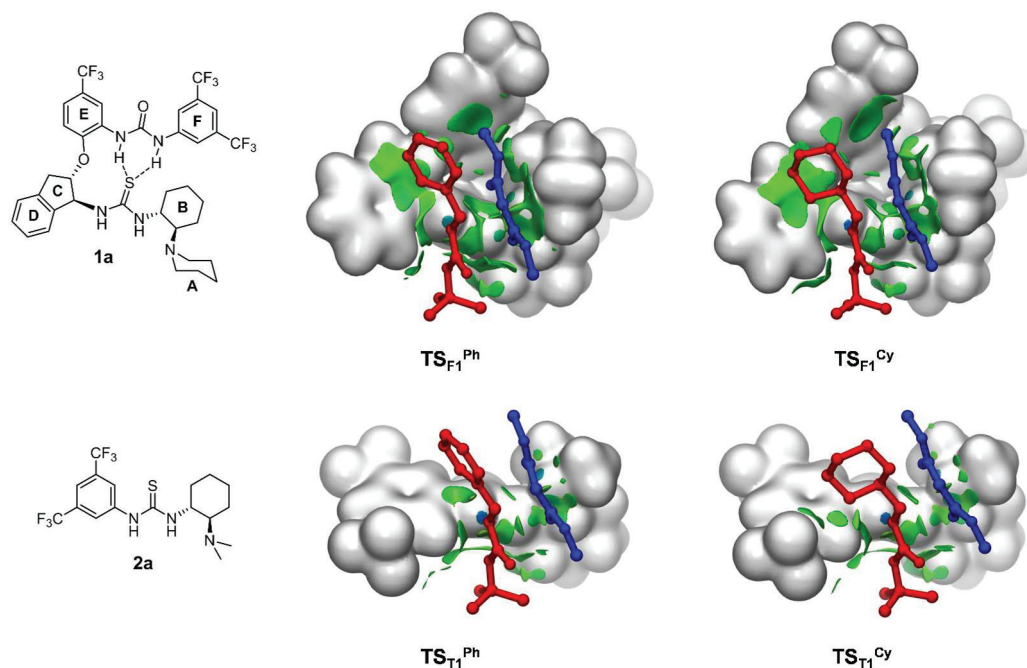


**Figure 12.** Noncovalent contacts in C–C bond formation transition states in route 1 in reactions **3a** + **4a** and **3a** + **4d** promoted by catalysts **1a** (upper structures) and **2a** (lower structures). The protonated catalyst is represented via an isodensity surface ( $\rho = 0.01$  au); imines **4a,d** are highlighted in red and malonate **3a** is shown in blue. Green regions represent weak noncovalent interactions as obtained from NCI analysis. The applied cutoff for reduced density gradient is  $s = 0.3$  au.

stabilities of the transition states and suggests that the foldamer catalyst cannot accommodate aromatic imines as efficiently as aliphatic imines into the catalytic pocket.

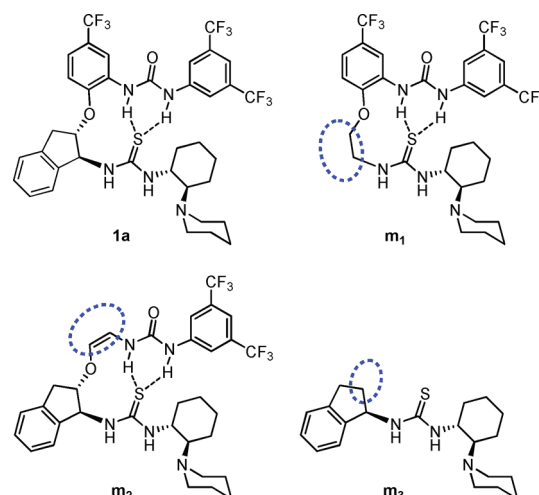
Figure 12 shows another representation of the four transition states and highlights the differences in noncovalent interactions between the catalyst and the evolving adduct species. It is apparent that the Ph/Cy groups of the imines and the Me substituents of dimethyl malonate have practically no contact with catalyst **2a**, but these groups do interact with various parts of catalyst **1a**. The presence of the urea side group in catalyst **1a** provides a well-defined binding pocket for the reacting substrates, which induces selectivity with respect to imine substitution. The cyclohexyl moiety of **4d** seems to accommodate more favorably into this pocket than the flat and more rigid phenyl group of **4a**, presumably because the more flexible cyclohexyl ring can bend and fit in the binding pocket generated by rings C–E of the catalyst. This is also visible from the more extended contact surface in  $TS_{F1}^{Cy}$ . The longer N–H...N distance in  $TS_{F1}^{Ph}$  in comparison to  $TS_{F1}^{Cy}$  (and also in comparison to  $TS_{T1}^{Ph}$ ) implies destabilizing steric hindrance.

The role of the urea side group in catalytic selectivity was further analyzed by calculations carried out for model catalysts derived from **1a** (Scheme 4).

C–C bond formation transition states analogous to  $TS_{F1}^{Ph}$  and  $TS_{F1}^{Cy}$  were computed for each model. The barriers related to the identified transition states are given in Table 4.

As reported above, the barriers computed for imines **4a,d** with the original catalyst (**1a**) are 17.7 and 15.3 kcal/mol, respectively, giving  $\Delta\Delta G = -2.4$  kcal/mol as a difference. The presence of the indene ring and the neighboring  $CF_3$ -substituted phenyl group appears to be important in getting enhanced reactivity with **4d**, because without these groups (models **m<sub>1</sub>** and **m<sub>2</sub>**) the computed  $\Delta\Delta G$  is close to 0 (similar barriers for **4a,d**). The elimination of the entire urea side group

#### Scheme 4. Model Catalysts Derived from **1a**<sup>a</sup>



<sup>a</sup>Units altered with respect to the original catalyst are highlighted in blue.

**Table 4.** Computed Barriers and Their Differences Obtained for Model Catalysts<sup>a</sup>

catalyst	$\Delta G^{Ph}$	$\Delta G^{Cy}$	$\Delta\Delta G = \Delta G^{Cy} - \Delta G^{Ph}$
<b>1a</b>	17.7	15.3	−2.4
<b>m<sub>1</sub></b>	18.5	18.6	+0.1
<b>m<sub>2</sub></b>	17.9	18.3	+0.4
<b>m<sub>3</sub></b>	19.9	21.1	+1.2
no cat.	11.8	14.9	+3.1 <sup>b</sup>

<sup>a</sup> $\Delta G^{Ph}$  and  $\Delta G^{Cy}$  refer to barriers computed for aromatic and aliphatic imines (**4a** and **4d**). <sup>b</sup>In the absence of catalyst, the barriers are computed relative to the  $3a^-$  + imine state.

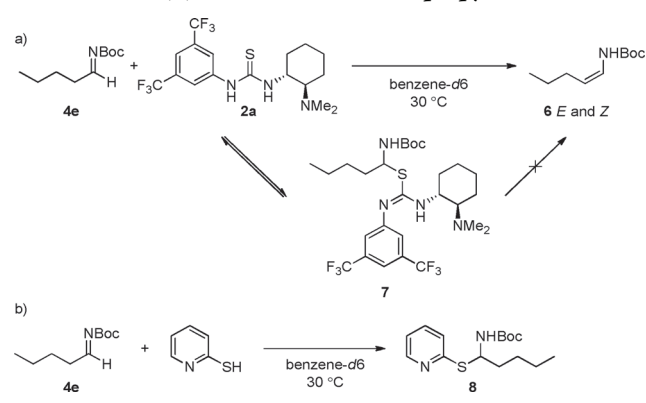
(model **m**<sub>3</sub>) gives  $\Delta\Delta G = +1.2$  kcal/mol; therefore, the catalysis becomes less efficient for the aliphatic imine similarly to that with Takemoto catalyst **2a** (for which  $\Delta\Delta G = +2.1$  kcal/mol). We note that, in the absence of catalyst, the C–C bond formation is clearly favored for the aromatic imine ( $\Delta\Delta G = +3.1$  kcal/mol).<sup>26</sup>

Our computational analysis thus suggests that the improved catalytic performance of foldamer catalysts in Mannich reactions with aliphatic imines cannot be explained solely by the cooperative effects of intramolecular H-bonding interactions between urea and thiourea, although cooperativity is clearly evident in the shortening of the intramolecular H bonds in the transition states. The structural fit of the substrates to the binding pocket of the folded structure appears to be better with the aliphatic imines, and this also contributes to their higher reactivity.

#### Catalyst Deactivation and Substrate Isomerization.

To further rationalize the differences between the catalysts **1a** and **2a**, we examined whether the aliphatic imines might suffer additional disadvantages with catalyst **2a** that are not present with **1a**. We were especially concerned about potential side reactions, which were investigated by using the less hindered and more reactive imine **4e** (Scheme 5).

#### Scheme 5. Deactivation of Catalyst **2a**: (a) Isomerization of Imine **4e** and (b) Addition of 2-Mercaptopyridine to **4e**



Indeed, we observed isomerization of the imine **4e** to the enamine (**6**) form with catalyst **2a** (Scheme 5). This isomerization leads to low conversion, as the isomerization is irreversible under the reaction conditions. Previously, Takemoto and co-workers have noted that problems with the bifunctional thiourea catalysts<sup>27</sup> can be avoided if the highly nucleophilic thiourea moiety is replaced with a less nucleophilic H-bond donor.<sup>28</sup>

The effect of the catalysts on the isomerization reaction was studied in more detail by <sup>1</sup>H NMR monitoring (Scheme 5a). Mixing an aliphatic imine **4e** and catalyst **2a** in a 1:1 ratio in benzene led to the immediate disappearance of the imine-related peaks. In addition, most of the catalyst had formed the new species **7**, which was stable enough to be detected on the <sup>1</sup>H NMR time scale. The degradation of this new species was directly related to formation of the enamines **6** and also to an increase in the catalyst peak integrals.

Mixing imine **4e** with 2-mercaptopyridine resulted in a stable product (**8**) that could be fully characterized with NMR (Scheme 5b; see the Supporting Information). <sup>1</sup>H, <sup>13</sup>C, COSY, and HMQC measurements were all consistent with a 1,2-addition product of 2-mercaptopyridine to imine **4e**. The

stability of this product implies that the amine base in the Takemoto catalyst is necessary for the adduct to decompose.

When the isomerization experiment was conducted with 20 mol % of **2a**, the isomerization process was sluggish, as only 73% conversion was obtained after 2 h (Table 5). However, a

**Table 5. Isomerization of Aliphatic Imine with Bifunctional Organocatalysts**

catalyst	conversion (%)	time (min)	E:Z
<b>1a</b>	80	120	1:1.5
<b>1b</b>	100	<8	3.8:1
<b>2a</b>	73	120	1:1.2
<b>2b</b>	97	40	1:1.8
Et <sub>3</sub> N	6	120	1:2.1

urea version of the Takemoto catalyst (**2b**) was more effective in the isomerization process, while no covalently bound species could be observed in the <sup>1</sup>H NMR spectra.

Catalyst **2b** also produced the enamine in higher *Z* selectivity in comparison to the Takemoto catalyst. Surprisingly, the foldamer catalyst **1b** was found to be the most effective in the isomerization of the imine to the enamine, implying that the isomerization process is favored by stronger H-bond donors. In addition, the selectivity for the double bond was inverted to favor the *E* enamine. With the bulkier piperidine catalyst **1a** the rate of isomerization was much slower than that with the *N*-dimethylamine foldamer catalyst (**1b**) and the *E*:*Z* selectivity was also close to those obtained with **2a,b**. These results demonstrate that blocking the sulfur atom of the catalyst by the foldamer structure does not solve the isomerization problem.

Overall, the deactivation and isomerization experiments suggest that the reactivity difference between the foldamer catalysts **1a,b** and Takemoto catalyst **2a** could at least partially be attributed to the nucleophilicity of the sulfur atom in **2a**, resulting in fast but reversible deactivation of the catalyst by an aliphatic imine such as **4e**. In catalysts **1a,b**, the intramolecular hydrogen bonds and the folding may completely block the nucleophilic attack of the thiourea sulfur and thus prevent deactivation of the catalyst. Isomerization of the imine appears to be a side reaction that is common to all catalysts. A control experiment with triethylamine showed that aliphatic imines are relatively stable under moderately basic non-nucleophilic conditions. The imine to enamine isomerization appears to require the presence of H-bond donors in the catalyst.

## CONCLUSIONS

The folded structure of the foldamer urea–thiourea–tertiary amine catalyst **1a** was confirmed by solution NMR, solid-state X-ray, and computational analyses, both in the free state as well as as a complex with the imine substrate or in an intramolecular salt form with substrate analogues (acac or hfacac). In all cases, evidence for the folded structure could be readily inferred from the structural data.

In competition experiments, aliphatic imine **4d** and aromatic imine **4a** reacted at comparable rates with dimethyl malonate when the foldamer catalysts **1a,b** were used. In contrast, with **2a** and its urea variant **2b**, **4d** reacted very slowly in comparison to **4a**.

The Hammett plot and the secondary kinetic isotope effects measured for the Mannich reaction with aromatic imines supported a mechanism where the C–C bond forming event is the turnover-limiting step. Computational studies revealed two viable C–C bond formation pathways in these reactions, route 1 and route 2, that differ in the alternate activation modes of the malonate and imine substrates. For aliphatic imine **4d** bearing a cyclohexyl group, route 1 allows a kinetically favored C–C bond formation process as well, which is found to be a unique feature of foldamer catalyst **1a**. For reactions with Takemoto catalyst, computations predict significantly reduced reactivity of **4d** in comparison to aromatic imines **4a–c**, which is in line with experimental observations. Our computational analysis suggests that, in addition to H-bonding interactions, the foldamer catalyst can further facilitate the C–C bond formation via dispersion forces provided by the catalyst's binding pocket. These stabilizing noncovalent interactions are scarcely present in C–C bond formation transition states with simpler thiourea–tertiary amine catalysts. These differences may explain the improved performance of the foldamer catalyst with aliphatic imines.

The folded structure of catalysts **1a,b** also helps to block the nucleophilicity of the thiourea sulfur atom, preventing catalyst deactivation via nucleophilic attack to imines. This provides an additional reason for the improved catalytic performance of the foldamer catalysts in the Mannich reactions with aliphatic imines.

In summary, the results obtained herein point to the importance of the folded structure with an active site cleft, in contrast to cooperative effects associated with the intramolecular hydrogen bond, as the explanation for the enhanced reactivity of foldamer catalysts **1a,b** with aliphatic imines.

## ■ ASSOCIATED CONTENT

### Supporting Information

The Supporting Information is available free of charge on the ACS Publications website at DOI: 10.1021/acscatal.7b00336.

Experimental procedures, additional experiments pertaining to the mechanism, characterization data, and computational details (PDF)

NMR spectra and GC chromatograms (PDF)

Crystallographic data (CIF)

## ■ AUTHOR INFORMATION

### Corresponding Authors

\*E-mail for I.P.: papai.imre@ttk.mta.hu.

\*E-mail for P.M.P.: petri.pihko@jyu.fi.

### ORCID

Petri M. Pihko: 0000-0003-0126-0974

### Notes

The authors declare no competing financial interest.

## ■ ACKNOWLEDGMENTS

Financial support from the Academy of Finland (project #259532), University of Jyväskylä (postgraduate fellowship to A.J.N.), and the Hungarian Scientific Research Fund (OTKA, grant K-112028) are gratefully acknowledged. Computer facilities provided by the NIIF HPC Hungary (project 85708 kataproc) is also acknowledged. We thank Dr. Élina Kalenius and Ms. Johanna Lind for assistance with mass spectrometry and Mr. Esa Haapaniemi for NMR assistance.

## ■ REFERENCES

- (1) For related discussions, see: (a) Frey, P. A.; Hegeman, A. D. *Enzymatic Reaction Mechanisms*; Oxford University Press: Oxford, U.K., 2007. (b) Petsko, G. A.; Ringe, D. In *Protein Structure and Function*; New Science Press: London, 2004.
- (2) For reviews, see: (a) Pihko, P. M.; Rahaman, H., Bifunctional Acid-Base Catalysts. In *Enantioselective Organocatalyzed Reactions 1*; Mahrwald, R., Ed.; Springer: Heidelberg, Germany, 2011; pp 185–207. (b) Takemoto, Y.; Inokuma, T. Bifunctional Thiourea Catalysts. In *Asymmetric Synthesis II: More Methods and Applications*; Christmann, M.; Bräse, S., Eds.; Wiley-VCH: Weinheim, Germany, 2012; pp 233–237. (c) Claraz, A.; Siitonen, J. H.; Pihko, P. M. Iminium catalysis. In *Lewis Base Catalysis in Organic Synthesis*; Vedejs, E., Denmark, S., Eds.; Wiley-VCH: Weinheim, Germany, 2016; Vol. 2, pp 805–856.
- (3) (a) Probst, N.; Madarász, Á.; Valkonen, A.; Pápai, I.; Rissanen, K.; Neuvonen, A.; Pihko, P. M. *Angew. Chem., Int. Ed.* **2012**, *51*, 8495–8499. (b) Neuvonen, A. J.; Pihko, P. M. *Org. Lett.* **2014**, *16*, 5152–5155.
- (4) (a) Okino, T.; Hoashi, Y.; Takemoto, Y. *J. Am. Chem. Soc.* **2003**, *125*, 12672–12673. (b) Okino, T.; Hoashi, Y.; Furukawa, T.; Xu, X.; Takemoto, Y. *J. Am. Chem. Soc.* **2005**, *127*, 119–125.
- (5) (a) Jones, C. R.; Pantoş, G. D.; Morrison, A. J.; Smith, M. D. *Angew. Chem., Int. Ed.* **2009**, *48*, 7391–7394. (b) So, S. S.; Burkett, J. A.; Mattson, A. E. *Org. Lett.* **2011**, *13*, 716–719. (c) A recent review on the topic: Auvil, T. J.; Schafer, A. G.; Mattson, A. E. *Eur. J. Org. Chem.* **2014**, *2014*, 2633–2646.
- (6) (a) Hamza, A.; Schubert, G.; Soós, T.; Pápai, I. *J. Am. Chem. Soc.* **2006**, *128*, 13151–13160. (b) Hammar, P.; Marcelli, T.; Hiemstra, H.; Himoto, F. *Adv. Synth. Catal.* **2007**, *349*, 2537–2548. (c) Almasi, D.; Alonso, D. A.; Gómez-Bengoa, E.; Nájera, C. *J. Org. Chem.* **2009**, *74*, 6163–6168. (d) Tan, B.; Lu, Y.; Zeng, X.; Chua, P. J.; Zhong, G. *Org. Lett.* **2010**, *12*, 2682–2685. (e) Zhu, J.-L.; Zhang, Y.; Liu, C.; Zheng, A.-M.; Wang, W. *J. Org. Chem.* **2012**, *77*, 9813–9825. (f) Han, X.; Lee, R.; Chen, T.; Luo, J.; Lu, Y.; Huang, K. W. *Sci. Rep.* **2013**, *3*, 2557. (g) Azuma, T.; Kobayashi, Y.; Sakata, K.; Sasamori, T.; Tokitoh, N.; Takemoto, Y. *J. Org. Chem.* **2014**, *79*, 1805–1817. (h) Žabka, M.; Šebesta, R. *Molecules* **2015**, *20*, 15500. (i) Grayson, M. N.; Houk, K. N. *J. Am. Chem. Soc.* **2016**, *138*, 1170–1173.
- (7) (a) Huynh, P. N. H.; Walvoord, R. R.; Kozłowski, M. C. *J. Am. Chem. Soc.* **2012**, *134*, 15621–15623. (b) Walvoord, R. R.; Huynh, P. N. H.; Kozłowski, M. C. *J. Am. Chem. Soc.* **2014**, *136*, 16055–16065.
- (8) X-ray structure of **1b** and its hfacac salt have been published in ref 3a.
- (9) In our computational analysis, most of the DFT calculations (geometry optimizations, vibrational analysis, estimation of solvent effects) were carried out at the M06-2X/6-311G(d,p) level of theory. For each located structure, we carried out additional single-point energy calculations using the same functional along with the larger 6-311++G(3df,3pd) basis set. The reported energetics refers to relative solution-phase Gibbs free energies (with benzene as a solvent). For further details, see the Supporting Information.
- (10) For details of the conformational analysis, see the Supporting Information.
- (11) For the corresponding transition state, see the Supporting Information. The experimentally observed ion pair complex formed between catalyst **1a** and hfacac is predicted to be 10.4 kcal/mol more stable than the reactant state.
- (12) Two different O-coordinated structures of complex **1a·4a** were also identified computationally, both lying about 2 kcal/mol higher than the N-coordinated form.
- (13) Entropic loss appears to be more important upon the coordination of the methoxy-substituted imine **4b** (rotational degrees of freedom of the OMe group are constrained in the **1a·4b** complex). The expected stability trend is well reproduced in terms of the binding energies computed from the electronic energies (–20.9, –19.5, and –18.5 kcal/mol for the **4b**, **4a**, and **4c** series, respectively).
- (14) Formation of exocyclic double bonds to a six-membered ring is known to be less favorable than acyclic double bonds, and as such isomerization to form the enamine is disfavored with **4d** in comparison

to other aliphatic imines. For a discussion see: Brown, H. C.; Brewster, J. H.; Shechter, H. J. *Am. Chem. Soc.* **1954**, *76*, 467–474.

(15) See the [Supporting Information](#) for details about rate measurements and initial rate determination.

(16) The reaction progress was followed by  $^1\text{H}$  NMR, and the data obtained were analyzed by linear regression of first measurement points: i.e., the method of initial rates. See the [Supporting Information](#) for details.

(17) Gajewski, J. J.; Ngermmeesri, P. *Org. Lett.* **2000**, *2*, 2813–2815.

(18) For the basic concepts of the energetic span model, see: Kozuch, S.; Shaik, D. *Acc. Chem. Res.* **2011**, *44*, 101–110.

(19) Although the analysis of stereoselectivity was not the main focus of the present study, we examined possible pathways toward the minor enantiomeric product as well. The most favored transition state corresponds to the activation mode of route 1 lying at 25.8 kcal/mol in free energy, implying that the sense and high degree of enantioselectivity are reproduced by computations (for details, see the [Supporting Information](#)).

(20) Kótai, B.; Kardos, G.; Hamza, A.; Farkas, V.; Pápai, I.; Soós, T. *Chem. - Eur. J.* **2014**, *20*, 5631–5639.

(21) On the basis of the results of competition experiments (see [Figure 2](#)), one expects a similar or slightly lower barrier for reaction with aromatic imine **4a**.

(22) Test calculations carried out with the  $\omega\text{B97X-D}$  functional give similar trends for the C–C bond formation barriers, suggesting that the discrepancy is probably not related to the choice of the approximated energy functional (for details, see the [Supporting Information](#)).

(23) C–C bond formation transition states and subsequent adduct intermediates show a close structural resemblance (for details, see the [Supporting Information](#)).

(24) The adequate description of the full pathway from the ion pair intermediate formed in route 1 to the reprotonation transition state is challenging for the large model used herein, because the structural rearrangement likely involves several steps. In our present work, we performed potential energy scan calculations using a single structural parameter: namely the distance between the adduct N atom and the H atom of the protonated amine. This simple approach can provide only an upper limit for the barrier of structural rearrangement.

(25) Computations predict very similar acidities of thiourea in catalysts **1a** and **2a**. Despite the aliphatic nature of the indene linker in **1a**, the  $\text{p}K_{\text{a}}$  of the N–H group that binds the imine in route 1 is computed to be only 1.1 unit higher than that in **2a**. For acidity enhancement via internal activation, see: Couch, E. D.; Auvil, T. J.; Mattson, A. E. *Chem. - Eur. J.* **2014**, *20*, 8283–8287.

(26) The barriers computed in the absence of catalyst are low because they do not involve the deprotonation and catalyst binding processes, which are both endergonic.

(27) Xu, X.; Yabuta, T.; Yuan, P.; Takemoto, Y. *Synlett* **2006**, 0137–0140.

(28) (a) Inokuma, T.; Furukawa, M.; Uno, T.; Suzuki, Y.; Yoshida, K.; Yano, Y.; Matsuzaki, K.; Takemoto, Y. *Chem. - Eur. J.* **2011**, *17*, 10470–10477. (b) Inokuma, T.; Furukawa, M.; Suzuki, Y.; Kimachi, T.; Kobayashi, Y.; Takemoto, Y. *ChemCatChem* **2012**, *4*, 983–985. (c) Xiao, H.; Kobayashi, Y.; Takemoto, Y.; Morokuma, K. *ACS Catal.* **2016**, *6*, 2988–2996.



### III

## DYNAMIC REFOLDING OF ION-PAIR CATALYSTS IN RESPONSE TO DIFFERENT ANIONS

by

Antti J. Neuvonen, Dimitris Noutsias, Filip Topić, Kari Rissanen, Tamás Földes,  
Imre Pápai and Petri M. Pihko

*The Journal of Organic Chemistry*, **2019**, 84, 15009–15019

DOI: 10.1021/acs.joc.9b01980

Reprinted with permission  
from *The Journal of Organic Chemistry*, **2019**, 84, 15009–15019. Copyright 2019  
American Chemical Society.



# Dynamic Refolding of Ion-Pair Catalysts in Response to Different Anions

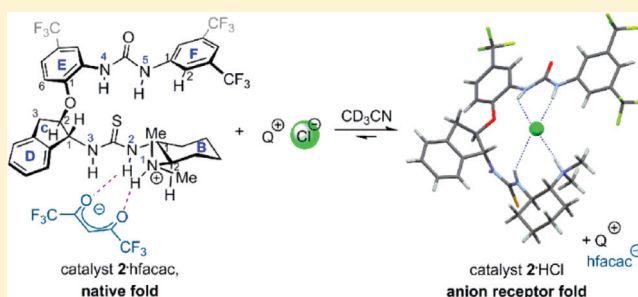
Antti J. Neuvonen,<sup>†,§</sup> Dimitris Noutsias,<sup>†,§</sup> Filip Topić,<sup>†,§</sup> Kari Rissanen,<sup>†,§</sup> Tamás Földes,<sup>‡</sup> Imre Pápai,<sup>‡</sup> and Petri M. Pihko<sup>\*,†,§</sup>

<sup>†</sup>Department of Chemistry and NanoScience Center, University of Jyväskylä, FI-40014 Jyväskylä, Finland

<sup>‡</sup>Institute of Organic Chemistry, Research Centre for Natural Sciences, Hungarian Academy of Sciences, Magyar tudósok körútja 2, H-1117 Budapest, Hungary

## Supporting Information

**ABSTRACT:** Four distinct folding patterns are identified in two foldamer-type urea–thiourea catalysts bearing a basic dimethylamino unit by a combination of X-ray crystallography, solution NMR studies, and computational studies (DFT). These patterns are characterized by different intramolecular hydrogen bonding schemes that arise largely from different thiourea conformers. The free base forms of the catalysts are characterized by folds where the intramolecular hydrogen bonds between the urea and the thiourea units remain intact. In contrast, the catalytically relevant salt forms of the catalyst, where the catalyst forms an ion pair with the substrate or substrate analogues, appear in two entirely different folding patterns. With larger anions that mimic the dialkyl malonate substrates, the catalysts maintain their native fold both in the solid state and in solution, but with smaller halide anions (fluoride, chloride, and bromide), the catalysts fold around the halide anion (anion receptor fold), and the intramolecular hydrogen bonds are disrupted. Titration of catalyst hexafluoroacetylacetonate salt with tetra-*n*-butylammonium chloride results in dynamic refolding of the catalyst from the native fold to the anion receptor fold.



## INTRODUCTION

The prevailing tenet in designing enantioselective catalysts is that the catalyst must be able to efficiently differentiate between two competing diastereomeric transition states, leading to different enantiomers of the product.<sup>1</sup> To this end, catalyst structures often include relatively bulky side chains to increase steric constraints<sup>2</sup> and to restrain conformational flexibility.

In contrast to the rigid design of synthetic catalysts, recent research has unearthed evidence that enzyme catalysis is highly tolerant of conformational flexibility in the structure of the protein.<sup>3</sup> In some cases, the binding of the substrate helps in preorganizing the active site of the enzyme.<sup>4</sup> It also appears that even after long periods of evolutionary optimization, enzymes often possess significant conformational flexibility that enables them to adapt to different substrates.<sup>5</sup> These properties are crucial for evolution of new functions and also for allosteric regulation. Although the importance of conformational adaptability is well-recognized in the realm of enzymes, conformational flexibility of synthetic catalysts has gained recognition only relatively recently.<sup>6</sup> In particular, synthetic peptides, in the same fashion as larger enzyme proteins, provide an important exception to the typical rigidity of synthetic catalysts.<sup>6c–e</sup>

Herein, we describe a pair of highly enantioselective synthetic catalysts displaying significant conformational flexi-

bility, with a native, active folded state and at least three alternative folded states.

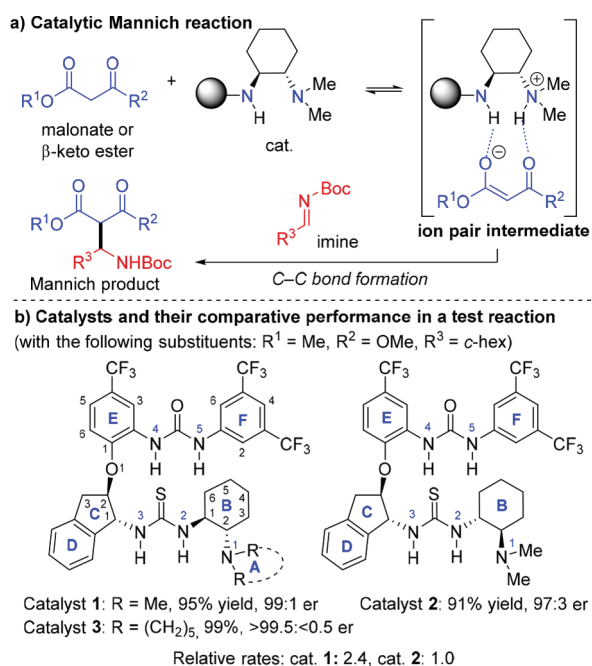
The catalysts that are the subject of the current study (1–3; see Scheme 1) are capable of highly enantioselective catalysis of Mannich reaction between malonate esters or  $\beta$ -keto esters and imines.<sup>7,8</sup> The intramolecular urea–thiourea hydrogen bond motif in these catalysts was originally designed by the Smith group as a  $\beta$ -turn mimic,<sup>9</sup> connecting the design of our catalysts to the realm of peptides. Mechanistically, in an initial proton transfer event, the malonate or  $\beta$ -keto ester anions are proposed to be tightly bound to the catalytic pocket via hydrogen bonds (Scheme 1a).<sup>7a</sup> Whereas all catalysts gave reasonable enantioselectivities in the catalytic Mannich reaction (Scheme 1b), catalyst 1 was superior to catalyst 2 in both selectivity as well as reactivity (Scheme 1b),<sup>7d</sup> and catalyst 3 was even more selective than either catalysts 1 or 2. We have earlier reported<sup>7a</sup> how important the catalytic pocket and the overall fold, including the rigid indane ring<sup>7c</sup> (rings C and D), are for catalysis with this catalyst family (Scheme 1c).

However, evidence for alternative folds with these catalysts was evident even in our first X-ray studies. For example, a completely different type of fold was characterized by X-ray when the counteranion was a small chloride ion (Figure 1). In

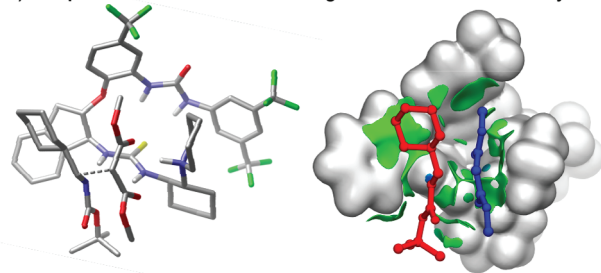
Received: July 20, 2019

Published: September 19, 2019

**Scheme 1.** (a) Catalytic Mannich Reaction via Ion-Pair Intermediate, (b) Structures of Catalysts 1–3 and Their Relative Performance in a Test Reaction,<sup>a</sup> and (c) Transition State (TS) Structure (DFT) Showing Catalyst 3 and the Test Substrates<sup>b</sup>



**c) Computational TS structure showing the active fold of the catalyst**



<sup>a</sup>With 10 mol % of catalyst, toluene, 0 °C for catalysts 1 and 3, –40 °C for 2; see refs 7a and 7c. <sup>b</sup>Showing the folding of the catalyst in the TS (left) and the surface of the active site cleft (right).<sup>7a</sup>

this case, the intramolecular hydrogen-bonded fold and the catalytic cleft were completely disrupted, and the catalyst instead folded around the chloride ion.

The presence of several different folds in catalysts is well-established in the realm of enzymes, where it is possible to distinguish between the native, catalytically competent state and other improperly folded or even denatured states.<sup>5</sup> Our foldamer-like catalysts are complex enough that different folding patterns may similarly emerge. These folding patterns, or folds, arise as a combination of four possible conformations for the thiourea unit (Figure 2a)<sup>10</sup> and the presence of hydrogen bond acceptors and donors within the catalyst, giving rise to additional conformational possibilities. Some of the possible folding patterns are shown in Figure 2b. Fold A is the fold that we have previously associated with catalytic activity,<sup>7a,c</sup> exhibiting the *anti-anti* thiourea unit and intramolecular urea–thiourea hydrogen bonds. Given its potential role in catalysis, fold A is herein called the “native fold”,

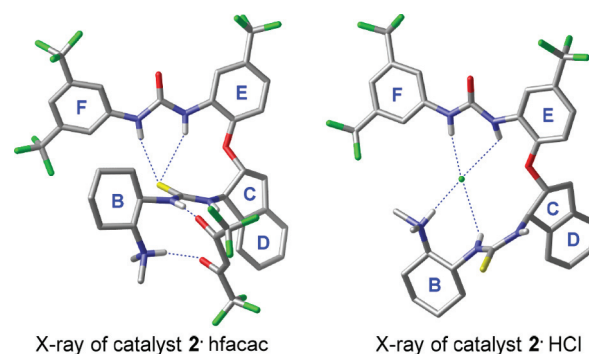
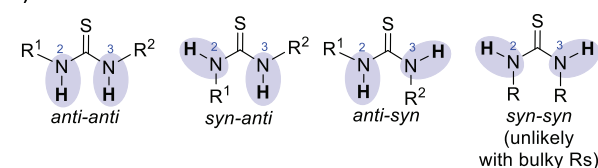
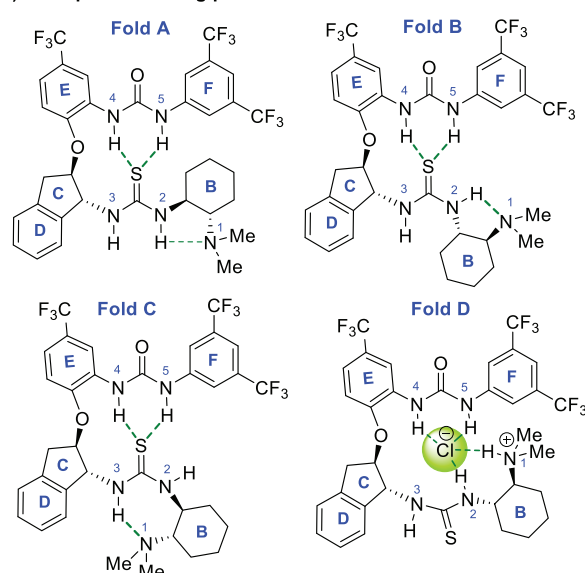


**Figure 1.** Two examples of previously characterized folding patterns of catalyst 2 (CCDC codes YEKPEL and YEKPIP) in their active salt form.<sup>7c</sup>

**a) Thiourea conformers**



**b) Examples of folding patterns**



	Fold A ("native")	Fold B	Fold C	Fold D "anion receptor"
Thiourea conformation	<i>anti-anti</i>	<i>syn-anti</i>	<i>syn-anti</i>	<i>anti-syn</i>
Urea–thiourea HBs	yes	yes	yes	no
N2–H···NMe <sub>2</sub> HB	yes	yes	no	no
N3–H···NMe <sub>2</sub> HB	no	no	yes	no

**Figure 2.** (a) Different thiourea conformations with unsymmetrical thioureas and (b) possible folding patterns in catalyst 1.

whereas the chloride-disrupted fold D is called “anion receptor fold”.<sup>11</sup>

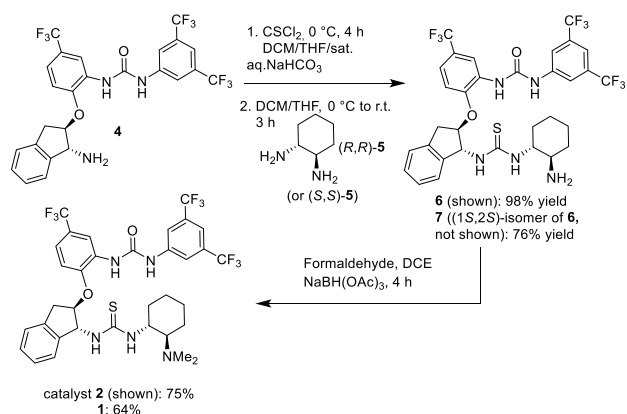
Our early studies, however, did not establish to what extent the native fold of these catalysts was maintained in solution. Furthermore, why did the chloride anion give rise to the anion receptor folding pattern, while the hexafluoroacetylacetonate (hfacac) anions maintained the native fold of the catalyst? In order to study the behavior of the catalysts in a more systematic manner, we decided to examine the original catalysts 1 and 2 and their salts with different anions, both

in solution and in the solid state. The free catalysts were examined first, followed by a more systematic variation of different anions, from small halides to larger organic anions mimicking possible pronucleophiles.

## RESULTS AND DISCUSSION

**Improved Synthesis of Catalysts 1 and 2.** We have found that the precursor 4 (Scheme 2) is hindered enough to

### Scheme 2. Improved Synthesis of Catalysts 1 and 2 Directly from Diamine 5



enable a straightforward and highly selective monothiourea formation between 4 and 5 (via an isothiocyanate derived from 4). In this manner, catalysts 1 and 2 can be obtained very easily from precursor 4 after reductive amination of intermediate 6 or 7.

**Solid-State Structures of Free Catalysts 1 and 2.** The X-ray structures of the free catalysts 1 and 2 were published previously.<sup>7c</sup> For comparison, the salient features of the structures are discussed herein.

Catalyst 1 exhibits the native folded conformation 1A in the X-ray structure (Figures 3 and 4). In this structure, the

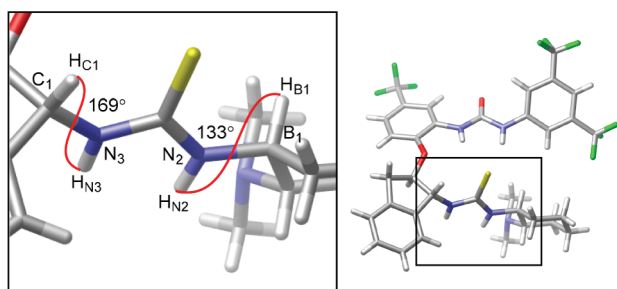


**Figure 3.**  $\varphi$ -Angle torsions in (*anti-anti*) conformer of the solid-state structure of catalyst 1.

thiourea sulfur atom is hydrogen bonded to the urea  $H_{N5}$ . The distance from the thiourea sulfur to  $N_5$  was 3.29 Å ( $H_{N5}\cdots S$  distance = 2.48 Å).<sup>12</sup> In turn, the hydrogen bond from thiourea sulfur to the second urea  $H_{N4}$  was weaker, with  $S\cdots N_4$  distance of 3.51 Å ( $H_{N4}\cdots S$  = 2.68 Å). The differentiation between the two urea H-bond donors is mainly caused by geometrical restraints from the aminoindanol linker and limited rotation around the ether bonds due to 1,5-interaction. In this structure, the angle between least-squares planes of the urea and thiourea is 75.8°. The thiourea unit is in the catalytically active (*anti-anti*) conformation, with the  $N_2-H$  and  $N_3-H$

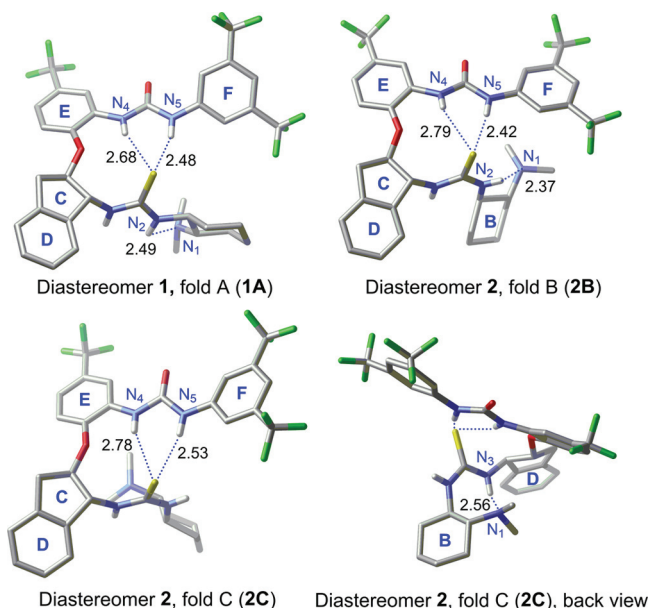


**Figure 4.** X-ray structures of diastereomers 1 (CSD: YEKQEM) and 2 (YEKPAH) showing three distinct folds for the catalysts. All except NH hydrogens are omitted for clarity.

bonds parallel, facing outward and open for coordination by hydrogen bond acceptors. The  $H_{N2}-N_2-C_{B1}-H_{B1}$  and  $H_{N3}-N_3-C_{C1}-H_{C1}$  dihedral angles on both sides of the thiourea are governed by allylic strain by minimizing the interaction between sulfur and the neighboring alkyl groups. This conformation is analogous to highly preferred 120 or 180°  $\varphi$ -angle clusters in peptides.<sup>13</sup> In fact, in catalyst 1, the torsion angle of  $H_{N2}-N_2-C_{B1}-H_{B1}$  is close to 120° (133°) and the torsion angle of  $H_{N3}-N_3-C_{C1}-H_{C1}$  is close to 180° (169°) (Figure 3). The thiourea hydrogens  $H_{N2}$  and  $H_{N3}$  form intermolecular hydrogen bonds to urea oxygen of the adjacent catalyst molecule with hydrogen bond lengths of 3.00 Å ( $N_2\cdots O'$ ) and 2.99 Å ( $N_3\cdots O'$ ) ( $H\cdots O'$  distance being 2.17 Å for both hydrogen bonds).

In contrast to the free catalyst 1, the X-ray structure of catalyst 2 shows two crystallographically independent conformations, 2B and 2C (Figure 4). Fold 2A was not observed in the solid state. In both conformations (2B and 2C), the catalyst backbone stays relatively unchanged, highlighting its rigidity. However, the folding of the rest of the catalyst is different from the fold 1A observed for 1 (Figure 4). In both 2B and 2C, the thiourea is the *syn-anti* conformer, and the intramolecular hydrogen bonds between the urea and thiourea units are retained. The difference between 2B and 2C lies in the orientation of cyclohexyl ring B. In 2B, the dimethylamino group ( $N_1$ ) can form one more intramolecular hydrogen bond with the thiourea  $H_{N2}$  ( $N_2\cdots N_1$  distance = 2.70 Å and  $H_{N2}\cdots N_1$  distance = 2.37 Å), but in 2C, a similar contact is not possible. A weaker hydrogen bond between  $N_1$  and  $H_{N3}$  is feasible based on the  $N_3\cdots N_1$  distance of 3.03 Å and  $H_{N3}\cdots N_1$  distance of 2.56 Å.

**Solution Structures of Free Catalysts 1 and 2.** The observation of three distinct folds in these X-ray structures supported the notion that these catalysts can adopt a variety of conformations in the solid state. The catalytic reactions, however, take place in solution. To assess the solution conformations, NOESY NMR spectra of the catalysts 1 and 2 were recorded in  $CD_2Cl_2$ . Different conformations of the

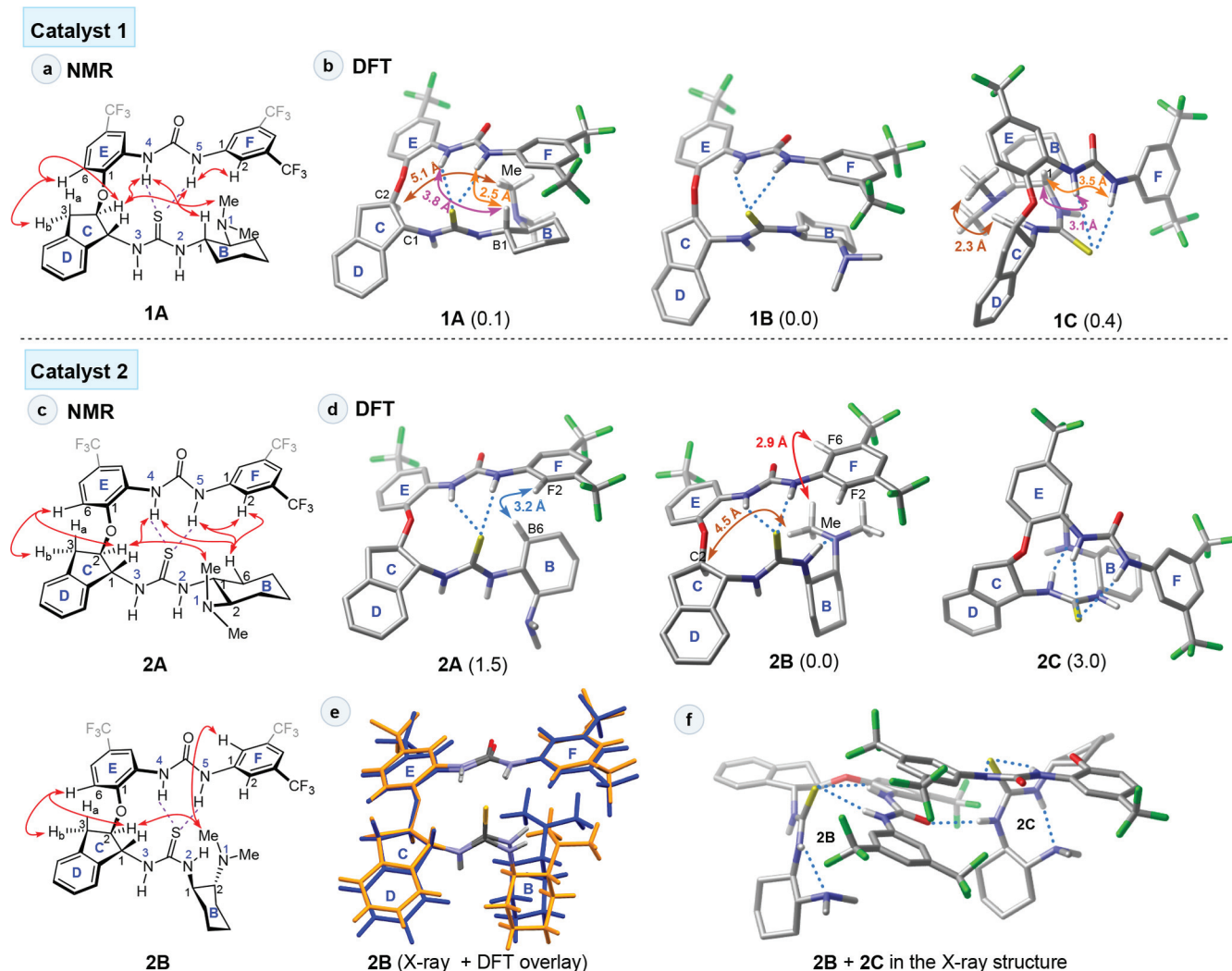


**Figure 5.** (a–d) Key NOESY correlations (NMR) and the most stable DFT structures of free catalysts **1** and **2**. To rationalize the NMR results for catalyst **2**, two different folds (**2A** and **2B**) are presented to account for the observed NOESY cross-peaks (see text). (e) Overlay of the X-ray of fold **2B** (gold) with the DFT structure (blue). (f) Packing of structures **2B** and **2C** in the X-ray structure of **2** (CSD: YEKPAH). The computed relative stabilities shown in parentheses (in kcal/mol) refer to solution-phase Gibbs free energies with respect to the most stable forms of catalysts **1** and **2**.

catalysts **1** and **2** were also examined computationally. We used DFT calculations at the M06-2X/6-311++G(3df,3pd)//M06-2X/6-311G(d,p) level to compute the structure and the relative stability of various catalyst conformers (for details, see [Supporting Information](#)).

The most stable computed structures are shown in [Figure 5b,d](#). For catalyst **1**, three conformers with very similar relative stabilities were identified. Conformer **1A** displays the conformation observed in the X-ray structure of **1**, with the *anti-anti* thiourea. Conformers **1B** and **1C**, in contrast, possess a *syn-anti* thiourea unit, but still involving intramolecular H-bonding interactions between the thiourea S atom and the urea NH groups. Neither of these folds was observed in the X-ray studies of **1**, but the **1B** fold is similar to the fold **2B** of catalyst **2**. For catalyst **2**, the most stable form corresponds to conformer **2B** displaying a *syn-anti* thiourea unit, whereas the *anti-anti* thiourea conformation (**2A**) is predicted to be 1.5 kcal/mol less favored in free energy. The overall fold of **2B** in the X-ray structure is almost identical with the DFT structure (see [Figure 5e](#)). Interestingly, although fold **2C** was present in the X-ray structure (see above), it turned

out to be 3.0 kcal/mol less stable than **2B**, even after optimization of the structure. The existence of fold **2C** in the X-ray crystal structure ([Figure 4](#)) may be attributed to intermolecular hydrogen bonds between structures **2B** and **2C** in the X-ray structure ([Figure 5f](#)). These hydrogen bonds could stabilize **2C** in the solid state.

In solution, the most diagnostic NOESY cross-peaks in catalyst **1** were those observed between  $N_1\text{-Me} \leftrightarrow H_{C2}$ ,  $H_{B1} \leftrightarrow H_{N5}$ , and  $H_{B1} \leftrightarrow H_{N4}$ . The observed  $N_1\text{-Me} \leftrightarrow H_{C2}$  interaction is consistent with the structures **1C** (computed distance = 2.3 Å) and possibly also with **1A** (5.1 Å) but appears inconsistent with the most stable conformer **1B** (6.1 Å). The  $H_{B1} \leftrightarrow H_{N5}$  interaction can be also supported by conformers **1A** (2.5 Å) and **1C** (3.5 Å), but the distance in **1B** is longer (4.8 Å). Last, the interaction between  $H_{B1} \leftrightarrow H_{N4}$  is expected on the basis of structure **1A** (computed distance = 3.8 Å) and **1C** (3.1 Å) but appears less likely for conformer **1B** (5.0 Å). Taken together, these results suggest that catalyst **1** is mostly populated by conformers **1A** and **1C** in the solution state, but we cannot rule out the contribution of conformer **1B** to the solution structure. The  $\Delta G^\ddagger$  for the rotation around the thiourea C–N bond is

13.5–14.4 kcal/mol,<sup>14</sup> and as such, NMR experiments at a 303 K probe temperature used herein are well above the coalescence temperature.<sup>14a</sup>

In catalyst **2**, the key diagnostic NOESY cross-peaks correspond to the correlations between  $N_1\text{-Me} \leftrightarrow H_{C2}$ ,  $H_{B6eq} \leftrightarrow H_{F2/F6}$  and the  $N_1\text{-Me} \leftrightarrow H_{F2/F6}$ . The most stable DFT structures, **2A** and **2B**, are consistent with most of the observed NOESY cross-peaks. The  $N_1\text{-Me} \leftrightarrow H_{C2}$  correlation is readily explained by fold **2B** (computed distance = 4.5 Å) but not by **2A** ( $\text{Me}_{N1} \cdots H_{C2}$  distance = 6.7 Å). Likewise, the correlation  $N_1\text{-Me} \leftrightarrow H_{F2/F6}$  is expected for **2B** (2.9 Å), but the corresponding computed distance in **2A** is 5.4 Å. In contrast, the correlation  $H_{B6eq} \leftrightarrow H_{F2/F6}$  cannot be readily rationalized by fold **2B** (distance = 7.3 Å), but it is very consistent with **2A** (distance = 2.9 Å). These data suggest that, in solution, both folds **2A** and **2B** may contribute to the averaged NMR structure as neither of these structures alone can fully rationalize the observed NOEs.

**Structures of the Halide Salts in the Solid State and in Solution.** We decided to probe the effect of anion size by generating a series of structures from two available catalyst diastereomers with hydrohalic acids. Indeed, we could successfully form salts and isolate good quality single crystals of hydrofluoric, hydrochloric, and hydrobromic acid salts of both catalysts **1** and **2**. Salts of hydroiodic acid, however, did not afford crystalline material with either catalyst diastereomer.

The X-ray structures (Figure 6) show that the structures of the hydrohalide salts are remarkably similar to those of different anions. In all structures, the halide anions are bound to the catalyst **1** via the urea  $H_{N4}$  and  $H_{N5}$  hydrogens and via one of the thiourea NH, the  $H_{N2}$ . The thiourea is in the *anti-syn* conformation.<sup>15</sup> The protonated ammonium  $H_{N1}$  forms a weaker hydrogen bond to the halide with a longer  $H \cdots N$  distance. For example, in **1**·HF, the  $H_{N1} \cdots F$  distance is 2.54 Å ( $N_1 \cdots F = 3.10$  Å), whereas the contacts to the thiourea and urea protons are shorter ( $H_{N2} \cdots F = 1.93$  Å,  $H_{N4} \cdots F = 2.08$  Å,  $H_{N5} \cdots F = 1.87$  Å). In addition, the fluoride ion also contacts the thiourea  $H_{N3}$  of the adjacent catalyst molecule in the solid-state structure (see the Supporting Information).<sup>16</sup>

All catalyst **1** halide salts show a similar bonding pattern, and the catalyst molecules overlap almost perfectly. Although the binding of the halide causes a small distortion in the upper CDEF urea segment of the catalyst molecule, the overlaid structures of the free catalyst **1** and **1**·HCl show a remarkable degree of similarity (Figure 6e).

The X-ray crystal structures of the hydrohalide salts of catalyst **2** are also remarkably similar to those of the HX salts of catalyst **1**. The only major change in the folding pattern is that the dimethylammonium group in this diastereomer is better able to contact the halide ion, even in the case of the smallest fluoride anion (see Figure 6b). In contrast, the thiourea  $H_{N2}$  is not ideally pointed toward the halide ion and forms only a weak contact with the anion, with a  $H_{N2} \cdots F$  distance of 2.96 Å in **2**·HF (Figure 6b).

It is evident from these solid-state structures that the halides do not fit the pocket perfectly and thus allow the formation of intermolecular hydrogen bonds on the exposed face of the anion. In particular, the bromide ion is large enough that it is bound only from one side of the sphere by one catalyst molecule, as exemplified by the spacefill structure of **1**·HBr (Figure 6f).

**Structures of Catalyst Hydrochloride Salts: Solution-State Structures.** The NOESY spectrum of the HCl salt of

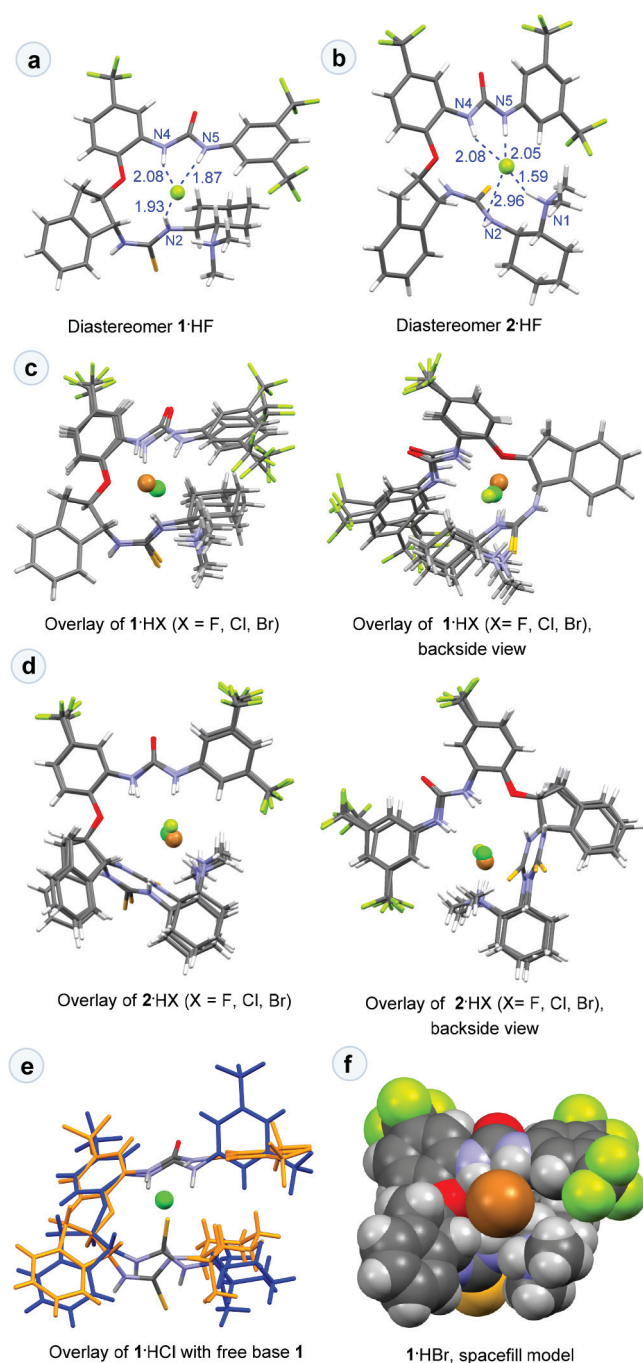


**Figure 6.** (a–d) Solid-state structures of the HX salts of catalysts **1** and **2**. (e) Overlay of the X-ray structures of **1**·HCl (blue, except for the urea and thiourea units) and free catalyst **1** (YEKQEM, gold) showing the similar folding of the CDEF region of the catalyst. (f) Spacefill model of **1**·HBr showing how the bromide ion protrudes out from the binding pocket.

catalysts *ent-1*<sup>17</sup> and **2** confirms most of the expected interactions that are observed in the X-ray structure (Figure 7). Many of the NOESY correlations observed in the free catalysts remained similar in the HCl salts. However, the correlation between  $H_{N2}$  and  $H_{C1}$  indicates a conformational change in the thiourea moiety to the *anti-syn* conformation. Furthermore, the cross-peaks between  $\text{Me}_{N1}$  and  $H_{F2}$  in both structures as well as  $H_{N5}$  and  $H_{B2}$  in *ent-1*·HCl were indicative

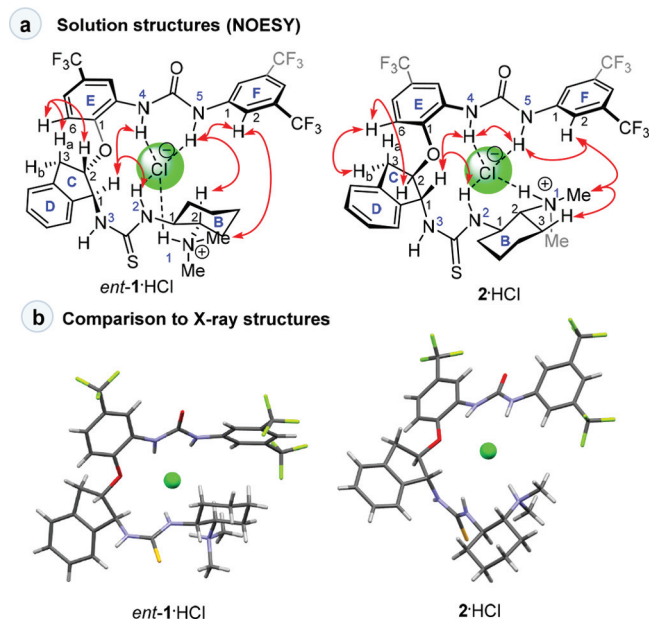


**Figure 7.** Structures of HCl salts of catalysts *ent-1* and *2* in (a)  $\text{CD}_3\text{CN}$  (with diagnostic NOESY cross-peaks indicated by arrows) and (b) in the solid state (X-ray). For the structure of *ent-1*·HCl, the mirror image of the X-ray of *1*·HCl is shown for clarity.

of a folded, compact conformation where the catalyst wraps around the chloride ion.

**Structures of Catalysts with Organic Acids.** In contrast to the salts of hydrohalic acids, we had already previously recorded examples where catalysts **1**–**3** exhibited the native fold **A** in the presence of organic acids.<sup>7c</sup> We therefore examined a series of acids with catalysts **1** and **2** to obtain further insight into how the size and the shape of the anions affect the overall fold of the catalyst.

Although it would have been desirable to obtain X-ray structures for a complete series of anions, in practice, these studies had to be limited to scattered cases where the crystal properties were satisfactory. In many cases, even if proper size crystals were obtained, they were often soft or brittle, making the experiments hard to conduct. Nevertheless, in addition to the previously characterized **2**·hfacac (Figure 1), we could also obtain the corresponding trifluoroacetate (TFA, Figure 8a), diphenylphosphate (DPP, Figure 8b), and bis(2,6-trifluoromethyl)benzoate (BTB, see Supporting Information) salts, all of which exhibited the expected native fold **A**. The

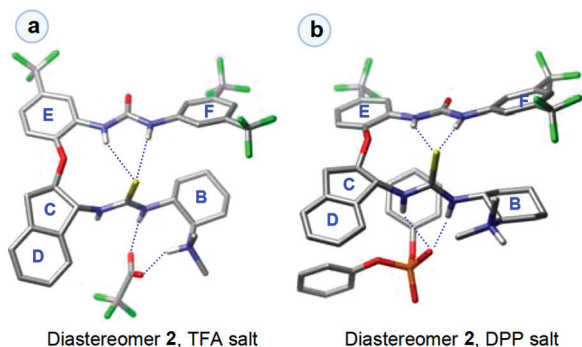


**Figure 8.** Solid-state structures of catalyst **2** as the (a) TFA salt and (b) DPP salt.

intermolecular hydrogen bonding patterns observed in these structures are, however, dependent on the hydrogen bond acceptor properties of the anion. For example, in the DPP salt, the ammonium  $\text{H}_{\text{N}1}$  contacts a neighboring diphenylphosphate anion in the solid state (see the Supporting Information) instead of forming a third hydrogen bond to the anion that is bound by the urea. For these reasons, these X-ray structures may not always offer a realistic insight into the conformers populated in solution.

**Structures of Catalyst hfacac Salts: Solution-State Structures.** The solution-state structures of the hfacac salts of catalysts **1** and **2** were obtained by recording NOESY spectra in  $\text{CD}_2\text{Cl}_2$  and analysis of the key correlations. The results (Figure 9) support the notion that these catalysts primarily

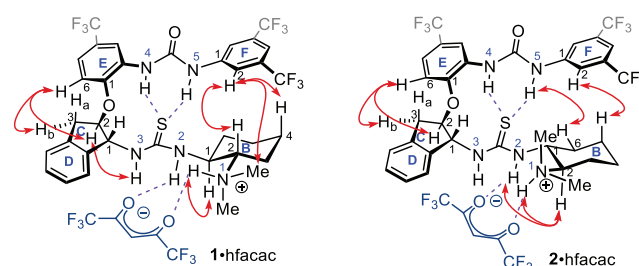


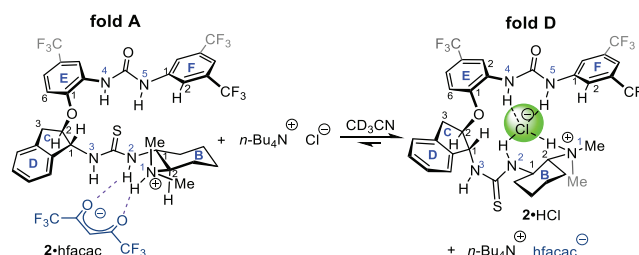
**Figure 9.** Solution-state structures of hfacac salts of catalysts **1** and **2**.

populate fold **A** in solution with larger anions such as hfacac and the enolate of dimethyl malonate.<sup>7a</sup> For example, the  $\text{H}_{\text{N}3} \leftrightarrow \text{H}_{\text{C}2}$  NOESY cross-peak observed in **1**·hfacac shows that the thiourea moiety is likely to adopt an *anti-anti* configuration. Most diagnostically, the cross-peaks between  $\text{H}_{\text{F}2}$  and  $\text{H}_{\text{B}2}$  and  $\text{H}_{\text{B}4\text{ax}}$  (**1**·hfacac) or  $\text{H}_{\text{F}2}$  and  $\text{H}_{\text{S}4\text{ax}}$  (**2**·hfacac) are consistent with fold **A** (Figure 9).

Interestingly, the lower reactivity and selectivity of catalyst **2** relative to that of **1** may be related to its relatively lower preference for the active *anti-anti* conformer (fold **A**). Catalyst **2** will need to adopt the active fold **2A** instead of the preferred folds **2B** or **2C** (with a *syn-anti* thiourea unit) upon binding to the malonate ion.<sup>7a,c</sup> In contrast, catalyst **1** appears to populate the native fold **1A** with greater occupancy in solution (see Figure 4a). If fold **A** is the fold required for catalysis, this difference may explain the higher reactivity and selectivity of catalyst **1** compared to **2**.

**Addition of Chloride Ion Source Dynamically Switches the Catalyst Conformation in Solution.** We also hypothesized that the refolding of the catalyst in the presence of different anions might be sufficiently rapid so that the event could be monitored by NMR. To this end, we

**Scheme 3. Dynamic Switching between the A and D Folds of the Catalyst with Addition of *n*-Bu<sub>4</sub>NCl as the Chloride Source**



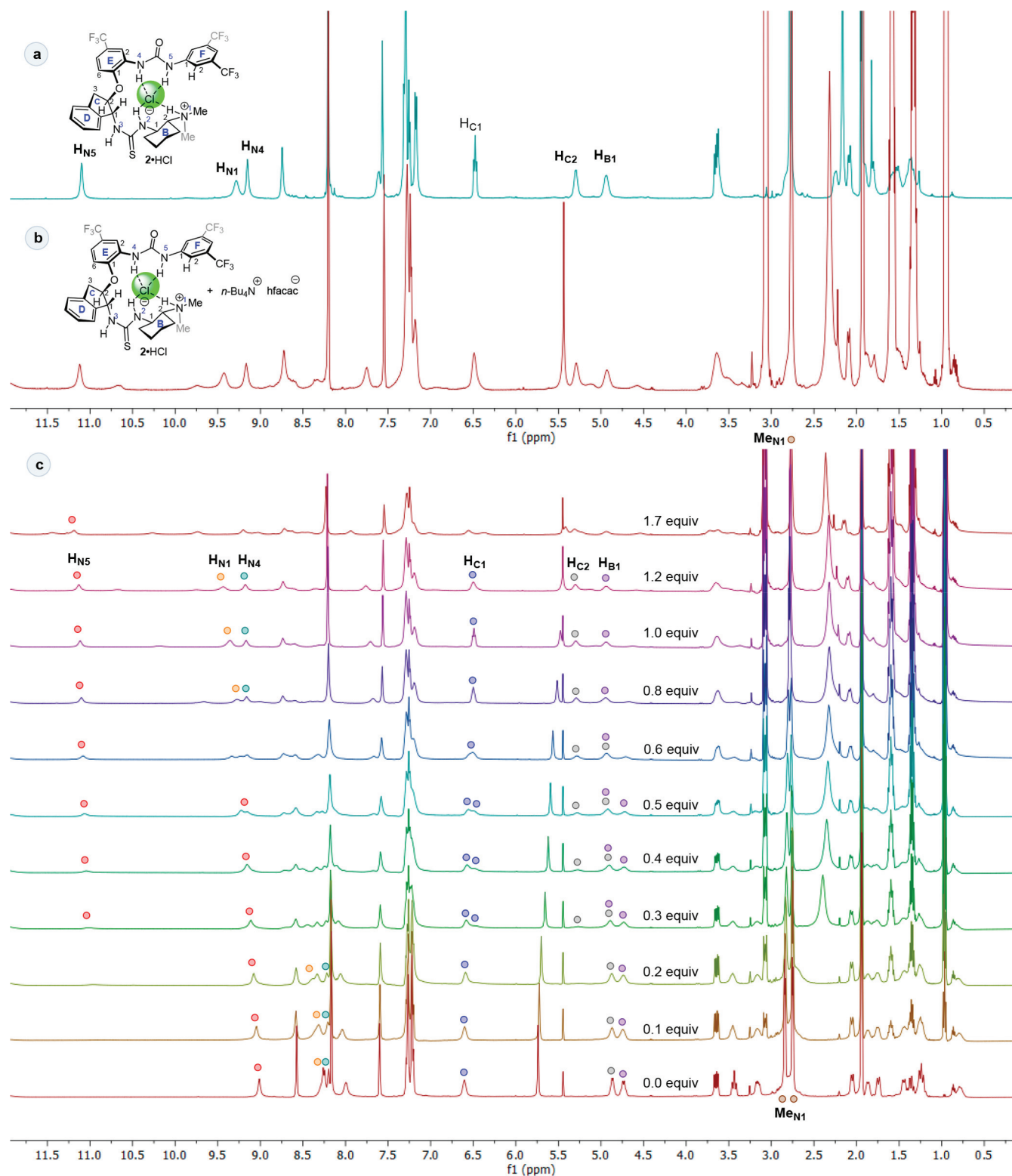


**Figure 10.** (a)  $^1\text{H}$  NMR spectrum of  $2\cdot\text{HCl}$ . (b)  $^1\text{H}$  NMR spectrum of  $2\cdot\text{hfacc}$  after addition of 1.2 equiv of  $n\text{-Bu}_4\text{NCl}$ . (c)  $^1\text{H}$  NMR titration of  $2\cdot\text{hfacc}$  with 0.5 M solution of  $n\text{-Bu}_4\text{NCl}$ . All spectra were recorded in  $\text{CD}_3\text{CN}$ .

selected  $n\text{-Bu}_4\text{NCl}$  as the chloride anion source that could potentially replace the hfacc anion in solution (Scheme 3).

Thus, a solution of  $2\cdot\text{hfacc}$  in  $\text{CD}_3\text{CN}$  was titrated with a solution of  $n\text{-Bu}_4\text{NCl}$  (0.5 M in  $\text{CD}_3\text{CN}$ ). During the titration, the  $^1\text{H}$  NMR of the mixture slowly began to resemble the spectrum of pure  $2\cdot\text{HCl}$  (compare panels a and b of Figure 10), and this species was still detectable beyond 1.2 equiv of  $n\text{-}$

$\text{Bu}_4\text{NCl}$  (Figure 10c). These data suggest that, during the titration, catalyst **2** had almost exclusively switched from the fold **2A** to the anion receptor fold **2D**. Similar results were obtained with catalyst **1** and  $n\text{-Bu}_4\text{NCl}$  (see the Supporting Information for details). The titration results with  $n\text{-Bu}_4\text{NCl}$  indicate that the equilibrium in this case lies on the side of the chloride complexes (**D** fold). However, titration of a solution

of 2-hfacac with *n*-Bu<sub>4</sub>NBr (a source of bromide ion) yielded a more complex NMR spectrum, suggesting that in this case the switch was either not complete or that other conformations were also populated.

## SUMMARY AND CONCLUSIONS

In conclusion, the folding patterns of our foldamer-type catalysts, capable of highly enantioselective Mannich reactions, have been characterized. The patterns that emerge from the solid-state XRD studies appear to be preserved in solution with high fidelity. Thus, the intramolecular hydrogen bonds in the native fold of the catalyst, where the catalytic pocket is intact, were maintained in the free base form of the catalyst as well as in its hfacac or TFA salts. However, the thiourea unit of the catalyst does not uniformly adopt the desired *anti-anti* conformation, and it turned out that the less-reactive catalyst **2** favored the undesired *syn-anti* thiourea conformer in solution, as established by a combination of NMR studies and computational conformational analysis.

In contrast, the salts with simple hydrohalic acids adopt a different, anion-receptor-type fold, where the intramolecular hydrogen bonding is completely disrupted, and the catalyst conformation changes to allow multiple hydrogen bond contacts with the small halide counteranion. This fold is made possible by the alternative *anti-syn* conformation of the thiourea unit, instead of the *syn-anti* conformation observed for catalyst **2**. These folding patterns were identified by X-ray structures in the solid state for both catalyst diastereomers and for different anions (F<sup>-</sup>, Cl<sup>-</sup>, and Br<sup>-</sup>), and the hydrochloride salts of two catalyst diastereomers were found to populate similar conformations in solution according to NOE studies.

The choice of the fold could also be modulated by addition of chloride ions. Titration of the hfacac salts of the catalysts **1** and **2**, possessing the native fold in solution, with a chloride source (*n*-Bu<sub>4</sub>NCl), resulted in a switch to the anion receptor mode as observed by <sup>1</sup>H NMR. The fact that different anions can affect the shapes of the catalysts suggests that anions could also be used to modulate the selectivities and activities of synthetic catalysts. Studies toward these goals are ongoing.

## EXPERIMENTAL SECTION

**General Information.** All reactions were carried out under an argon atmosphere in flame-dried glassware, unless otherwise noted. When needed, nonaqueous reagents were transferred under argon via syringe or cannula and dried prior to use. THF and CH<sub>2</sub>Cl<sub>2</sub> were obtained by passing deoxygenated solvents through activated alumina columns (MBraun SPS-800 Series solvent purification system). Other solvents and reagents were used as obtained from supplier, unless otherwise noted. Analytical TLC was performed using Merck silica gel F<sub>254</sub> (230–400 mesh) plates and analyzed by UV light or by staining upon heating with anisaldehyde solution (2.8 mL of anisaldehyde, 2 mL of concentrated H<sub>2</sub>SO<sub>4</sub>, 1.2 mL of concentrated CH<sub>3</sub>COOH, 100 mL of EtOH), vanillin solution (6 g of vanillin, 5 mL of concentrated H<sub>2</sub>SO<sub>4</sub>, 3 mL of glacial acetic acid, 250 mL of EtOH), or KMnO<sub>4</sub> solution (1 g of KMnO<sub>4</sub>, 6.7 g of K<sub>2</sub>CO<sub>3</sub>, 1.7 mL of 1 M NaOH, 100 mL of H<sub>2</sub>O). For silica gel chromatography, the flash chromatography technique was used, with Merck silica gel 60 (230–400 mesh) and p.a. grade solvents unless otherwise noted.

The <sup>1</sup>H NMR and <sup>13</sup>C NMR spectra were recorded in CD<sub>2</sub>Cl<sub>2</sub> or CD<sub>3</sub>CN on Bruker Avance 500, 400, or 250 spectrometers. The chemical shifts are reported in parts per million relative to CHD<sub>2</sub>CN (δ 1.94) or CHDCl<sub>2</sub> (δ 5.32) for <sup>1</sup>H NMR. For the <sup>13</sup>C NMR spectra, the residual CD<sub>3</sub>CN (δ 118.26) or CD<sub>2</sub>Cl<sub>2</sub> (δ 53.84) were used as the internal standards. The enantiomeric excesses (ee) of the products were determined by HPLC in comparison to the corresponding

racemic samples using a Waters 501 pump and a Waters 486 detector. Melting points (mp) were determined in open capillaries using a Gallenkamp melting point apparatus. IR spectra were recorded on a Tensor27 FT-IR spectrometer. Optical rotations were obtained with a PerkinElmer 343 polarimeter. High-resolution mass spectrometric data were measured using MicroMass LCT Premier spectrometer.

Single-crystal X-ray diffraction analyses were performed at indicated, measuring temperature on an Agilent Super-Nova diffractometer using mirror monochromatized Mo Kα (λ = 0.71073 Å) or Cu Kα (λ = 1.54184 Å) radiation. CrysAlisPro program was used for the data collection and processing. The intensities were corrected for absorption using the analytical face index absorption correction method. The structure was solved by the charge-flipping method with SUPERFLIP and refined by full-matrix least-squares methods using the OLEX2-1.2 software, which utilizes the SHELXL module. All non-hydrogen atoms were refined with anisotropic thermal parameters. Hydrogen atoms were introduced in proper positions with isotopic thermal parameters using the “riding model”. The ORTEP figure was plotted and structure was analyzed with Mercury v 3.10.

**Synthesis of Catalysts.** CAUTION: CCl<sub>4</sub> (thiophosgene) is a toxic and corrosive reagent that must be used in an efficient fume cupboard.

**1-(2-(((1*R*,2*R*)-1-(3-(((1*R*,2*R*)-2-Aminocyclohexyl)thioureido)-2,3-dihydro-1*H*-inden-2-yl)oxy)-5-(trifluoromethyl)phenyl)-3-(3,5-bis-(trifluoromethyl)phenyl)urea (6).** Amine **4** (430 mg, 0.76 mmol, 100 mol %) was dissolved in a stirred biphasic mixture of DCM, THF, and saturated aqueous NaHCO<sub>3</sub> (10:1:10, total volume 21 mL) at 0 °C. The stirring was stopped, and thiophosgene (117 μL, 1.52 mmol, 200 mol %) was added via syringe to the organic layer. Stirring was started and continued for 4 h at 0 °C after which the layers were separated and the aqueous layers extracted with DCM (3 × 20 mL). The combined organic extracts were dried over Na<sub>2</sub>SO<sub>4</sub> and concentrated. The crude isothiocyanate was dissolved in a mixture of dry DCM and THF (5:1, total volume 12 mL) under argon, and diamine (*R,R*)-**5** (174 mg, 1.52 mmol, 200 mol %) was added in one portion at 0 °C. The reaction mixture was stirred at rt for 3 h, after which most of the solvents were removed under reduced pressure (2 mL of solvent left in the flask). Purification of the residue by flash chromatography (100:1:1 DCM/MeOH/triethylamine) afforded the desired product **6** as an off-white solid (535 mg, 98%): *R*<sub>f</sub> (4% 7 N NH<sub>3</sub>/MeOH in DCM) = 0.35; mp 141–142 °C; [α]<sub>D</sub><sup>25</sup> = –50.7 (c 1.0, CH<sub>2</sub>Cl<sub>2</sub>); IR (film, cm<sup>-1</sup>) ν 3259, 3083, 2934, 2860, 1709, 1543, 1385, 1276, 1170, 1121, 681; <sup>1</sup>H NMR (500 MHz, CD<sub>2</sub>Cl<sub>2</sub>) δ 10.25 (s, 1H), 9.21 (s, 1H), 8.69 (s, 1H), 8.67 (brs, 1H), 8.17 (s, 2H), 7.53 (s, 1H), 7.34–7.30 (m, 4H), 7.25 (d, *J* = 8.4 Hz, 1H), 7.05 (d, *J* = 8.4 Hz, 1H), 6.64 (brs, 1H), 6.13 (brs, 1H), 4.61 (app q, *J* = 8.2 Hz, 1H), 3.66 (dd, *J* = 14.9, 7.2 Hz, 1H), 3.25 (app. dd, *J* = 14.9, 9.1 Hz, 1H), 2.51 (app. td, *J* = 10.1, 3.7 Hz, 1H), 2.04 (m, 1H), 1.78–1.13 (m, 9H); <sup>13</sup>C{<sup>1</sup>H} NMR (125 MHz, CD<sub>2</sub>Cl<sub>2</sub>) δ 184.1, 152.6, 150.0, 141.7, 138.9, 138.0, 132.3 (q, *J* = 33.1 Hz), 131.1, 129.1, 128.1, 125.7, 124.7 (q, *J* = 32.6), 123.9 (q, *J* = 272.6 Hz), 123.4, 122.7 (q, *J* = 271.1 Hz), 119.5, 118.5, 115.9 (quint, *J* = 3.8 Hz), 115.4, 113.7, 90.1, 66.1, 63.5, 56.4, 37.3, 35.2, 32.8, 25.0, 24.9; HRMS (ESI<sup>+</sup>, TOF) *m/z* calcd for [C<sub>32</sub>H<sub>31</sub>F<sub>9</sub>N<sub>5</sub>O<sub>2</sub>S]<sup>+</sup> 720.2049, found 720.2045, Δ = 0.6 ppm.

**1-(2-(((1*R*,2*R*)-1-(3-(((1*S*,2*S*)-2-Aminocyclohexyl)thioureido)-2,3-dihydro-1*H*-inden-2-yl)oxy)-5-(trifluoromethyl)phenyl)-3-(3,5-bis-(trifluoromethyl)phenyl)urea (7).** The reaction performed using **4** (300 mg, 0.53 mmol, 100 mol %) and (*S,S*)-**5** (121 mg, 1.06 mmol, 200 mol %) using the procedure used for the preparation of **6**. The product was purified by flash chromatography (100:1:1 DCM/MeOH/triethylamine) to afford **7** as an off-white solid (290 mg, 76%): *R*<sub>f</sub> (4% 7N NH<sub>3</sub>/MeOH in DCM) = 0.45; mp 142–143 °C; [α]<sub>D</sub><sup>25</sup> = –183.0 (c 1.0, DCM); IR (film, cm<sup>-1</sup>) 3273, 2932, 2859, 1710, 1542, 1442, 1384, 1276, 1122, 681; <sup>1</sup>H NMR (500 MHz, CD<sub>2</sub>Cl<sub>2</sub>) δ 10.23 (s, 1H), 9.51 (s, 1H), 8.70 (d, *J* = 1.9 Hz, 1H), 8.53 (s, 1H), 8.19 (s, 2H), 7.52 (s, 1H), 7.31–7–24 (m, 5H), 7.08 (d, *J* = 8.4 Hz, 1H), 6.73 (d, *J* = 8.1 Hz, 1H), 6.07 (br s, 1H), 4.59 (q, *J* = 8.2 Hz, 1H), 3.67 (dd, *J* = 15.2, 7.4 Hz, 1H), 3.25 (dd, *J* = 15.1, 8.9 Hz, 1H), 3.08 (brs, 1H), 2.62 (td, *J* = 10.3, 3.5 Hz, 1H), 1.81 (app. d, *J* =



12.5 Hz, 1H), 1.75–1.63 (m, 5H), 1.21–1.07 (m, 4H);  $^{13}\text{C}\{^1\text{H}\}$  NMR (125 MHz,  $\text{CD}_2\text{Cl}_2$ )  $\delta$  183.7, 152.5, 150.0, 141.7, 138.4, 137.9, 132.2 (q,  $J = 33.0$  Hz), 131.1, 129.1, 127.9, 125.7, 124.8 (q,  $J = 271.6$  Hz), 124.6 (q,  $J = 33.7$  Hz), 123.9 (q,  $J = 272.7$ ), 123.5, 119.4, 118.4, 115.7, 115.4, 113.9, 91.4, 66.3, 63.1, 56.4, 37.4, 35.1, 32.6, 24.9; HRMS (ESI<sup>+</sup>, TOF)  $m/z$  calcd for  $[\text{C}_{32}\text{H}_{31}\text{F}_9\text{N}_3\text{O}_2\text{S}]^+$  720.2049, found 720.2062,  $\Delta = -1.8$  ppm.

**1-(3,5-Bis(trifluoromethyl)phenyl)-3-(2-(((1R,2R)-1-(3-(((1R,2R)-2-(dimethylamino)cyclohexyl)thioureido)-2,3-dihydro-1H-inden-2-yl)oxy)-5-(trifluoromethyl)phenyl)urea (2).** To a solution of compound 6 (200 mg, 0.28 mmol, 100 mol %) in DCE (6 mL) was added formaldehyde (38%  $\text{CH}_2\text{O}$  in water, 61  $\mu\text{L}$ , 0.84 mmol, 300 mol %) at rt. The reaction mixture was stirred at rt for 15 min, after which  $\text{NaBH}(\text{OAc})_3$  (237 mg, 1.12 mmol, 400 mol %) was added in one portion. The reaction mixture was stirred at rt for 4 h before saturated aqueous  $\text{NaHCO}_3$  (18 mL) was added. The mixture was allowed to stir for 15 min, and then the layers were separated. The aqueous layer was washed with DCM (3  $\times$  18 mL). The combined organic extracts were dried over  $\text{Na}_2\text{SO}_4$  and concentrated. Purification of the residue by flash chromatography (4% 7N  $\text{NH}_3/\text{MeOH}$  in DCM) afforded the desired product 2 as a pale crystalline solid (133 mg, 64%). Characterization data are in full agreement with our previous publication:<sup>7c</sup>  $^1\text{H}$  NMR (500 MHz,  $\text{CD}_2\text{Cl}_2$ )  $\delta$  9.40 (b rs, 1H), 8.71 (s, 1H), 8.61 (s, 1H), 8.20 (s, 2H), 7.53 (s, 1H), 7.33–7–28 (m, 4H), 7.26 (dd,  $J = 8.4, 1.4$  Hz, 1H), 7.09 (d,  $J = 8.4$  Hz, 1H), 6.65 (s, 1H), 6.34 (brs, 1H), 4.46 (app. q,  $J = 8.1$  Hz, 1H), 3.65 (dd,  $J = 14.6, 6.9$  Hz, 1H), 3.49 (brs, 1H), 3.29 (dd,  $J = 14.6, 9.1$  Hz, 1H), 2.31 (m, 1H), 2.21 (m, 1H), 1.93 (brs, 6H), 1.79 (m, 1H), 1.75 (m, 1H), 1.64 (brs, 1H), 1.27 (m, 1H), 1.16–1.12 (m, 3H);  $^{13}\text{C}\{^1\text{H}\}$  NMR (75 MHz,  $\text{CD}_2\text{Cl}_2$ )  $\delta$  183.5, 152.6, 150.0, 141.8, 138.5, 138.1, 132.3 (q,  $J = 33.1$  Hz), 129.2, 128.2, 125.8, 124.9 (q,  $J = 271.5$  Hz), 124.9 (q,  $J = 31.7$  Hz), 123.9 (q,  $J = 272.7$  Hz), 119.5, 118.4, 115.7 (sept,  $J = 4.0$  Hz), 115.4, 114.2, 90.9, 67.8, 65.6, 57.0, 40.1, 37.4, 33.8, 24.8 (2C), 22.6.

**1-(3,5-Bis(trifluoromethyl)phenyl)-3-(2-(((1R,2R)-1-(3-(((1S,2S)-2-(dimethylamino)cyclohexyl)thioureido)-2,3-dihydro-1H-inden-2-yl)oxy)-5-(trifluoromethyl)phenyl)urea (1).** The reaction was performed using 7 (187 mg, 0.28 mmol, 100 mol %) utilizing the procedure used for the preparation of 2. The product was purified by flash chromatography (4% 7N  $\text{NH}_3/\text{MeOH}$  in DCM) to afford 1 as a pale crystalline solid (145 mg, 75%). Characterization data are in full agreement with our previous publication.<sup>7c</sup>  $^1\text{H}$  NMR (500 MHz,  $\text{CD}_2\text{Cl}_2$ )  $\delta$  9.61 (br s, 1H), 8.71 (s, 1H), 8.46 (s, 1H), 8.21 (s, 2H), 7.53 (s, 1H), 7.34 (m, 3H), 7.27 (d,  $J = 8.2$  Hz, 2H), 7.09 (d,  $J = 8.4$  Hz, 1H), 6.65 (brs, 1H), 6.00 (brs, 1H), 4.47 (app. q,  $J = 7.5$  Hz, 1H), 3.65 (dd,  $J = 15.3, 7.6$  Hz, 1H), 3.27 (app. dd,  $J = 15.3, 8.8$  Hz, 2H), 2.34 (app. td,  $J = 10.5, 3.5$  Hz, 1H), 2.02 (s, 6H), 1.79 (app. d,  $J = 11.2$  Hz, 1H), 1.69 (m, 2H), 1.62 (m, 1H), 1.17 (m, 1H), 1.09–1.01 (m, 3H);  $^{13}\text{C}\{^1\text{H}\}$  NMR (125 MHz,  $\text{CD}_2\text{Cl}_2$ )  $\delta$  184.3, 152.5, 150.0, 141.7, 138.4, 138.1, 132.3 (q,  $J = 33.1$  Hz), 131.4, 129.2, 128.0, 125.8, 124.8 (q,  $J = 271.6$  Hz), 124.8 (q,  $J = 32.4$  Hz), 123.9 (q,  $J = 272.6$  Hz), 123.3, 119.4 (app. q,  $J = 4.0$  Hz), 118.4 (app. d,  $J = 3.0$  Hz), 115.8 (quint,  $J = 3.9$  Hz), 115.5, 114.7, 91.8, 68.3, 65.9, 57.2, 40.2, 37.5, 33.8, 24.8, 24.7, 22.5.

**Typical Procedure for the Preparation of HCl Salts of Catalysts 1 and 2.** To a solution of catalyst (10 mg, 0.013 mmol, 100 mol %) in DCM (2 mL) was added aqueous HCl (concentrated, 53  $\mu\text{L}$ , 0.65 mmol, 5000 mol %) at 0 °C. A white precipitate was immediately formed, and the mixture was stirred for 5 min at rt. The solvent and the excess HCl were removed carefully under reduced pressure.

All other catalyst HX salts were prepared in an analogous manner except that, for nonvolatile acids, 110 mol % of the corresponding acid was used. The crystalline salts were grown using a diffusion method from a binary solvent mixture consisting of either cyclopentane, benzene, or toluene (first component) and dichloromethane (second component).

**Note:** The 2D NOESY spectrum of both HCl salts were measured with a 500 MHz spectrometer at 30 °C (303 K). Both salts show some instability after 24 h in  $\text{CD}_3\text{CN}$ . *ent*-1-HCl salt is only sparingly

soluble in  $\text{CD}_3\text{CN}$ , and as such, the NMR sample was warmed to 70 °C before the start of the measurement and then recooled to the probe temperature (303 K).

**(1R,2R)-2-(3-(((1R,2R)-2-(2-(3-(3,5-Bis(trifluoromethyl)phenyl)ureido)-4-(trifluoromethyl)phenoxy)-2,3-dihydro-1H-inden-1-yl)thioureido)-N,N-dimethylcyclohexan-1-aminium chloride (2-HCl):**  $^1\text{H}$  NMR (500 MHz,  $\text{CD}_3\text{CN}$ )  $\delta$  11.10 (s, 1H), 9.28 (brs, 1H), 9.15 (s, 1H), 8.74 (s, 1H), 8.21 (s, 2H), 7.61 (br s, 1H), 7.57 (s, 1H), 7.32–7.24 (m, 5H), 7.17 (app. d,  $J = 8.3$  Hz, 2H), 6.48 (t,  $J = 8.2$  Hz, 1H), 5.29 (brs, 1H), 4.93 (brs, 1H), 3.63 (m, 2H), 2.83 (m, 1H), 2.78 (s, 3H), 2.77 (s, 3H), 2.24 (m, 1H), 2.08 (m, 1H), 1.90 (m, 1H), 1.80 (m, 1H), 1.59–1.49 (m, 2H), 1.41–1.26 (m, 2H);  $^{13}\text{C}\{^1\text{H}\}$  NMR (125 MHz,  $\text{CD}_3\text{CN}$ ) 182.8, 153.7, 149.3, 143.1, 140.1, 138.6, 132.4 (q,  $J = 32.9$  Hz), 131.0, 129.6, 128.9, 128.7, 128.5, 128.4, 125.7 (q,  $J = 271.9$ ), 126.3, 124.6, 124.5 (q,  $J = 272.0$  Hz), 123.4 (q,  $J = 33.9$  Hz), 119.9, 115.6, 112.6, 110.9, 84.2, 67.2, 63.2, 56.2, 42.9, 37.4, 36.2, 32.8, 25.1, 24.7, 23.3.

**(1R,2R)-2-(3-(((1S,2S)-2-(2-(3-(3,5-Bis(trifluoromethyl)phenyl)ureido)-4-(trifluoromethyl)phenoxy)-2,3-dihydro-1H-inden-1-yl)thioureido)-N,N-dimethylcyclohexan-1-aminium chloride (ent-1-HCl):**  $^1\text{H}$  NMR (500 MHz,  $\text{CD}_3\text{CN}$ ) 11.20 (s, 1H), 9.39 (s, 1H), 8.68 (s, 1H), 8.20 (s, 3H), 7.90 (br s, 1H), 7.59 (s, 1H), 7.38–7.28 (m, 4H), 7.24 (m, 1H), 6.78 (br s, 1H), 5.24 (m, 1H), 4.80 (m, 1H), 3.98 (m, 1H), 3.60 (dd,  $J_1 = 15.5, 7.1$  Hz, 1H), 2.90 (d,  $J = 3.7$  Hz, 3H), 2.83 (m, 1H), 2.79 (d,  $J = 4.3$  Hz, 3H), 1.88 (m, 1H), 1.65 (app. d,  $J = 11.9$  Hz, 1H), 1.47 (m, 1H), 1.42 (m, 1H), 1.26–1.12 (m, 3H), 0.75 (m, 1H);  $^{13}\text{C}\{^1\text{H}\}$  NMR (125 MHz,  $\text{CD}_3\text{CN}$ ) 183.1, 153.7, 149.0, 143.0, 139.5, 139.0, 132.6 (q,  $J = 32.9$  Hz), 131.0, 129.9, 128.5, 126.2, 125.6 (q,  $J = 270.2$  Hz), 125.1, 124.5 (q,  $J = 271.9$  Hz), 123.7 (q,  $J = 32.2$  Hz), 120.1, 116.0, 115.7, 113.1, 110.9, 87.5, 67.4, 63.2, 56.1, 42.8, 37.8, 36.5, 32.9, 24.9, 24.7, 23.1.

**Catalyst Solution Structure Elucidation.** Catalyst 1 solution structure: The sample was prepared by dissolving catalyst 1 (10 mg, 0.0134 mmol, 100 mol %) in 0.6 mL  $\text{DCM-d}_2$ . The 2D NOESY spectrum was measured with 500 MHz spectrometer at 303 K. Catalyst 2 solution structure: The sample was prepared by dissolving catalyst 2 (10 mg, 0.0134 mmol, 100 mol %) in 0.6 mL of  $\text{DCM-d}_2$ . The 2D NOESY spectrum was measured with 500 MHz spectrometer at 303 K.

**Solution Structures of Hexafluoroacetylacetonate Salt Catalysts.** The sample of catalyst 1-hfacac salt was prepared by dissolving catalyst 1 (10 mg, 0.0134 mmol, 100 mol %) in 0.6 mL of  $\text{DCM-d}_2$ , and hfacac (1.9  $\mu\text{L}$ , 0.0134 mmol, 100 mol %) was subsequently added. The 2D NOESY spectrum was measured with a 500 MHz spectrometer at 303 K. The sample of catalyst 2-hfacac salt was prepared by using the procedure used for the 1-hfacac salt. The 2D NOESY spectrum was measured with a 300 MHz spectrometer at 303 K.

**Titration Experiments.** Titration of catalyst 1-hfacac with tetra-*n*-butylammonium chloride (*n*- $\text{Bu}_4\text{NCl}$ ) catalyst 1 (11.2 mg, 0.015 mmol, 100 mol %) was dissolved in  $\text{CD}_3\text{CN}$  (0.6 mL), and hfacac (2.1  $\mu\text{L}$ , 0.015 mmol, 100 mol %) was subsequently added and transferred to a NMR tube. This solution was titrated with 0.5 M solution of *n*- $\text{Bu}_4\text{NCl}$  in  $\text{CD}_3\text{CN}$ . The  $^1\text{H}$  NMR (300 MHz) measurement was performed every 30 min after the addition of *n*- $\text{Bu}_4\text{NCl}$ , insertion of the sample into the magnet, and initial shimming and receiver gain adjustment. All measurements were carried out at a probe temperature of 303 K.

## ■ ASSOCIATED CONTENT

### Supporting Information

The Supporting Information is available free of charge on the ACS Publications website at DOI: 10.1021/acs.joc.9b01980.

Details of the X-ray structural characterization, and computational details: total energies and Cartesian coordinates for the considered stationary points (PDF) NMR spectra (PDF) X-ray data for 1·HBr (CIF) X-ray data for 1·HCl (CIF)

X-ray data for 1·HF (CIF)  
 X-ray data for 2·DPP (CIF)  
 X-ray data for 2·HBr (CIF)  
 X-ray data for 2·HF (CIF)  
 X-ray data for 2·hfacac (CIF)  
 X-ray data for 2·TFA (CIF)

## AUTHOR INFORMATION

### Corresponding Author

\*E-mail: [petri.pihko@jyu.fi](mailto:petri.pihko@jyu.fi)

### ORCID

Filip Topić: 0000-0003-3811-6036

Kari Rissanen: 0000-0002-7282-8419

Imre Pápai: 0000-0002-4978-0365

Petri M. Pihko: 0000-0003-0126-0974

### Author Contributions

§A.J.N. and D.N. contributed equally.

### Notes

The authors declare no competing financial interest.

## ACKNOWLEDGMENTS

Financial support for this work was provided by the Academy of Finland (Grant Nos. 297874 and 307624) and the Hungarian Scientific Research Fund (OTKA, Grant No. K-112028). We thank Dr. Nicolas Probst for earlier synthetic and mechanistic efforts.

## REFERENCES

- (1) (a) Walsh, P. J.; Kozlowski, M. C. *Fundamentals of Asymmetric Catalysis*; University Science Books: Sausalito, CA, 2008. (b) Sunoj, R. B. Transition State Models for Understanding the Origin of Chiral Induction in Asymmetric Catalysis. *Acc. Chem. Res.* **2016**, *49*, 1019–1028.
- (2) Harper, K. C.; Sigman, M. S. Predicting and Optimizing Asymmetric Catalyst Performance Using the Principles of Experimental Design and Steric Parameters. *Proc. Natl. Acad. Sci. U. S. A.* **2011**, *108*, 2179–2183.
- (3) Sharma, R.; Raduly, Z.; Miskei, M.; Fuxreiter, M. Fuzzy Complexes: Specific Binding without Complete Folding. *FEBS Lett.* **2015**, *589*, 2533–2542.
- (4) Roca, M.; Messer, B.; Hilvert, D.; Warshel, A. On the Relationship between Folding and Chemical Landscapes in Enzyme Catalysis. *Proc. Natl. Acad. Sci. U. S. A.* **2008**, *105*, 13877–13882.
- (5) Petrović, D.; Rizzo, V. A.; Kamerlin, S. C. L.; Sanchez-Ruiz, J. M. Conformational Dynamics and Enzyme Evolution. *J. R. Soc., Interface* **2018**, *15*, 20180330.
- (6) (a) Hua, M.-Q.; Cui, H.-F.; Wang, L.; Nie, J.; Ma, J.-A. Reversal of Enantioselectivity by Tuning the Conformational Flexibility of Phase Transfer Catalysts. *Angew. Chem., Int. Ed.* **2010**, *49*, 2772–2776. (b) Sohtome, Y.; Tanaka, S.; Takada, K.; Yamaguchi, T.; Nagasawa, K. Solvent-Dependent Enantiodivergent Mannich-Type Reaction: Utilizing a Conformationally Flexible Guanidine/Bisthiourea Organocatalyst. *Angew. Chem., Int. Ed.* **2010**, *49*, 9254–9257. (c) Metrano, A. J.; Abascal, N. C.; Mercado, B. Q.; Paulson, E. K.; Hurlley, A. E.; Miller, S. J. Diversity of Secondary Structure in Catalytic Peptides with  $\beta$ -Turn-Biased Sequences. *J. Am. Chem. Soc.* **2017**, *139*, 492–516. (d) Yan, X. C.; Metrano, A. J.; Robertson, M. J.; Abascal, N. C.; Tirado-Rives, J.; Miller, S. J.; Jorgensen, W. L. Molecular Dynamics Simulations of a Conformationally Mobile Peptide-Based Catalyst for Atroposelective Bromination. *ACS Catal.* **2018**, *8*, 9968–9979. (e) For a recent insightful review, see: Crawford, J. M.; Sigman, M. S. Conformational Dynamics in Asymmetric Catalysis: Is Catalyst Flexibility a Design Element? *Synthesis* **2019**, *51*, 1021–1036.
- (7) (a) Neuvonen, A. J.; Földes, T.; Madarász, Á.; Pápai, I.; Pihko, P. M. Organocatalysts Fold to Generate an Active Site Pocket for the Mannich Reaction. *ACS Catal.* **2017**, *7*, 3284–3294. (b) Neuvonen, A. J.; Pihko, P. M. Enantioselective Mannich Reaction of  $\beta$ -Keto Esters with Aromatic and Aliphatic Imines Using a Cooperatively Assisted Bifunctional Catalyst. *Org. Lett.* **2014**, *16*, 5152–5155. (c) Probst, N.; Madarász, Á.; Valkonen, A.; Pápai, I.; Rissanen, K.; Neuvonen, A.; Pihko, P. M. Cooperative Assistance in Bifunctional Organocatalysis: Enantioselective Mannich Reactions with Aliphatic and Aromatic Imines. *Angew. Chem., Int. Ed.* **2012**, *51*, 8495–8499. (d) The relative rates for catalysts 1 and 2 in the test reaction were estimated from the initial rates reported in ref 7c.
- (8) For leading references to enantioselective Mannich reactions catalyzed by (thio)urea tertiary amine catalysts, see: (a) Tillman, A. L.; Ye, J.; Dixon, D. J. Direct enantio- and diastereoselective Mannich reactions of malonate and  $\beta$ -keto esters with *N*-Boc and *N*-Cbz aldimines catalyzed by a bifunctional cinchonine derivative. *Chem. Commun.* **2006**, 1191–1193. (b) Song, J.; Wang, Y.; Deng, L. The Mannich Reaction of Malonates with Simple Imines Catalyzed by Bifunctional Cinchona Alkaloids: Enantioselective Synthesis of  $\beta$ -Amino Acids. *J. Am. Chem. Soc.* **2006**, *128*, 6048–6049. (c) Guo, Q.; Zhao, J. C.-G. Highly Enantioselective Three-Component Direct Mannich Reactions of Unfunctionalized Ketones Catalyzed by Bifunctional Organocatalysts. *Org. Lett.* **2013**, *15*, 508–510. (d) Kobayashi, S.; Mori, Y.; Fossey, J. S.; Salter, M. M. Catalytic Enantioselective Formation of C–C Bonds by Addition to Imines and Hydrazones: A Ten-Year Update. *Chem. Rev.* **2011**, *111*, 2626–2704.
- (9) Jones, C. R.; Dan Pantoş, G.; Morrison, A. J.; Smith, M. D. Plagiarizing Proteins: Enhancing Efficiency in Asymmetric Hydrogen-Bonding Catalysis through Positive Cooperativity. *Angew. Chem., Int. Ed.* **2009**, *48*, 7391–7394.
- (10) (a) Supady, A.; Hecht, S.; Baldauf, C. About Underappreciated Yet Active Conformations of Thiourea Organocatalysts. *Org. Lett.* **2017**, *19*, 4199–4202. (b) Luchini, G.; Ascough, D. M. H.; Alegre-Requena, J. V.; Gouverneur, V.; Paton, R. S. Data-mining the Diaryl(thio)urea Conformational Landscape: Understanding the Contrasting Behavior of Ureas and Thioureas with Quantum Chemistry. *Tetrahedron* **2019**, *75*, 697–702. (c) For a recent example of an *anti-syn* bisurea catalyst capable of binding fluoride, see: Pupo, G.; Ibba, F.; Ascough, D. M. H.; Vicini, A. C.; Ricci, P.; Christensen, K. E.; Pfeifer, L.; Morphy, J. R.; Brown, J. M.; Paton, R. S.; Gouverneur, V. Asymmetric nucleophilic fluorination under hydrogen bonding phase-transfer catalysis. *Science* **2018**, *360*, 638–642. (d) Pupo, G.; Vicini, A. C.; Ascough, D. M. H.; Ibba, F.; Christensen, K. E.; Thompson, A. L.; Brown, J. M.; Paton, R. S.; Gouverneur, V. Hydrogen Bonding Phase-Transfer Catalysis with Potassium Fluoride: Enantioselective Synthesis of  $\beta$ -Fuoroamines. *J. Am. Chem. Soc.* **2019**, *141*, 2878–2883. (e) For a leading references to dimeric thiourea catalysts with halogen binding, see: Ford, D. D.; Lehnher, D.; Kennedy, C. R.; Jacobsen, E. N. On- and Off-Cycle Catalyst Cooperativity in Anion-Binding Catalysis. *J. Am. Chem. Soc.* **2016**, *138*, 7860–7863. (f) Park, Y.; Harper, K. C.; Kuhl, N.; Kwan, E. E.; Liu, R. Y.; Jacobsen, E. N. Macrocyclic bis-thioureas catalyze stereospecific glycosylation reactions. *Science* **2017**, *355*, 162–166.
- (11) (a) Gale, P. A.; Howe, E. N. W.; Wu, X. Anion Receptor Chemistry. *Chem.* **2016**, *1*, 351–422. (b) Blazek Bregovic, V.; Basaric, N.; Mlinaric-Majerski, K. Anion Binding with Urea and Thiourea Derivatives. *Coord. Chem. Rev.* **2015**, *295*, 80–124.
- (12) All reported distances to hydrogens in the X-ray structures refer to calculated positions of the hydrogen atoms.
- (13) Dunbrack, R. L., Jr.; Karplus, M. Conformational Analysis of the Backbone-dependent Rotamer Preferences of Protein Sidechains. *Nat. Struct. Mol. Biol.* **1994**, *1*, 334–340.
- (14) (a) Haushalter, K. A.; Lau, J.; Roberts, J. D. An NMR Investigation of the Effect of Hydrogen Bonding on the Rates of Rotation about the C–N Bonds in Urea and Thiourea. *J. Am. Chem. Soc.* **1996**, *118*, 8891–8896. (b) Chambers, C. C.; Archibong, E. F.; Jabalameli, A.; Sullivan, R. H.; Giesen, D. J.; Cramer, C. J.; Truhlar, D. G. Quantum mechanical and  $^{13}\text{C}$  dynamic NMR study of 1,3-

dimethylthiourea conformational isomerizations. *J. Mol. Struct.: THEOCHEM* **1998**, *425*, 61–68.

(15) (a) Interestingly, thioureas appear to strongly prefer the *anti-anti* conformation when bound to chloride ions, based on a search of the CSD database. *CSD: ConQuest V2.02* (2019). Groom, C. R.; Bruno, I. J.; Lightfoot, M. P.; Ward, S. C. *Acta Crystallogr., Sect. B: Struct. Sci., Cryst. Eng. Mater.* **2016**, *B72*, 171–179. Of the 98 hits found with thiourea N–H contacting the chloride ion, only a single example of an *anti-syn* or *syn-anti* conformation of a thiourea bound to chloride ion has been reported outside of these studies. See: (b) Soriano, M. L.; Lenthall, J. T.; Anderson, K. W.; Smith, S. J.; Steed, J. W. Enhanced Anion Binding from Unusual Coordination Modes of Bis(thiourea) Ligands in Platinum Group Metal Complexes. *Chem. - Eur. J.* **2010**, *16*, 10818–10831.

(16) For a review of fluoride sensors, see: Cametti, M.; Rissanen, K. Highlights on Contemporary Recognition and Sensing of Fluoride Anion in Solution and in the Solid State. *Chem. Soc. Rev.* **2013**, *42*, 2016–2038.

(17) In these experiments, *ent-1* was used due to temporary shortage of supply of catalyst **1**.

DEPARTMENT OF CHEMISTRY, UNIVERSITY OF JYVÄSKYLÄ  
RESEARCH REPORT SERIES

1. Vuolle, Mikko: Electron paramagnetic resonance and molecular orbital study of radical ions generated from (2.2)metacyclophane, pyrene and its hydrogenated compounds by alkali metal reduction and by thallium(III)trifluoroacetate oxidation. (99 pp.) 1976
2. Pasanen, Kaija: Electron paramagnetic resonance study of cation radical generated from various chlorinated biphenyls. (66 pp.) 1977
3. Carbon-13 Workshop, September 6-8, 1977. (91 pp.) 1977
4. Laihia, Katri: On the structure determination of norbornane polyols by NMR spectroscopy. (111 pp.) 1979
5. Nyrönen, Timo: On the EPR, ENDOR and visible absorption spectra of some nitrogen containing heterocyclic compounds in liquid ammonia. (76 pp.) 1978
6. Talvitie, Antti: Structure determination of some sesquiterpenoids by shift reagent NMR. (54 pp.) 1979
7. Häkli, Harri: Structure analysis and molecular dynamics of cyclic compounds by shift reagent NMR. (48 pp.) 1979
8. Pitkänen, Ilkka: Thermodynamics of complexation of 1,2,4-triazole with divalent manganese, cobalt, nickel, copper, zinc, cadmium and lead ions in aqueous sodium perchlorate solutions. (89 pp.) 1980
9. Asunta, Tuula: Preparation and characterization of new organometallic compounds synthesized by using metal vapours. (91 pp.) 1980
10. Sattar, Mohammad Abdus: Analyses of MCPA and its metabolites in soil. (57 pp.) 1980
11. Bibliography 1980. (31 pp.) 1981
12. Knuuttila, Pekka: X-Ray structural studies on some divalent 3d metal compounds of picolinic and isonicotinic acid N-oxides. (77 pp.) 1981
13. Bibliography 1981. (33 pp.) 1982
14. 6<sup>th</sup> National NMR Symposium, September 9-10, 1982, Abstracts. (49 pp.) 1982
15. Bibliography 1982. (38 pp.) 1983
16. Knuuttila, Hilka: X-Ray structural studies on some Cu(II), Co(II) and Ni(II) complexes with nicotinic and isonicotinic acid N-oxides. (54 pp.) 1983
17. Symposium on inorganic and analytical chemistry May 18, 1984, Program and Abstracts. (100 pp.) 1984
18. Knuutinen, Juha: On the synthesis, structure verification and gas chromatographic determination of chlorinated catechols and guaiacols occurring in spent bleach liquors of kraft pulp mill. (30 pp.) 1984
19. Bibliography 1983. (47 pp.) 1984
20. Pitkänen, Maija: Addition of BrCl, B<sub>2</sub> and Cl<sub>2</sub> to methyl esters of propenoic and 2-butenic acid derivatives and <sup>13</sup>C NMR studies on methyl esters of saturated aliphatic mono- and dichlorocarboxylic acids. (56 pp.) 1985
21. Bibliography 1984. (39 pp.) 1985
22. Salo, Esa: EPR, ENDOR and TRIPLE spectroscopy of some nitrogen heteroaromatics in liquid ammonia. (111 pp.) 1985

DEPARTMENT OF CHEMISTRY, UNIVERSITY OF JYVÄSKYLÄ  
RESEARCH REPORT SERIES

23. Humppi, Tarmo: Synthesis, identification and analysis of dimeric impurities of chlorophenols. (39 pp.) 1985
24. Aho, Martti: The ion exchange and adsorption properties of sphagnum peat under acid conditions. (90 pp.) 1985
25. Bibliography 1985 (61 pp.) 1986
26. Bibliography 1986. (23 pp.) 1987
27. Bibliography 1987. (26 pp.) 1988
28. Paasivirta, Jaakko (Ed.): Structures of organic environmental chemicals. (67 pp.) 1988
29. Paasivirta, Jaakko (Ed.): Chemistry and ecology of organo-element compounds. (93 pp.) 1989
30. Sinkkonen, Seija: Determination of crude oil alkylated dibenzothiophenes in environment. (35 pp.) 1989
31. Kolehmainen, Erkki (Ed.): XII National NMR Symposium Program and Abstracts. (75 pp.) 1989
32. Kuokkanen, Tauno: Chlorocymenes and Chlorocymenenes: Persistent chlorocompounds in spent bleach liquors of kraft pulp mills. (40 pp.) 1989
33. Mäkelä, Reijo: ESR, ENDOR and TRIPLE resonance study on substituted 9,10-anthraquinone radicals in solution. (35 pp.) 1990
34. Veijanen, Anja: An integrated sensory and analytical method for identification of off-flavour compounds. (70 pp.) 1990
35. Kasa, Seppo: EPR, ENDOR and TRIPLE resonance and molecular orbital studies on a substitution reaction of anthracene induced by thallium(III) in two fluorinated carboxylic acids. (114 pp.) 1990
36. Herve, Sirpa: Mussel incubation method for monitoring organochlorine compounds in freshwater recipients of pulp and paper industry. (145 pp.) 1991
37. Pohjola, Pekka: The electron paramagnetic resonance method for characterization of Finnish peat types and iron (III) complexes in the process of peat decomposition. (77 pp.) 1991
38. Paasivirta, Jaakko (Ed.): Organochlorines from pulp mills and other sources. Research methodology studies 1988-91. (120 pp.) 1992
39. Veijanen, Anja (Ed.): VI National Symposium on Mass Spectrometry, May 13-15, 1992, Abstracts. (55 pp.) 1992
40. Rissanen, Kari (Ed.): The 7. National Symposium on Inorganic and Analytical Chemistry, May 22, 1992, Abstracts and Program. (153 pp.) 1992
41. Paasivirta, Jaakko (Ed.): CEOEC'92, Second Finnish-Russian Seminar: Chemistry and Ecology of Organo-Element Compounds. (93 pp.) 1992
42. Koistinen, Jaana: Persistent polychloroaromatic compounds in the environment: structure-specific analyses. (50 pp.) 1993
43. Virkki, Liisa: Structural characterization of chlorolignins by spectroscopic and liquid chromatographic methods and a comparison with humic substances. (62 pp.) 1993
44. Helenius, Vesa: Electronic and vibrational excitations in some

DEPARTMENT OF CHEMISTRY, UNIVERSITY OF JYVÄSKYLÄ  
RESEARCH REPORT SERIES

- biologically relevant molecules. (30 pp.) 1993
45. Leppä-aho, Jaakko: Thermal behaviour, infrared spectra and x-ray structures of some new rare earth chromates(VI). (64 pp.) 1994
46. Kotila, Sirpa: Synthesis, structure and thermal behavior of solid copper(II) complexes of 2-amino-2-hydroxymethyl-1,3-propanediol. (111 pp.) 1994
47. Mikkonen, Anneli: Retention of molybdenum(VI), vanadium(V) and tungsten(VI) by kaolin and three Finnish mineral soils. (90 pp.) 1995
48. Suontamo, Reijo: Molecular orbital studies of small molecules containing sulfur and selenium. (42 pp.) 1995
49. Hämäläinen, Jouni: Effect of fuel composition on the conversion of fuel-N to nitrogen oxides in the combustion of small single particles. (50 pp.) 1995
50. Nevalainen, Tapio: Polychlorinated diphenyl ethers: synthesis, NMR spectroscopy, structural properties, and estimated toxicity. (76 pp.) 1995
51. Aittola, Jussi-Pekka: Organochloro compounds in the stack emission. (35 pp.) 1995
52. Harju, Timo: Ultrafast polar molecular photophysics of (dibenzylmethine)borondifluoride and 4-aminophthalimide in solution. (61 pp.) 1995
53. Maatela, Paula: Determination of organically bound chlorine in industrial and environmental samples. (83 pp.) 1995
54. Paasivirta, Jaakko (Ed.): CEOEC'95, Third Finnish-Russian Seminar: Chemistry and Ecology of Organo-Element Compounds. (109 pp.) 1995
55. Huuskonen, Juhani: Synthesis and structural studies of some supramolecular compounds. (54 pp.) 1995
56. Palm, Helena: Fate of chlorophenols and their derivatives in sawmill soil and pulp mill recipient environments. (52 pp.) 1995
57. Rantio, Tiina: Chlorohydrocarbons in pulp mill effluents and their fate in the environment. (89 pp.) 1997
58. Ratilainen, Jari: Covalent and non-covalent interactions in molecular recognition. (37 pp.) 1997
59. Kolehmainen, Erkki (Ed.): XIX National NMR Symposium, June 4-6, 1997, Abstracts. (89 pp.) 1997
60. Matilainen, Rose: Development of methods for fertilizer analysis by inductively coupled plasma atomic emission spectrometry. (41 pp.) 1997
61. Koistinen, Jari (Ed.): Spring Meeting on the Division of Synthetic Chemistry, May 15-16, 1997, Program and Abstracts. (36 pp.) 1997
62. Lappalainen, Kari: Monomeric and cyclic bile acid derivatives: syntheses, NMR spectroscopy and molecular recognition properties. (50 pp.) 1997
63. Laitinen, Eira: Molecular dynamics of cyanine dyes and phthalimides in solution: picosecond laser studies. (62 pp.) 1997
64. Eloranta, Jussi: Experimental and theoretical studies on some

DEPARTMENT OF CHEMISTRY, UNIVERSITY OF JYVÄSKYLÄ  
RESEARCH REPORT SERIES

- quinone and quinol radicals. (40 pp.) 1997
65. Oksanen, Jari: Spectroscopic characterization of some monomeric and aggregated chlorophylls. (43 pp.) 1998
66. Häkkänen, Heikki: Development of a method based on laser-induced plasma spectrometry for rapid spatial analysis of material distributions in paper coatings. (60 pp.) 1998
67. Virtapohja, Janne: Fate of chelating agents used in the pulp and paper industries. (58 pp.) 1998
68. Airola, Karri: X-ray structural studies of supramolecular and organic compounds. (39 pp.) 1998
69. Hyötyläinen, Juha: Transport of lignin-type compounds in the receiving waters of pulp mills. (40 pp.) 1999
70. Ristolainen, Matti: Analysis of the organic material dissolved during totally chlorine-free bleaching. (40 pp.) 1999
71. Eklin, Tero: Development of analytical procedures with industrial samples for atomic emission and atomic absorption spectrometry. (43 pp.) 1999
72. Väლისаari, Jouni: Hygiene properties of resol-type phenolic resin laminates. (129 pp.) 1999
73. Hu, Jiwei: Persistent polyhalogenated diphenyl ethers: model compounds syntheses, characterization and molecular orbital studies. (59 pp.) 1999
74. Malkavaara, Petteri: Chemometric adaptations in wood processing chemistry. (56 pp.) 2000
75. Kujala Elena, Laihia Katri, Nieminen Kari (Eds.): NBC 2000, Symposium on Nuclear, Biological and Chemical Threats in the 21<sup>st</sup> Century. (299 pp.) 2000
76. Rantalainen, Anna-Lea: Semipermeable membrane devices in monitoring persistent organic pollutants in the environment. (58 pp.) 2000
77. Lahtinen, Manu: *In situ* X-ray powder diffraction studies of Pt/C, CuCl/C and Cu<sub>2</sub>O/C catalysts at elevated temperatures in various reaction conditions. (92 pp.) 2000
78. Tamminen, Jari: Syntheses, empirical and theoretical characterization, and metal cation complexation of bile acid-based monomers and open/closed dimers. (54 pp.) 2000
79. Vatanen, Virpi: Experimental studies by EPR and theoretical studies by DFT calculations of  $\alpha$ -amino-9,10-anthraquinone radical anions and cations in solution. (37 pp.) 2000
80. Kotilainen, Risto: Chemical changes in wood during heating at 150-260 °C. (57 pp.) 2000
81. Nissinen, Maija: X-ray structural studies on weak, non-covalent interactions in supramolecular compounds. (69 pp.) 2001
82. Wegelius, Elina: X-ray structural studies on self-assembled hydrogen-bonded networks and metallosupramolecular complexes. (84 pp.) 2001
83. Paasivirta, Jaakko (Ed.): CEOEC'2001, Fifth Finnish-Russian Seminar: Chemistry and Ecology of Organo-Element Compounds. (163 pp.) 2001
84. Kiljunen, Toni: Theoretical studies on spectroscopy and

DEPARTMENT OF CHEMISTRY, UNIVERSITY OF JYVÄSKYLÄ  
RESEARCH REPORT SERIES

- atomic dynamics in rare gas solids. (56 pp.) 2001
85. Du, Jin: Derivatives of dextran: synthesis and applications in oncology. (48 pp.) 2001
86. Koivisto, Jari: Structural analysis of selected polychlorinated persistent organic pollutants (POPs) and related compounds. (88 pp.) 2001
87. Feng, Zhinan: Alkaline pulping of non-wood feedstocks and characterization of black liquors. (54 pp.) 2001
88. Halonen, Markku: Lahon havupuun käyttö sulfaattiprosessin raaka-aineena sekä havupuun lahontorjunta. (90 pp.) 2002
89. Falábu, Dezső: Synthesis, conformational analysis and complexation studies of resorcarene derivatives. (212 pp.) 2001
90. Lehtovuori, Pekka: EMR spectroscopic studies on radicals of ubiquinones Q-*n*, vitamin K<sub>3</sub> and vitamine E in liquid solution. (40 pp.) 2002
91. Perkkalainen, Paula: Polymorphism of sugar alcohols and effect of grinding on thermal behavior on binary sugar alcohol mixtures. (53 pp.) 2002
92. Ihalainen, Janne: Spectroscopic studies on light-harvesting complexes of green plants and purple bacteria. (42 pp.) 2002
93. Kunttu, Henrik, Kiljunen, Toni (Eds.): 4<sup>th</sup> International Conference on Low Temperature Chemistry. (159 pp.) 2002
94. Väisänen, Ari: Development of methods for toxic element analysis in samples with environmental concern by ICP-AES and ETAAS. (54 pp.) 2002
95. Luostarinen, Minna: Synthesis and characterisation of novel resorcarene derivatives. (200 pp.) 2002
96. Louhelainen, Jarmo: Changes in the chemical composition and physical properties of wood and nonwood black liquors during heating. (68 pp.) 2003
97. Lahtinen, Tanja: Concave hydrocarbon cyclophane  $\pi$ -prismans. (65 pp.) 2003
98. Laihia, Katri (Ed.): NBC 2003, Symposium on Nuclear, Biological and Chemical Threats – A Crisis Management Challenge. (245 pp.) 2003
99. Oasmaa, Anja: Fuel oil quality properties of wood-based pyrolysis liquids. (32 pp.) 2003
100. Virtanen, Elina: Syntheses, structural characterisation, and cation/anion recognition properties of nano-sized bile acid-based host molecules and their precursors. (123 pp.) 2003
101. Nättinen, Kalle: Synthesis and X-ray structural studies of organic and metallo-organic supramolecular systems. (79 pp.) 2003
102. Lampiselkä, Jarkko: Demonstraatio lukion kemian opetuksessa. (285 pp.) 2003
103. Kallioinen, Jani: Photoinduced dynamics of Ru(dcbpy)<sub>2</sub>(NCS)<sub>2</sub> – in solution and on nanocrystalline titanium dioxide thin films. (47 pp.) 2004
104. Valkonen, Arto (Ed.): VII Synthetic Chemistry Meeting and XXVI Finnish NMR Symposium. (103 pp.) 2004



DEPARTMENT OF CHEMISTRY, UNIVERSITY OF JYVÄSKYLÄ  
RESEARCH REPORT SERIES

105. Vaskonen, Kari: Spectroscopic studies on atoms and small molecules isolated in low temperature rare gas matrices. (65 pp.) 2004
106. Lehtovuori, Viivi: Ultrafast light induced dissociation of Ru(dcbpy)(CO)<sub>2</sub>I<sub>2</sub> in solution. (49 pp.) 2004
107. Saarenketo, Pauli: Structural studies of metal complexing Schiff bases, Schiff base derived *N*-glycosides and cyclophane  $\pi$ -prismoids. (95 pp.) 2004
108. Paasivirta, Jaakko (Ed.): CEOEC'2004, Sixth Finnish-Russian Seminar: Chemistry and Ecology of Organo-Element Compounds. (147 pp.) 2004
109. Suontamo, Tuula: Development of a test method for evaluating the cleaning efficiency of hard-surface cleaning agents. (96 pp.) 2004
110. Güneş, Minna: Studies of thiocyanates of silver for nonlinear optics. (48 pp.) 2004
111. Ropponen, Jarmo: Aliphatic polyester dendrimers and dendrons. (81 pp.) 2004
112. Vu, Mân Thi Hong: Alkaline pulping and the subsequent elemental chlorine-free bleaching of bamboo (*Bambusa procera*). (69 pp.) 2004
113. Mansikkamäki, Heidi: Self-assembly of resorcinarenes. (77 pp.) 2006
114. Tuononen, Heikki M.: EPR spectroscopic and quantum chemical studies of some inorganic main group radicals. (79 pp.) 2005
115. Kaski, Saara: Development of methods and applications of laser-induced plasma spectroscopy in vacuum ultraviolet. (44 pp.) 2005
116. Mäkinen, Riika-Mari: Synthesis, crystal structure and thermal decomposition of certain metal thiocyanates and organic thiocyanates. (119 pp.) 2006
117. Ahokas, Jussi: Spectroscopic studies of atoms and small molecules isolated in rare gas solids: photodissociation and thermal reactions. (53 pp.) 2006
118. Busi, Sara: Synthesis, characterization and thermal properties of new quaternary ammonium compounds: new materials for electrolytes, ionic liquids and complexation studies. (102 pp.) 2006
119. Mäntykoski, Keijo: PCBs in processes, products and environment of paper mills using wastepaper as their raw material. (73 pp.) 2006
120. Laamanen, Pirkko-Leena: Simultaneous determination of industrially and environmentally relevant aminopolycarboxylic and hydroxycarboxylic acids by capillary zone electrophoresis. (54 pp.) 2007
121. Salmela, Maria: Description of oxygen-alkali delignification of kraft pulp using analysis of dissolved material. (71 pp.) 2007
122. Lehtovaara, Lauri: Theoretical studies of atomic scale impurities in superfluid <sup>4</sup>He. (87 pp.) 2007
123. Rautiainen, J. Mikko: Quantum chemical calculations of structures, bonding, and spectroscopic properties of some sulphur and selenium iodine cations. (71 pp.) 2007
124. Nummelin, Sami: Synthesis, characterization, structural and

- retrostructural analysis of self-assembling pore forming dendrimers. (286 pp.) 2008
125. Sopo, Harri: Uranyl(VI) ion complexes of some organic aminobisphenolate ligands: syntheses, structures and extraction studies. (57 pp.) 2008
126. Valkonen, Arto: Structural characteristics and properties of substituted cholanoates and *N*-substituted cholanamides. (80 pp.) 2008
127. Lähde, Anna: Production and surface modification of pharmaceutical nano- and microparticles with the aerosol flow reactor. (43 pp.) 2008
128. Beyeh, Ngong Kodiah: Resorcinarenes and their derivatives: synthesis, characterization and complexation in gas phase and in solution. (75 pp.) 2008
129. Välisaari, Jouni, Lundell, Jan (Eds.): Kemian opetuksen päivät 2008: uusia oppimisympäristöjä ja ongelmalähtöistä opetusta. (118 pp.) 2008
130. Myllyperkiö, Pasi: Ultrafast electron transfer from potential organic and metal containing solar cell sensitizers. (69 pp.) 2009
131. Käkölä, Jaana: Fast chromatographic methods for determining aliphatic carboxylic acids in black liquors. (82 pp.) 2009
132. Koivukorpi, Juha: Bile acid-arene conjugates: from photoswitchability to cancer cell detection. (67 pp.) 2009
133. Tuuttila, Tero: Functional dendritic polyester compounds: synthesis and characterization of small bifunctional dendrimers and dyes. (74 pp.) 2009
134. Salorinne, Kirsi: Tetramethoxy resorcinarene based cation and anion receptors: synthesis, characterization and binding properties. (79 pp.) 2009
135. Rautiainen, Riikka: The use of first-thinning Scots pine (*Pinus sylvestris*) as fiber raw material for the kraft pulp and paper industry. (73 pp.) 2010
136. Ilander, Laura: Uranyl salophens: synthesis and use as ditopic receptors. (199 pp.) 2010
137. Kiviniemi, Tiina: Vibrational dynamics of iodine molecule and its complexes in solid krypton - Towards coherent control of bimolecular reactions? (73 pp.) 2010
138. Ikonen, Satu: Synthesis, characterization and structural properties of various covalent and non-covalent bile acid derivatives of N/O-heterocycles and their precursors. (105 pp.) 2010
139. Siitonen, Anni: Spectroscopic studies of semiconducting single-walled carbon nanotubes. (56 pp.) 2010
140. Raatikainen, Kari: Synthesis and structural studies of piperazine cyclophanes – Supramolecular systems through Halogen and Hydrogen bonding and metal ion coordination. (69 pp.) 2010
141. Leivo, Kimmo: Gelation and gel properties of two- and three-component Pyrene based low molecular weight organogelators. (116 pp.) 2011
142. Martiskainen, Jari: Electronic energy transfer in light-harvesting complexes isolated from *Spinacia oleracea* and from three

- photosynthetic green bacteria  
*Chloroflexus aurantiacus*,  
*Chlorobium tepidum*, and  
*Prosthecochloris aestuarii*. (55  
pp.) 2011
143. Wichmann, Oula: Syntheses,  
characterization and structural  
properties of [O,N,O,X']  
aminobisphenolate metal  
complexes. (101 pp.) 2011
144. Ilander, Aki: Development of  
ultrasound-assisted digestion  
methods for the determination of  
toxic element concentrations in  
ash samples by ICP-OES. (58 pp.)  
2011
145. The Combined XII Spring  
Meeting of the Division of  
Synthetic Chemistry and XXXIII  
Finnish NMR Symposium. Book  
of Abstracts. (90 pp.) 2011
146. Valto, Piia: Development of fast  
analysis methods for extractives  
in papermaking process waters.  
(73 pp.) 2011
147. Andersin, Jenni: Catalytic activity  
of palladium-based nanostructures  
in the conversion of simple  
olefinic hydro- and  
chlorohydrocarbons from first  
principles. (78 pp.) 2011
148. Aumanen, Jukka: Photophysical  
properties of dansylated  
poly(propylene amine)  
dendrimers. (55 pp.) 2011
149. Kärnä, Minna: Ether-  
functionalized quaternary  
ammonium ionic liquids –  
synthesis, characterization and  
physicochemical properties. (76  
pp.) 2011
150. Jurček, Ondřej: Steroid conjugates  
for applications in pharmacology  
and biology. (57 pp.) 2011
151. Nauha, Elisa: Crystalline forms of  
selected Agrochemical actives:  
design and synthesis of cocrystals.  
(77 pp.) 2012
152. Ahkola, Heidi: Passive sampling  
in monitoring of nonylphenol  
ethoxylates and nonylphenol in  
aquatic environments. (92 pp.)  
2012
153. Helttunen, Kaisa: Exploring the  
self-assembly of resorcinarenes:  
from molecular level interactions  
to mesoscopic structures. (78 pp.)  
2012
154. Linnanto, Juha: Light excitation  
transfer in photosynthesis  
revealed by quantum chemical  
calculations and exciton theory.  
(179 pp.) 2012
155. Roiko-Jokela, Veikko: Digital  
imaging and infrared  
measurements of soil adhesion  
and cleanability of semihard and  
hard surfaces. (122 pp.) 2012
156. Noponen, Virpi: Amides of bile  
acids and biologically important  
small molecules: properties and  
applications. (85 pp.) 2012
157. Hulkko, Eero: Spectroscopic  
signatures as a probe of structure  
and dynamics in condensed-phase  
systems – studies of iodine and  
gold ranging from isolated  
molecules to nanoclusters. (69  
pp.) 2012
158. Lappi, Hanna: Production of  
Hydrocarbon-rich biofuels from  
extractives-derived materials. (95  
pp.) 2012
159. Nykänen, Lauri: Computational  
studies of Carbon chemistry on  
transition metal surfaces. (76 pp.)  
2012
160. Ahonen, Kari: Solid state studies  
of pharmaceutically important  
molecules and their derivatives.  
(65 pp.) 2012

DEPARTMENT OF CHEMISTRY, UNIVERSITY OF JYVÄSKYLÄ  
RESEARCH REPORT SERIES

161. Pakkanen, Hannu: Characterization of organic material dissolved during alkaline pulping of wood and non-wood feedstocks. (76 pp.) 2012
162. Moilanen, Jani: Theoretical and experimental studies of some main group compounds: from closed shell interactions to singlet diradicals and stable radicals. (80 pp.) 2012
163. Himanen, Jatta: Stereoselective synthesis of Oligosaccharides by *De Novo* Saccharide welding. (133 pp.) 2012
164. Bunzen, Hana: Steroidal derivatives of nitrogen containing compounds as potential gelators. (76 pp.) 2013
165. Seppälä, Petri: Structural diversity of copper(II) amino alcohol complexes. Syntheses, structural and magnetic properties of bidentate amino alcohol copper(II) complexes. (67 pp.) 2013
166. Lindgren, Johan: Computational investigations on rotational and vibrational spectroscopies of some diatomics in solid environment. (77 pp.) 2013
167. Giri, Chandan: Sub-component self-assembly of linear and non-linear diamines and diacylhydrazines, formylpyridine and transition metal cations. (145 pp.) 2013
168. Riisiö, Antti: Synthesis, Characterization and Properties of Cu(II)-, Mo(VI)- and U(VI) Complexes With Diaminotetraphenolate Ligands. (51 pp.) 2013
169. Kiljunen, Toni (Ed.): Chemistry and Physics at Low Temperatures. Book of Abstracts. (103 pp.) 2013
170. Hänninen, Mikko: Experimental and Computational Studies of Transition Metal Complexes with Polydentate Amino- and Aminophenolate Ligands: Synthesis, Structure, Reactivity and Magnetic Properties. (66 pp.) 2013
171. Antila, Liisa: Spectroscopic studies of electron transfer reactions at the photoactive electrode of dye-sensitized solar cells. (53 pp.) 2013
172. Kemppainen, Eeva: Mukaiyama-Michael reactions with  $\alpha$ -substituted acroleins – a useful tool for the synthesis of the pectenotoxins and other natural product targets. (190 pp.) 2013
173. Virtanen, Suvi: Structural Studies of Dielectric Polymer Nanocomposites. (49 pp.) 2013
174. Yliniemelä-Sipari, Sanna: Understanding The Structural Requirements for Optimal Hydrogen Bond Catalyzed Enolization – A Biomimetic Approach. (160 pp.) 2013
175. Leskinen, Mikko V: Remote  $\beta$ -functionalization of  $\beta'$ -keto esters. (105 pp.) 2014
176. 12<sup>th</sup> European Conference on Research in Chemistry Education (ECRICE2014). Book of Abstracts. (166 pp.) 2014
177. Peuronen, Anssi: N-Monoalkylated DABCO-Based N-Donors as Versatile Building Blocks in Crystal Engineering and Supramolecular Chemistry. (54 pp.) 2014
178. Perämäki, Siiri: Method development for determination and recovery of rare earth elements from industrial fly ash. (88 pp.) 2014

DEPARTMENT OF CHEMISTRY, UNIVERSITY OF JYVÄSKYLÄ  
RESEARCH REPORT SERIES

179. Chernyshev, Alexander, N.: Nitrogen-containing ligands and their platinum(IV) and gold(III) complexes: investigation and basicity and nucleophilicity, luminescence, and aurophilic interactions. (64 pp.) 2014
180. Lehto, Joni: Advanced Biorefinery Concepts Integrated to Chemical Pulping. (142 pp.) 2015
181. Tero, Tiia-Riikka: Tetramethoxy resorcinarenes as platforms for fluorescent and halogen bonding systems. (61 pp.) 2015
182. Löfman, Miika: Bile acid amides as components of microcrystalline organogels. (62 pp.) 2015
183. Selin, Jukka: Adsorption of softwood-derived organic material onto various fillers during papermaking. (169 pp.) 2015
184. Piisola, Antti: Challenges in the stereoselective synthesis of allylic alcohols. (210 pp.) 2015
185. Bonakdarzadeh, Pia: Supramolecular coordination polyhedra based on achiral and chiral pyridyl ligands: design, preparation, and characterization. (65 pp.) 2015
186. Vasko, Petra: Synthesis, characterization, and reactivity of heavier group 13 and 14 metallylenes and metalloid clusters: small molecule activation and more. (66 pp.) 2015
187. Topić, Filip: Structural Studies of Nano-sized Supramolecular Assemblies. (79 pp.) 2015
188. Mustalahti, Satu: Photodynamics Studies of Ligand-Protected Gold Nanoclusters by using Ultrafast Transient Infrared Spectroscopy. (58 pp.) 2015
189. Koivisto, Jaakko: Electronic and vibrational spectroscopic studies of gold-nanoclusters. (63 pp.) 2015
190. Suhonen, Aku: Solid state conformational behavior and interactions of series of aromatic oligoamide foldamers. (68 pp.) 2016
191. Soikkeli, Ville: Hydrometallurgical recovery and leaching studies for selected valuable metals from fly ash samples by ultrasound-assisted extraction followed by ICP-OES determination. (107 pp.) 2016
192. XXXVIII Finnish NMR Symposium. Book of Abstracts. (51 pp.) 2016
193. Mäkelä, Toni: Ion Pair Recognition by Ditopic Crown Ether Based bis-Urea and Uranyl Salophen Receptors. (75 pp.) 2016
194. Lindholm-Lehto, Petra: Occurrence of pharmaceuticals in municipal wastewater treatment plants and receiving surface waters in Central and Southern Finland. (98 pp.) 2016
195. Härkönen, Ville: Computational and Theoretical studies on Lattice Thermal conductivity and Thermal properties of Silicon Clathrates. (89 pp.) 2016
196. Tuokko, Sakari: Understanding selective reduction reactions with heterogeneous Pd and Pt: climbing out of the black box. (85 pp.) 2016
197. Nuora, Piia: Monitapaustutkimus LUMA-Toimintaan liittyvissä oppimisympäristöissä tapahtuvista kemian oppimiskokemuksista. (171 pp.) 2016

DEPARTMENT OF CHEMISTRY, UNIVERSITY OF JYVÄSKYLÄ  
RESEARCH REPORT SERIES

198. Kumar, Hemanathan: Novel Concepts on The Recovery of By-Products from Alkaline Pulping. (61 pp.) 2016
199. Arnedo-Sánchez, Leticia: Lanthanide and Transition Metal Complexes as Building Blocks for Supramolecular Functional Materials. (227 pp.) 2016
200. Gell, Lars: Theoretical Investigations of Ligand Protected Silver Nanoclusters. (134 pp.) 2016
201. Vaskuri, Juhani: Oppiennätyksistä opetussuunnitelman perusteisiin - lukion kemian kansallisen opetussuunnitelman kehittyminen Suomessa vuosina 1918-2016. (314 pp.) 2017
202. Lundell Jan, Kiljunen Toni (Eds.): 22<sup>nd</sup> Horizons in Hydrogen Bond Research. Book of Abstracts. 2017
203. Turunen, Lotta: Design and construction of halogen-bonded capsules and cages. (61 pp.) 2017
204. Hurmalainen, Juha: Experimental and computational studies of unconventional main group compounds: stable radicals and reactive intermediates. (88 pp.) 2017
205. Koivistoinen Juha: Non-linear interactions of femtosecond laser pulses with graphene: photo-oxidation, imaging and photodynamics. (68 pp.) 2017
206. Chen, Chengcong: Combustion behavior of black liquors: droplet swelling and influence of liquor composition. (39 pp.) 2017
207. Mansikkamäki, Akseli: Theoretical and Computational Studies of Magnetic Anisotropy and Exchange Coupling in Molecular Systems. (190 p. + included articles) 2018.
208. Tatikonda, Rajendhraprasad: Multivalent N-donor ligands for the construction of coordination polymers and coordination polymer gels. (62 pp.) 2018
209. Budhathoki, Roshan: Beneficiation, desilication and selective precipitation techniques for phosphorus refining from biomass derived fly ash. (64 pp.) 2018
210. Siitonen, Juha: Synthetic Studies on 1-azabicyclo[5.3.0]decane Alkaloids. (140 pp.) 2018
211. Ullah, Saleem: Advanced Biorefinery Concepts Related to Non-wood Feedstocks. (57 pp.) 2018
212. Ghalibaf, Maryam: Analytical Pyrolysis of Wood and Non-Wood Materials from Integrated Biorefinery Concepts. (106 pp.) 2018

1. Bulatov, Evgeny: Synthetic and structural studies of covalent and non-covalent interactions of ligands and metal center in platinum(II) complexes containing 2,2'-dipyridylamine or oxime ligands. (58 pp.) 2019. JYU Dissertations 70.
2. Annala, Riia: Conformational Properties and Anion Complexes of Aromatic Oligoamide Foldamers. (80 pp.) 2019. JYU Dissertations 84.
3. Isoaho, Jukka Pekka: Dithionite Bleaching of Thermomechanical Pulp - Chemistry and Optimal Conditions. (73 pp.) 2019. JYU Dissertations 85.
4. Nygrén, Enni: Recovery of rubidium from power plant fly ash. (98 pp.) 2019. JYU Dissertations 136.
5. Kiesilä, Anniina: Supramolecular chemistry of anion-binding receptors based on concave macromolecules. (68 pp.) 2019. JYU Dissertations 137.
6. Sokolowska, Karolina: Study of water-soluble p-MBA-protected gold nanoclusters and their superstructures. (60 pp.) 2019. JYU Dissertations 167.
7. Lahtinen, Elmeri: Chemically Functional 3D Printing: Selective Laser Sintering of Customizable Metal Scavengers. (71 pp.) 2019. JYU Dissertations 175.
8. Larijani, Amir: Oxidative reactions of cellulose under alkaline conditions. (102 pp.) 2020. JYU Dissertations 217.
9. Kolari, Kalle: Metal-metal contacts in late transition metal polymers. (60 pp.) 2020. JYU Dissertations 220.
10. Kauppinen, Minttu: Multiscale computational investigation of catalytic properties of zirconia supported noble metals. (87 pp.) 2020. JYU Dissertations 231.
11. Ding, Xin: Halogen Bond in Crystal Engineering: Structural Studies on Crystals with Ruthenium Centered Complexes and 1-(4-Pyridyl)-4-thiopyridine Zwitterion as Halogen Bond Acceptors. 2020. JYU Dissertations.
12. Kortet, Sami: 2,5-Diarylpiperidines and Pyroglutamic-Acid-Derived 2-Diarylmethyl-5-Aryl-Piperidines: Their Synthesis and Use in Asymmetric Synthesis. 2020. JYU Dissertations.